POLITECNICO DI MILANO

School of Industrial and Information Engineering

Master of Science in Energy Engineering

Three-dimensional inverse modelling of two-phase flows at the core scale

Supervisor:
Prof. Alberto Guadagnini

Co-Supervisor:
Ph. D. Martina Siena
Ph. D. Aronne Dell'Oca

Autor:
Andrea Manzoni
Matr. 915052

Academic Year 2019/2020

Occam's principle: a simulation model should be as simple as possible, but not simpler.

ABSTRACT

È stata sviluppata una metodologia per il problema inverso di flussi multifase all'interno di mezzi porosi alla scala dei campioni in carota. L'obbiettivo è stato quello di creare una metodologia in grado di ricavare accuratamente le informazioni necessarie alla realizzazione di un modello alla scala di giacimento; e.g. è in grado di ricavare i parametri necessari all'ottenimento delle permeabilità relative e delle pressioni capillari durante le operazioni di waterflooding. L'input richiesto dalla metodologia comprende un dataset tridimensionale di valori di saturazione all'interno del campione e la caduta di pressione ai capi dello stesso. Nello specifico è stato utilizzato un set di dati sintetico che simula i risultati ottenuti da un'analisi ai raggi X del campione e i risultati ricavati dalla misura della caduta di pressione durante un esperimento di iniezione di flusso costante alla base del provino. Il dataset realizzato numericamente comprende un errore di misura imposto artificialmente.

Una versione iniziale della metodologia è stata realizzata utilizzando solo le informazioni presenti in letteratura riguardo l'impiego di vari metodi e di applicazioni simili. Alla versione iniziale sono stati apportati molti aggiornamenti per ottenere una efficace versione finale della metodologia. I confronti delle diverse funzioni obbiettivo sono stati effettuati servendosi dell'analisi di sensitività allo scopo di ottenere il peso relativo del componente legato ai dati di saturazione e quello legato alla caduta di pressione. Inoltre, è stato verificato l'effetto provocato dalla riduzione del peso del dataset da trattare attraverso un'operazione di upscaling dei dati. Nelle varie versioni della metodologia sono stati impiegati due diversi algoritmi di ottimizzazione (Particle Swarm Optimization e Differential Evolution); il confronto dei risultati ha portato all'utilizzo del DE nella versione finale. Anche i parametri dell'algoritmo hanno richiesto diversi confronti per ottenere un settaggio efficace.

Utilizzando le informazioni acquisite è stata realizzata la versione finale della metodologia che ha dimostrato di essere efficace per alcuni dei casi reali più comuni.

ABSTRACT

An approach to tackle the inverse problem of multiphase flows within core-scale porous media has been developed. The objective was to create a methodology able to accurately derive the information necessary to create a model at the reserve scale; e.g. it is able to derive the parameters necessary to obtain the relative permeabilities and the capillary pressures during waterflooding operations. The input required by the methodology includes a three-dimensional dataset of saturation values within the sample and the pressure drop at the ends of it. Specifically, a synthetic dataset that simulates the results obtained from an X-ray analysis of the sample and the results obtained from the measurement of the pressure drop during a constant flow injection experiment at the base of the sample has been used. The dataset produced, from a numerical simulation, includes an artificially imposed measurement error.

An initial version of the methodology has been realized using only the information present in the literature regarding the use of the various methods and similar applications. Many updates have been made to the initial version in order to obtain an effective final version of the methodology. The comparisons of the various objective functions have been carried out using the sensitivity analysis in order to obtain the relative weight of the component linked to the saturation data and that linked to the pressure drop. Furthermore, the effect caused by the reduction of the weight of the dataset to be treated through an upscaling of the data has been verified. In the various versions of the methodology, two different optimization algorithms were used (Particle Swarm Optimization and Differential Evolution); the comparison of the results led to the use of DE in the final version. The parameters of the algorithm also required different comparisons in order to obtain an effective setting.

Using the acquired information, the final version of the methodology has been realized, which has proved to be effective for some of the most common real cases.

ACKNOWLEDGEMENTS

Ringrazio in primis il professor Guadagnini che, trasmettendomi un po' della sua passione per la materia e per la ricerca, mi ha prima concesso di scegliere l'argomento di tesi e poi invogliato a proseguire gli studi. Lo ringrazio anche e soprattutto per la disponibilità che mi ha sempre dimostrato durante lo svolgimento di questo progetto e per l'aiuto nelle scelte per la mia carriera. Un ringraziamento alla Dottoressa Siena e al Dottor Dell'Oca che, con grande disponibilità, mi hanno fornito un supporto tecnico comprensivo di codici ed aggiornamenti e degli ottimi spunti per la prosecuzione del lavoro. Grazie anche al professor Inzoli che, grazie ai suoi buoni consigli, mi ha assistito nella scelta dei corsi di Laurea Magistrale e del (futuro) corso di dottorato. Inoltre, vorrei ringraziare i componenti della mia famiglia, Diego, Antonella e Francesca, per il sostegno e la pazienza che hanno dimostrato durante tutti gli anni della mia formazione. Un ringraziamento particolare va alla mia Laura che ha condiviso con me tutte le fatiche e le gioie che questo duro percorso ci ha messo davanti, che mi ha insegnato tanto e che anche durante la stesura di questo scritto è riuscita come sempre a migliorare un po' le cose. Ringrazio tutti i compagni di avventura, di cui ho grande stima: Federica, Gabriele, Paolo e specialmente Michela con cui ho sempre avuto un'ottima intesa. E infine, per ultimi ma non meno importanti ringrazio tutti i miei amici per esserci sempre stati nonostante tutti i miei 'non posso, devo studiare' tra tutti: Riccardo, Nicolò, Mobassiro, Moses, Cristiana, Sabrina, Mireille, Simone, Debora, Stefano, Luca, Silvia e Letizia.

EXTENDED ABSTRACT

The information obtained from experiments in the laboratory is a fundamental aspect for modelling at the reserve scale, and consequently for the development of a hydrocarbon extraction project. One of the most used experiments for the determination of important properties of the system is the injection of a fluid into a rock sample taken directly from the reserve. The oil production may consist of injecting water into the reserve with the aim of displacing the oil (economically interesting good). The objective of the thesis project was to create a useful methodology for extrapolating information from data obtained from experiments conducted on core samples into which water is injected (simulating the extraction process). Thanks to the instrumentation available today, it is possible to obtain three-dimensional data of the saturation values inside the sample during the discrete temporal steps of the experiment. To create an effective workflow, it was necessary to create artificial data that were completely similar to those obtainable from the experiments. The synthetic data were generated using commercial software widely used for developing models for multiphase flows within porous media. The software for the representation of a two-phase flow consisting of water and oil, within a sample taken from an oil reservoir, was created using specific simulation programs within the MATLAB MRST toolbox and adding the necessary closure equations and boundary conditions. The closure equations used are: the Corey's model for the representation of the relative permeability trend of the fluids involved as the water saturation inside the sample varies, the Skjaeveland's model that expresses the relationship between capillary pressure and water saturation and the porosity-absolute permeability relationship that relates the porosity and absolute permeability inside a heterogeneous porous medium. The simulation program was updated during the development of the work by adding correlations able to express the links between the various parameters present in the program itself. Starting from the data generated with the above mentioned program, an artificial error has been inserted to simulate the one committed by a measuring instrument. The use of synthetic data has allowed to have more advantages compared to the use of data coming from real experiments. The first benefit was the a priori knowledge of the information to be obtained from the data, because they are the same used to generate the dataset. The second advantage was the possibility of generating datasets able to represent different situations of the system, specifically with different wettability and more significant measurement errors; this has allowed the methodology to be tested under different conditions.

To acquire the information from the (synthetic) data, an inverse problem has been set. The inverse problem consists in determining the characteristics of the system that characterizes a given phenomenon starting from the observations of its advancement. Given the complexity of the model, which is able to generate a discrete three-dimensional dataset, the direct approach has been excluded because it is impossible to invert the system of equations to set up an analytical solution. The indirect approach has therefore been chosen. It consists in minimizing an objective function to make the data generated by the model similar to those obtained from the measurements. The appropriate objective function was chosen by observing the system and then choosing the one that best suits the context. Moreover, for the specific case, based on theoretical formulations, the equivalence between the maximization of the Likelihood function and the least square error has been obtained. Besides the minimization of the local saturation residues, the information concerning the difference in pressure at the heads of the sample (time-dependent) has been added to the objective function. The relative weight of the two components of the

objective function (the one linked to saturation and the one linked to pressure difference) has been determined thanks to the sensitivity analysis on the residues.

Another key step in the development of the methodology was the choice of the optimization algorithm for determining the minimum of the objective function. Two optimisation algorithms were compared for this purpose: the Particle Swarm Optimization and the Differential Evolution. The particle swarm optimization proved to be ineffective during the first iterations; its dispersive behaviour has led the flow simulation program to have in input combinations of parameters with no physical meaning with the consequent blockage of the optimization process. The final choice fell on differential evolution, as it proved capable of identifying good results without problems during the first iterations.

Finally, a solution was found to reduce the computational cost of the inversion process. The realization of a coarser grid allowed to reduce the cost of each single simulation, conducted by the optimization algorithm, resulting in a considerable time saving in the optimization procedure. Although the final grid was composed of a small number of cells, it has proven to be able to obtain the necessary information with sufficient accuracy. The reduced time of the evaluations has also allowed the optimization algorithm to be set in the most suitable way, increasing the number of population components to that recommended in the literature.

Some specific evaluation parameters were introduced to compare the different versions of workflow. They were able to determine how much the solution identified by a given methodology was different from the exact one. These evaluation parameters were used to assess the goodness of the overall solution but also the goodness of every single piece of information obtained. Another important parameter of comparison was the time that a methodology took to obtain the solution.

The final version of the workflow was verified on datasets that represented systems in different possible conditions. Specifically, the methodology proved to be effective in systems with different wettability conditions and more significant measurement errors. Thanks to the carried out analyses, it was also possible to identify the limits and the criticalities that define the applicability of the developed workflow.

CONTENTS

LIST OF FIGURES

LIST OF TABLES

1 INTRODUCTION

In the study of the motion of the fluids in subsurface systems, usually the information available is scarce and unreliable; indeed, the measurements from which the data are obtained are often conducted at different scales or estimated using interpolation methods. A further factor that complicates the evaluations is that in the majority of underground systems the flows are composed by two or more phases. In order to produce sufficiently accurate large-scale models useful for commercial extraction purposes (in the case of hydrocarbon reserves) or for research and study (in the case of aquifers) a large amount of information is required. One of the most effective methods for the determination of some of the fundamental properties is laboratory testing. In these tests the samples of the fluids present in the system and the core samples are analysed. A core sample is a piece of material (in the case treated of sandstone) usually of cylindrical shape taken directly from the layers of reservoir. The sample is extracted thanks to special drills made for specific sampling processes or installed on drilling devices for the construction of wells. In the core drilling process, the rock is transported more or less intact to the surface. Transferred to the laboratory, the core sample is inspected and analysed using different techniques and equipment depending on the type of data desired. Therefore, to date, the realization of a method able to extrapolate as much information as possible from the experiments on core samples is an aspect of great interest.

The aim of the project is to create a methodology (workflow) for the inverse problem on multi-phase flow within a core sample; i.e. the objective is to determine the parameters of the equations that characterise the phenomena, and all information derived from them, at the laboratory scale starting from a set of three-dimensional saturation data. To this end, a real experiment conducted by Eni on a core sample taken directly from an oil reserve has been used as starting point.

To validate the methodology, it has been decided to create a synthetic dataset that reproduces a fictitious experiment, which is similar to the real experiments carried out in the laboratory. The data come from a simulate water injection experiment through an oil saturated rock. So, a non-steady state two phase (water and oil) flow through a porous media has been represented. Artificial errors have been inserted in the synthetic dataset to simulate the error made by the measuring instrument. The synthetic datasets have made possible to carry out experiments on systems characterized by different properties with the benefit to know the results that the methodology should have been able to determine.

Thanks to the large amount of information acquired on the phenomena that characterize the experimentation and the study of the inverse problem, a first version of workflow has been presented.

In the various sections all the methodology updates have been deeply described. The steps carried out in order to obtain the final version of the workflow have been numerous. The first version of the workflow was unable to complete the calibration process; so, the optimization algorithm has been replaced in favour of one, that maintaining the same characteristics, was able to solve problems occurred during the evaluation of the candidate solutions. The choice has been made by observing the behaviours of the different algorithms and comparing this information with the information present in the literature. The methodology at that point has been refined in order to make possible to individuate the correct parameters that characterize the system starting from the synthetic data. To

carry out the necessary modifications, various simulations and sensitivity analyses have been performed. The acquired information has been used for understanding the specific inverse problem issues. Once the issues have been stated, the settings of the optimisation algorithm have been updated and an effective objective function has been selected. The last update of the methodology concerned the modification of the grid of the model for the simulation of the experiment. The aim of this last updates has been the reduction of the computational time in order to make the methodology applicable.

Finally, the ultimate version of the workflow for determining the parameters has been tested in different systems (with different properties and with worse measurement errors) to verify its applicability and criticality.

2 THEORETICAL FRAMEWORK

To build an effective methodology for the parameter estimation, a rich theoretical background has been required.

The first topic of the study has been oriented to the understanding of the phenomena occurring inside the core sample during the waterflooding experiment. In fact, the immiscible two-phase flow inside the porous media has been analysed starting from the understanding of the simplest single-phase flow and extending the parameters and the equations.

The second topic has deal with the construction of the models. Although a personal model has been not realized during the thesis project, it has been fundamental to understand how to build a conceptual model for the representation of the flow and how to pass from it to the mathematical model; then the knowledge of the methods used to numerically solve the mathematical model on the computer has been required.

The third argument explored has been the inverse problem. Regarding this topic it has been fundamental to understand: the approach for the estimation of the parameters, the different approaches available (direct and indirect) and the advantages and disadvantages in the different applications of the various approaches. Finally, the main problems of the inverse problem have been studied.

The fourth and last topic have been the optimization algorithms. Once understood their purpose within the inverse problem, the five main categories in which the optimization algorithms are usually subdivided have been analysed and of these the most common algorithms have been briefly explored. In the end the algorithms that have been chosen and used in the various versions of the methodology have been studied in detail.

The topics just presented has proven to be interdependent, and by combining the acquired knowledge a methodology for obtaining information from 3D saturation datasets (from experiments at the core sample scale) has been created.

The four topics mentioned above are a brief introduction to the content of the following four subchapters. Following these subchapters, a summary of the history of the methodologies used for the estimation of the parameters in problems involving sub-surface flows is presented, with particular attention to the most recent developments (state of the art).

2.1 MULTI-PHASE FLOW BASIC CONCEPTS

In order to understand the motion of multiphase flow in porous media it is fundamental to introduce the basic concepts starting from the homogeneous flow in porous media.

The micro scale solution of the fluid motion through the pore will require a large computational cost and will give a too detailed solution unnecessary in most cases for petroleum industries. So, the fluid is treated as continuum and the conservative equations of mass and momentum for a homogeneous flow are not resolved, but the Darcy equation is introduced to simplify the solution. [1]

2.1.1 Darcy's experiment

The Darcy's law is an empirical equation obtained for slow flow in porous media [2]. The Darcy experience investigate a flow that pass through a vertical sand filters from the top to the floor. From the just mentioned experiment Darcy has discovered that the volumetric flow (Q) is proportional to the constant cross section area (A) and to the piezometric head difference between the head and the bottom of the filter (h_1-h_2) however, it is inversely proportional to the filter length L.

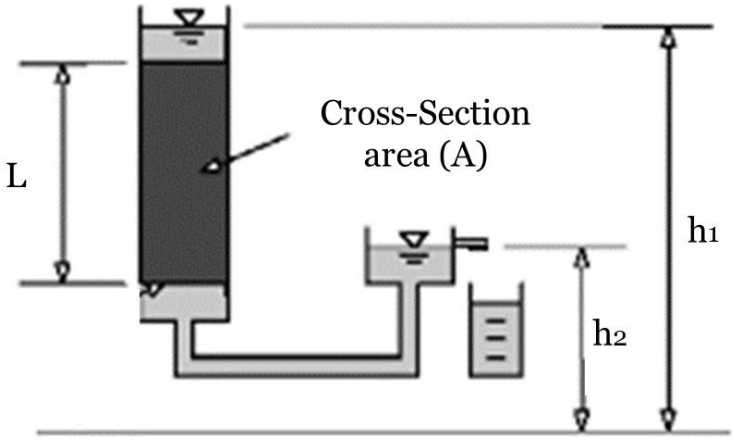

Figure 1:scheme of Darcy's experiment, flow of water passing through a sand filter from top to bottom. Source:SNU OPEN COURSEWARESEOUL NATIONAL UNIVERSITY, Darcy's Law - Darcy experiment

Combining these inferences, it has been obtained the famous Darcy formula:

$$Q = \frac{KA(h_1 - h_2)}{L} \tag{2.1}$$

It is possible to notice that (h_1-h_2) refers to the potential plus the pressure energy different across the filter. So, the hydraulic gradient can be defined as $J = (h_1 - h_2)/L$. A common version of the Darcy is $q = KJ$ where q is defined as Q/A and it is the volumetric flow that pass through a unit area.

The experimentally derived Darcy's law is valid for one dimensional flow. In practice one dimensional flow are not present, so an extension to a three-dimensional homogeneous isotropic condition is:

$$\mathbf{q} = K\mathbf{J} = -K \operatorname{grad} \varphi \tag{2.2}$$

Where $\varphi = z + p/\gamma$ is the piezometric head , $\mathbf{J} = -\operatorname{grad} \varphi$ is the hydraulic gradient composed by $J_x = -\frac{\partial \varphi}{\partial x}, J_y = -\frac{\partial \varphi}{\partial y}, J_z = -\frac{\partial \varphi}{\partial z}$ and **q** is the specific flux vector composed by q_x, q_y, q_z. The subscripts x,y,z refers to the cartesian coordinates.

Other forms of Darcy's law (eq. 2.2) are:

$$\begin{aligned}\mathbf{q} &= -\frac{k}{\mu}\left[\frac{\partial p}{\partial x}\mathbf{x} + \frac{\partial p}{\partial y}\mathbf{y} + \left(\frac{\partial p}{\partial z} + \rho g\right)\mathbf{z}\right] \\ &= -\frac{k}{\mu}(\text{grad } p + \rho\mathbf{g}\mathbf{1}z) = -\frac{k}{\mu}(\text{grad } \beta - \rho\mathbf{g})\end{aligned} \tag{2.3}$$

For a further extension of the law to non-homogeneous media it must be considered the K dependence to the position: $K = K(x, y, z)$. For the anisotropic medium the Darcy law accounts the directional dependence of a property, in the specific of the hydraulic conductivity K (or its main component the permeability k).

Subsurface systems are typically anisotropic with respect to conductivity. It might be caused by many occurrences; here are reported the most common [1]:

- The sediments are formed by stratified deposits that due to the different formation time have different properties. In such manner the non-homogeneous material has different behaviour in different direction.
- The stratification may also be a result from the shape of the particles.
- Another mechanism that creates anisotropicity is the formation of fractures. Along the fracture direction the permeability (and with it the hydraulic conductivity) is typically greater than in the other directions.

The extended forms for the Darcy's law for anisotropic medium are:

$$\begin{aligned} q_x &= K_{xx}J_x + K_{xy}J_y + K_{xz}J_z \\ q_v &= K_{yx}J_x + K_{yy}J_y + K_{yz}J_z \\ q_x &= K_{zx}J_x + K_{zy}J_y + K_{zz}J_z \end{aligned} \tag{2.4}$$

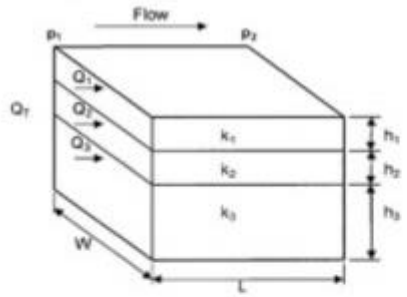

$$K_{avg} = \frac{\sum_{j=1}^{n} K_j h_j}{h_t}$$

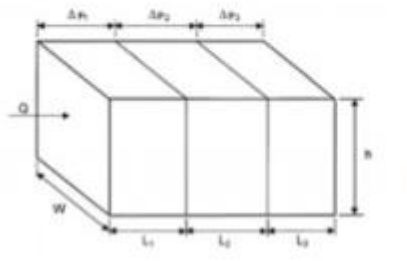

$$K_{avg} = \frac{\sum_{i=1}^{n} L_i}{\sum_{i=1}^{n} (L/K)_i}$$

Figure 2:Eexample of a non-histotrophic layered medium with different hydraulic conductivity for different flow orientations. - Source: https://perminc.com/

An intuitive example is shown in the picture above. It makes easy understanding that the flow has different characteristics for the same media in different directions. In the image

are also reported the different evaluation of the global hydraulic conductivity (K) in the two different orientations (for more information on average permeability in the two examples in figure 2 see https://perminc.com/ in the permeability section combination).

2.1.2 Darcy law limits of applicability:

As the specific flow (q) increases it has been demonstrated that Darcy's law is invalid [1]. It is therefore necessary to define an upper limit.

The Reynolds dimensionless number (Re) expresses the ratio of inertial to viscous forces. In fluid dynamic it is used to differentiate the laminar with respect to the turbulent flow.

For flow in porous media it is defined a Re in analogy with the fluid-dynamic, as:

$$\mathrm{Re} = \frac{\mathrm{qd}}{v} \tag{2.4}$$

Where q is the volumetric flow rate through a unit area, v is the kinematic viscosity of the fluid and d is a characteristic dimension of the porous matrix, for which it is typically used the mean grain diameter (Re is defined without an universal agreement, so in literature are present different definition of d). [1]

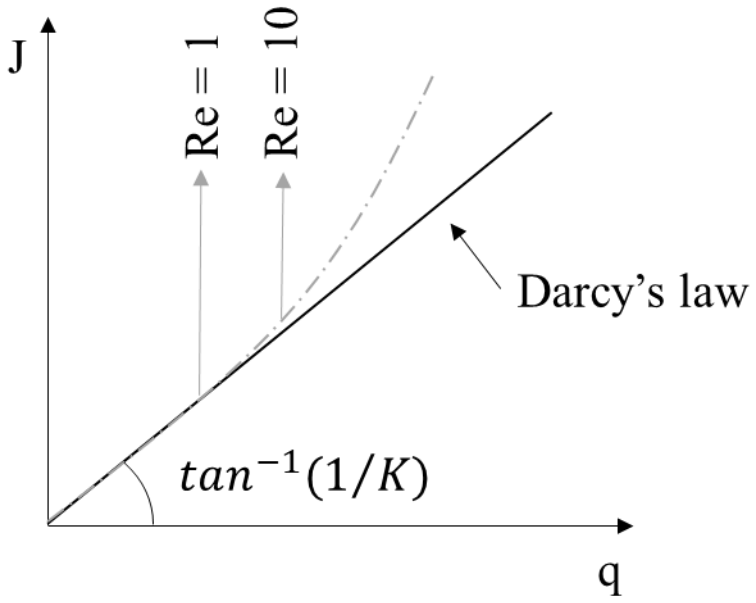

Figure 3: the linear trend of Darcy's law compared with the typical trend of real data that deviates when the specific flow increase. - Source: [1]

Darcy's law expresses a linear relationship between the hydraulic gradient and volumetric flow rate. It is possible to notice from the graph that the interpolation of real data is not anymore linear at Re greater than a value comprised between one and ten (it depends on how it is defined). At Re greater than ten the inertia forces became relevant so the hypothesis of a Darcian flow decays.

It also exists a lower limit where phenomena of interaction between rock and the fluid become more significative leading to a non-Darcian flow [1].

Another possibility of the flow to have a behaviour that deviates from the one described by the Darcy's law is the occurrence of the slip phenomenon. It occurs when a gas or a gas-liquid flow passes through a pore that has a diameter of a capillary tube that approaches the mean free path of the molecules. In the just described situation the flow is faster than the predicted one.

2.1.3 Hydraulic Conductivity and Permeability

The coefficient K, appearing in the Darcy's law discussed in the section 2.1.1., is called hydraulic conductivity. In homogeneous and isotropic media, as already seen in the previous paragraph, it is a scalar value (dimensions L/T) that express the specific flow rate (dim. L/T) per unit of hydraulic gradient (dimensionless). K depends on the kinematic viscosity of the fluid ν (that is μ/ρ) and from the rock properties: porosity, tortuosity, pore size and pore space distribution. However, the hydraulic conductivity can be expressed as $K = k\gamma/\mu = kg/v$, where k is called permeability (dim L^2) of the porous matrix.

In literature exist various formulas that relate the various rock properties. These are divided in three main categories: (1) the purely empirical formulas, (2) the purely theoretical formulas obtained from the theoretical derivation of the Darcy's law, (3) the semi empirical formulas, that requires calibration for every specific rock matrix. [1]

When k varies in space the porous media is called inhomogeneous, k=k(x,y,z). The rock is called anisotropic if k is function of the direction. When the fluid thermodynamic condition varies in time and in space also the fluid properties change affecting the hydraulic conductivity.

In summary:

Isotropic and homogeneous: $\mathbf{q} = -K\,\mathrm{grad}(\varphi(\mathbf{x}))$. (2.5)

Anisotropic and homogeneous: $\mathbf{q} = -\underline{\mathbf{K}}\,\mathrm{grad}(\varphi(\mathbf{x}))$. (2.6)

Isotropic and non-homogeneous: $\mathbf{q} = -K(\mathbf{x})\mathrm{grad}(\varphi(\mathbf{x}))$. (2.7)

Anisotropic and non-homogeneous: $\mathbf{q} = -\underline{\mathbf{K}}(\mathbf{x})\,\mathrm{grad}(\varphi(\mathbf{x}))$. (2.8)

with: $\underline{\mathbf{K}} = \begin{bmatrix} K_{xx} & K_{xy} & K_{xz} \\ K_{yx} & K_{yy} & K_{yz} \\ K_{zx} & K_{zy} & K_{zz} \end{bmatrix}$ (2.9)

2.1.4 Flow of immiscible fluids

In the oil & gas industries or in groundwater flow, two of the most important field where flow through porous media is investigated, the two-phase flow is very common. Below are reported some examples.

When more than one fluid occupies the same porous domains only two types of flow are possible. If the two fluids are completely soluble, it is called miscible displacement. The interfacial tension between the two fluids is zero. Hence, it is not possible to find a fluid-

fluid interface. On the other hand, when the interfacial tension between the fluids is not zero, the displacement is called immiscible. The capillary pressure difference is not zero and it is possible to identify different streams inside the flow in number equal to the fluids present. For both the types of fluid an abrupt interface between the phases in macroscopic scale does not exist. The hydrodynamic dispersion generates a transition zone

In many cases of interest, the transition zone is relatively very small or in immiscible fluids the displacement is almost complete. [1] In such cases it is a practical use assume a fictitious abrupt interface considering them as separated flows.

In an oil reservoir usually with the liquid hydrocarbon is present a gas phase composed by inert gases (as CO2) and the most volatile hydrocarbon (as methane). It is also very common in oil and gas reservoir find some brine. It is of extreme interest to study their interaction in order to be able to predict and maximise the valuable hydrocarbon production. In the oil industries is also very common to inject an external fluid, that may be water or specific fluid, in order to increase the productivity and therefore the revenues.

Those, just mentioned, are typical problem where understanding the interaction between the phases and its effect on the flow is highly important.

It is now necessary to define a new state variable that indicates how much space is occupied by that particular fluid (α):

$$S_\alpha = \frac{\text{volume of fluid } \alpha \text{ within an REV}}{\text{volume of voids within an REV}} \tag{2.10}$$

where S_α is called saturation and represents the fraction of a reference elementary volume (REV) with $\sum s_\alpha = 1$.

$$C_\alpha = \frac{\text{volume of fluid } \alpha \text{ within an REV}}{\text{bulk volume of REV}} = \phi S_\alpha \; ; \sum c_\alpha = \phi \tag{2.11}$$

where C_α is the concentration and ϕ is the porosity.

2.1.5 Interfacial tension and wettability

When one liquid comes in contact with another immiscible fluid or a solid, a free interfacial energy is present between them. The interfacial energy is originated by the difference between the inward attraction of the molecules in the interior of each phase and those at the surface of contact. [3]

σ_{ik} is the interfacial tension between any pairs of substance in contact. It is the amount of work required to separate a unit area of the two substances i and k. σ_i is defined as the interfacial tension between a substance i and its own vapor.

The interfacial tensions are temperature dependent and so is the capillary pressure.

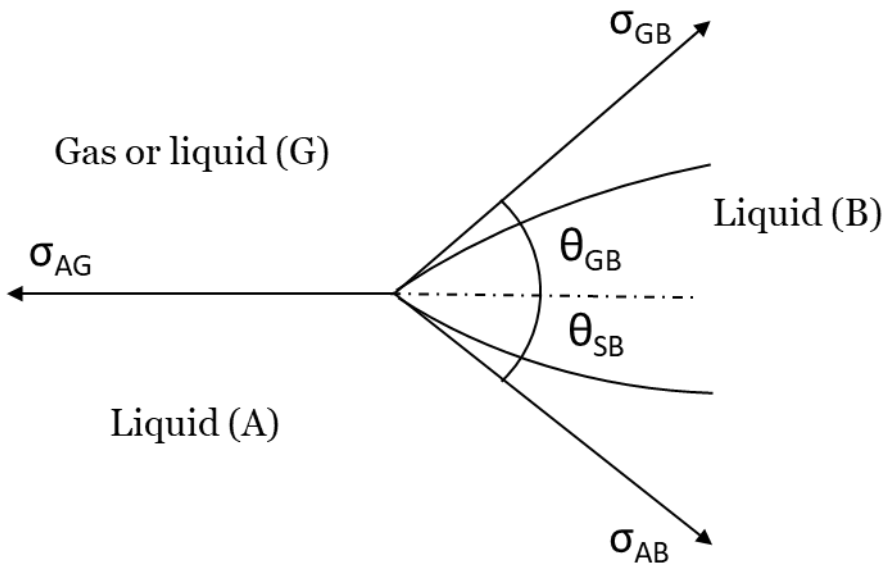

Figure 4: interfacial tensions between two liquids (A and B) and a gas (G) (e.g. oil, water and gas) - Source: [1]

$$\sigma_{AG} = \sigma_{AB} \cos\theta_{AB} + \sigma_{GB} \cos\theta_{GB}. \quad (2.12)$$

The equation (2.12) can be satisfied if $\sigma_{AG} < (\sigma_{AB} + \sigma_{GB})$, and a lens of liquid B will be formed. If $\sigma_{AG} > (\sigma_{AB} + \sigma_{GB})$, the equilibrium is not possible and liquid B will spread out between A and G.

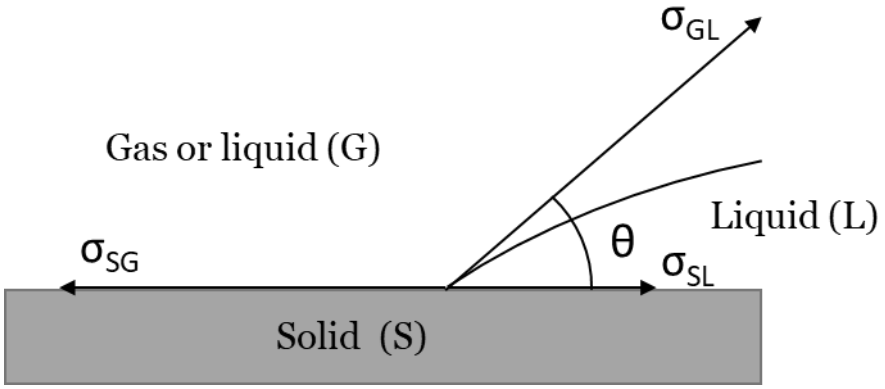

Figure 5:interfacial tensions between a liquid phase and another liquid or gas phase in contact with a solid wall (e.g. water or gas with oil in porous duct) - Source: [1]

Young's equation:

$$\cos\theta = \frac{\sigma_{SG} - \sigma_{SL}}{\sigma_{GL}} \quad (2.13)$$

If $\frac{\sigma_{SG}-\sigma_{SL}}{\sigma_{GL}} > 1$, the liquid L will spread indefinitely over the solid. This leads to the concept of wettability of a solid by a liquid.

θ angle is called contact angle and $\sigma_{GL} \cos\theta$ is the adhesion tension. When $\theta < 90°$, L is a wetting fluid (otherwise it is called non wetting fluid). Wettability depends on the chemical composition of the fluids and the solid. It has also been demonstrated that also the history of the porous media can influence wettability [3].

When a non-wetting phase is injected in a porous medium initially saturated by the wetting fluid, the process is called drainage. On the other hand, the phenomena characterized by a wetting fluid that displace a non-wetting phase that originally saturates the rock is called imbibition only if it occurs thanks to the capillary pressure.

2.1.6 Capillary pressure

Across the (fictitious) interface, that exist between two immiscible fluids, a discontinuity in pressure it is observed. It is called capillary pressure and its magnitude depends on the interface curvature:

$$P_o = P_{nw} - P_w \tag{2.14}$$

At the microscale it is possible to define an idealized model aimed at determining P as $P = P_c(s_p)$. This approach fails at macroscopic scale even if it is useful to identify the effect of various factors.

Laboratory experiment remains the only way to derive the relationship for any given porous medium. Indeed, empirical, and semi-empirical relationship are largely available in literature. [1]

It is obviously impossible evaluate the saturation-capillary pressure relation $p_c = p_0(S_w)$ using the mechanical relations between tension stresses and the pressure: $p_c = \left(\frac{2\sigma}{r}\right)\cos\theta$, because the pore shape are typically very irregular and also very complex to measure. However, there are many laboratory methods used to determine that relationship:

- Displacement method: the measurements are conducted into a successive state of hydrostatic equilibrium obtained during the experiment.
- Dynamic methods: differently from the previous method are established successive steady state flow conditions; the flux is composed of wetting and non-wetting fluid multiphase flow.

2.1.7 Capillary pressure hysteresis

A typical observation of hysteresis of contact angle (θ) is present on the so-called rain drop effect. There it is possible to observe the difference between the downwards angle (θ_1) and the upwards angle (θ_2).

The hysteresis effect is also observable on a flow inside a pipe. The angles are different as the direction of the flow is different. Specifically, if the flow has the direction towards the fluid G the theta angle is different with respect to the case where the direction is toward the fluid L.

Capillary pressure is subjected to hysteresis as the contact angle θ is. The behaviour of the contact angle is the reason of the capillary pressure difference between the one evaluated from static experiment and those observed in dynamic conditions. [1]

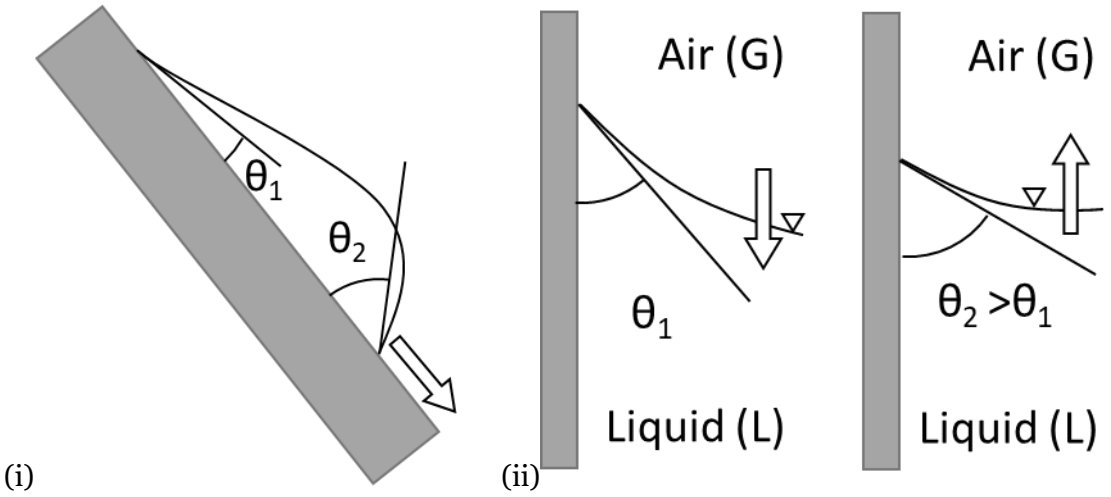

Figure 6: Examples of contact angle hysteresis: (i) raindrop effect, (ii) different contact angles for the same system with opposite flow direction - Source: [1]

2.1.8 The basic motion equation of multiphase flow.

It has been investigated from experiments that two immiscible fluids flowing simultaneously through a porous media form two independent paths. [1]

Observing a multiphase flow composed by a wetting (S_w) and a non-wetting (S_{nw}) fluid, as the saturation of the wetting phase reduces, the channel containing the non-wetting phase gets progressively cut off until it remains only in isolated regions . What remains is the residual non-wetting phase saturation. It is not possible to remove this remaining part of non-wetting fluids because it is trapped by the other fluid. [3]

In contrast, if S_w reduces, the channels containing the wetting fluid progressively break down and become discontinuous until S_w is equal to the irreducible saturation. It is the minimum value of wetting fluid saturation reachable. [3]

Now it is intuitive applying the well understood concept seen for the single-phase to the multi-phase conditions. The idea is to adapt the notion of permeability accounting the presence of the other phases modifying its value.

Considering a two phase flow and assuming a steady state condition for both the phases, the Darcy's law, that originally describes the flow of a single-phase fluid completely saturating the media, may be modified to describe the flow of each of the two immiscible fluids obtaining:

$$q_1 = \frac{\left(\frac{k_1}{\mu_1}\right)\Delta p_1}{L};\ q_2 = \frac{\left(\frac{k_2}{\mu_2}\right)\Delta p_2}{L} \tag{2.15}$$

where $q_\alpha = Q_\alpha/A_\alpha$ with $\alpha = 1,2$ are the volumetric flow rate the two phases, Δp_α is the pressure drop in the α^{th} fluid, k1 and k2 are called effective permeabilities of the medium to fluids 1 and 2, respectively. The relative permeabilities are defined as:

$$k_{r1} = k_1/k, k_{r2} = k_2/k \tag{2.16}$$

Likewise, it is common to introduce phase mobilities $\lambda_\alpha = kk_{r\alpha}/\mu\alpha$ or relative phase mobilities $\lambda_\alpha = \lambda_\alpha k$ to simplify the notation slightly. [3]

Those depend on the structure of the porous medium involved specifically, on the permeability k of the medium to a single-phase fluid completely saturating it, on the respective saturations and the wettability.

The relative permeabilities start to be related to the flow of the other phases and to the flow rate when (and/or where) the latter becomes sufficiently large. Moreover, the relevance of the viscosity ratio between the two phases may increases when the velocity is higher. These last mentioned effects can become more important when the capillary forces are not anymore dominant at the pore scale.

2.1.9 Relative permeability curves

Below it is reported an example of relative permeability curve for a waterflooding in a rock sample initially filled by oil.

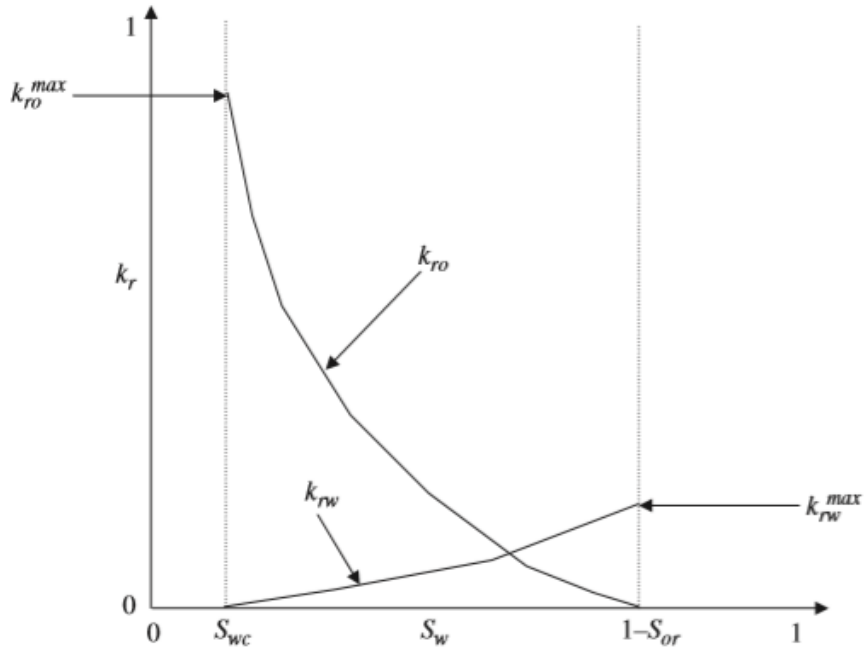

Figure 7:Example of the trend of the relative permeability curves as water saturation varies in a two-phase (oil & water) mixed-wet system. - Source: [3]

It is of common use the representation of the permeability function of the saturation as reported above. [3] From this kind of graph, analysing some key feature, it is possible to

determine the wettability of the rock and it is possible to determine some important parameters.

Examples:

- In a water wet (figure 11,ii)medium during water flooding the saturation of water increases. The water starts flowing in the narrow region leaving the oil in the middle of the channels. It implies that the oil permeability is close to 1 (≤0.8) and the water permeability is close to zero. While the water saturation increases, the water permeability remains low, even if it increases slightly. The water continues to flow in the narrow region and at the same time the oil permeability reduces because the water traps the oil. This behaviour continues until the water cut all the oil escape route. At that point, the oil permeability is zero. The oil remains embedded by water in large pores, implying a typical large residual oil saturation (0.2-0.5).
- In oil wet media (figure 11,i) the water remains in the big pores and oil flow through the narrow regions. It means that during water flooding, of an initially oil saturated porous media, the permeability is initially high because it is well connected. When the water is injected it goes to the large pores obliging the oil to flow in narrow duct so, the permeability of oil is easily reduced when the saturation of water increase. On the other hand, the water permeability grows fast when the saturation increases, and it gets very high value when the residual oil saturation is reached. The oil is moved to smaller and smaller channels until it is blocked. It means that the residual oil saturation is small (<0.1).

Those just described in the examples are the two extreme cases. Typically, the situation is in the middle and it is called mixed-wet condition. The mixed wet condition presents region more oil wet and other more water wet. Those regions are not constant in time, which means that the passage of a fluid alters the wettability depositing or removing layers on the rock surface. Sometimes special components are injected to artificially induce the change of wettability. In a mixed wet system, the key features are the low residual oil saturation and the low water relative permeability. When the water is first injected, it preferentially fills the water wet regions. The water saturation increases but the water connectivity remains low, even if the permeability grows earlier than for oil wet flow. Then the water fills the oil wet regions, the largest oil-wet pores first. [3]

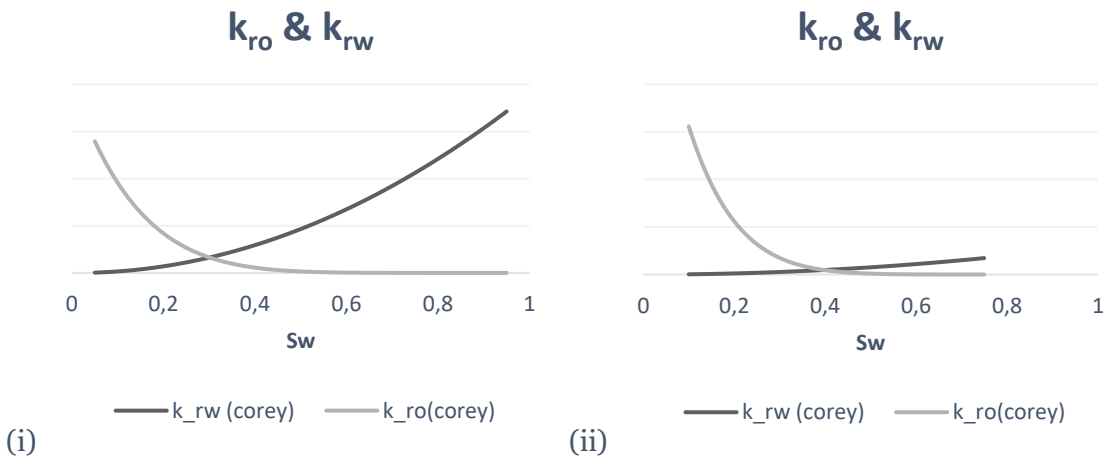

Figure 8:Examples of relative permeability vs water saturation graphs in a two-phase system (water & oil) . (i)oil wet (ii) water wet. these graphs have been realized with the Corey model (section 3.2.3.) and have been used for a verification on chosen parameter

Experience has shown that carbonates rock has a stronger wettability alteration when comes in contact with crude oil respect sandstones.

Typically carbonates rock shows mix-wet and oil-wet behaviour, while the sandstones have comportment that comprises the whole possibilities from water-wet to oil-wet. [3]

In oil recovery industries the ideal condition is: low permeability of the water to extract as little as possible of it, and a high oil relative permeability that would allow the oil to flow rapidly. A low residual oil saturation is also important, in order to recover has much oil as possible from the reservoir.

There are two distinct recovery processes for water flooding:

- Water is injected and essentially pushes out oil
- The imbibition process in which the water enters spontaneously inside the rock under the influence of capillary pressure. It is the dominant process in fractured reservoirs.

2.2 MATHEMATICAL CORE MODEL

The realization of a model representing the flow, however, is not the ultimate goal. Actually, in the specific case of the sample flow model, the objective is to identify the parameters that characterize the rock-oil-water system of a specific reserve.

A hydrocarbon reserve is a porous domain through which a mixture mainly composed of hydrocarbons and water flows. Usually the flows that characterize an oil reserve are multiphase flows that mainly involve: (1) gases composed of light hydrocarbons, e.g. methane, and inert gases trapped in the reserve, e.g. carbon dioxide, (2) liquid hydrocarbons (oil) (3) reserve water or brine. (subchapter 2.1.)

In the sample supplied by Eni the mixture includes mainly water and oil (liquid hydrocarbon).

In the following section an overview of the modelling process of flows within porous media is presented. During the thesis project an already available model (largely used in literature) has been chosen and has been analysed in detail in order to understand its characteristics and to be able to implement an effective methodology for the determination of its parameters. The understanding of the methodology for the realization of the model has been of concrete help for the development of the workflow of the thesis.

2.2.1 Objective of modelling

A model is a simplified version of a real system that represents the phenomena that occur within it, simulating the excitation-response relationship of interest that characterize the system itself [4].

The most common objectives of modelling activity are:

- Predict the response of a system to some solicitation, often imposed because of the implementation of management decisions, to which it is subjected. E.g. the injection of water in reserve in order to increase the productivity of the valuable hydrocarbons.
- To improve the knowledge of the system from a hydrogeological and/or chemical point of view.
- Upscaling the properties obtained from laboratory scale models and experiment to the field size.

Although a model is expressed in mathematical terms, it is important to say that this kind of notation is a resource to represent in a compact way the physical and chemical phenomena that influence the aspects of interest of the system. Often the ultimate goal is to maximize an objective, e.g. the extraction of the economically interesting hydrocarbons identifying which are the input that causes a favourably reaction of the system towards the objectives. [4]

2.2.2 Overview of the modelling process

A typical conceptual modelling process can be resumed in the following steps:

a) It is, first of all, necessary to find all the information needed to identify and evaluate the ultimate goal (e.g. the oil production).
   To select the best model which considers the pursued goal, it is necessary to identify, a priori, one or more parameters able to evaluate the goodness of the performed simulations. These parameters are assessed by one or more objective functions that combine the acquired information. This type of information will be also used to verify whether the proposed alternative, chosen as optimal, does not exceed some of the constraints imposed on the system. The model evaluation parameters must be defined first to ensure that all the choices made in the development of the conceptual model are consistent with the goal.
b) The next step is Development of the conceptual model.
   A real system can be very complex. It often depends on the quality of the details wanted or needed for the description.
   A too detailed descriptions of the system are actually hard to interpret and therefore may be useless or inapplicable for the ultimate purpose of evaluation and choice. In addition, excessive scrupulousness in representation is often the cause of excessive computational costs or even not manageable by the technologies available for the project.
   Therefore, of particular interest is the identification of the best compromise between the information added and the benefits that are derived from it.
   Citing J. Bear [4]: *The art of modelling is to simplify the description of the system and its behaviour to a degree that will be useful for the purpose of planning and making management decisions in specific cases.*
   Since the model is a simplification of the real system, its uniqueness does not exist. The conceptual model should introduce a series of hypotheses that reduce the real domain and make easier the problem by obtaining simplified versions that must be satisfactory to the ultimate goal of the modelling.

Usually the hypotheses refer to:

- The dimensionality of the model (e.g. two or three dimensions)
- The domain in which parameters can be searched.
- The behaviour of the system over time (e.g. stationary or transient).
- The characteristics of the porous medium; the main ones are the homogeneity, the isotropicity and the deformability of the materials that compose it.
- The phases of the flows in terms of number, interactions and changing state.
- The chemical species present, and if necessary, the reactions that occur between them.
- The properties of the materials present (density, viscosity, porosity, etc.).
- The transport mechanisms and the extensive quantities transported.
- The flow regimes that develop in the system.
- The thermo-fluid dynamic conditions
- The discretization if it is present
- The presence of sources or sinks
- The initial and the boundary conditions.

The choice of the appropriate model depends on the objective(s) of the assessment, in order to ensure that sufficient information is obtained to make decisions. [4]

c) Finally, considering the resources available by including the accessible data for model validation is fundamental. The degree of detail is constrained by computational resources (computer power) and requires more experience in modelling and the use of more sophisticated codes.

Remember that: if the model is oversimplified. It is not possible to get the required information, instead an under-simplification could lead to not having enough data for calibration; ultimately inappropriate or inadequate assumptions would lead to a bad representation of the real system. [4]

The established conceptual model must be converted into a mathematical model.

The development of a continuous mathematical model provides the definition of geometry and domain boundaries, the equations that link the extensive quantities, the equations that relate the extensive quantities and the flows and the constitutive equations that define the behaviour of particular phases and of the chemical species involved. The number of equations needed to define the problem in sufficient detail varies according to the assumptions applied to each individual case. If present, the terms of accumulation and source must be defined, and finally the initial conditions (in the case of transient) and the boundary conditions must be included so to have a well-posed mathematical problem.

It is possible that the heterogeneity of the system does not allow to identify an adequate elementary volume, so it is necessary to apply lumped parameters model.

In ground flow analysis the Darcy's law can be applied due to the very low speed of the flux. It is used to model, in a simplified manner, the transport of the two extensive properties: mass of a fluid phase and momentum. (section 2.1.1.)

To pass from the microscopic scale to the macroscopic scale, various storage coefficients and quantities are used. Permeability and dispersivity of a phase are examples of coefficients that express the macroscopic effects of the microscopic configuration of the

boundaries between a considered phase and all other phases present in a representative elementary volume (REV). For further information [1]

The analytical solution is the fastest way and the preferred-one. But unfortunately, usually the analytical solution is not applicable.

More than fifty years of prior research in this area has led to some understanding in terms of how subsurface flow processes can be modelled adequately with numerical simulation technology. State-of-the-art simulators employ numerical methods that can take advantage of multiple processors, distributed memory computer architectures, adaptive grid refinement strategies, and iterative techniques with linear complexity [4].

Once the code has been produced, to be declared ready for the use it must undergo an appropriate verification procedure. The way to verify the accuracy is to compare, if available, the solution obtained with the analytical solution; the analytical solution is usually available only for specific and simple geometry. [5] Where analytical solution cannot be obtained, the results are compared with the ones obtained with other simulation codes.

The whole model validation is usually combined with the model calibration. [4] The only way to validate a model is to compare its results, that describe the phenomena, with a laboratory experiment conducted in a controlled environment.

The goal of model verification and model validation is to understand if the code has the following characteristic:

- Accuracy: the model must represent as faithfully as possible the process, e.g. it must be able to represent the multi-phase flows in the sandstone core.
- Robustness: the model must be able to find a correct solution for all the possible input values.
- Stability: the model returns a small variation in results at the imposition of a small variation in the inputs.

2.2.3 Model calibration and parameter estimation.

In this phase the numerical values are assigned to all the coefficients (e.g. permeability, transmissivity, storativity). The activity of identifying the coefficients is called 'invers problem' or 'parameter estimation problem'. [4] To obtain these coefficients for a specific domain, it is necessary to investigate the domain itself.

The combination of the model validation activity with the estimation of the parameters of a specific system is called 'calibration'. These two activities are actually performed simultaneously.

Historical data are analysed to identify the information related to the initial conditions of the system and the reactions of the system in terms of temporal and spatial distributions of state variables, caused by possible excitations that may be useful for the estimation process (e.g. pumping , natural replenishment, introduction of contaminants, or changes in boundary conditions).

Trial-and-error approach: trial coefficients values are assumed, and the model's response is derived; this response is then compared with the observed data. The ideally correct

values of the coefficients are those that would make the model solution and the observed data identical. However, since the model is a simplification of reality, these are not expected to be identical; the aim is therefore to obtain them as similar as possible.

When at a reserve scale it is not possible to obtain sufficient information suitable for the determination of the coefficients, laboratory experiments are carried out with the specific aim of acquiring enough data for the application in an inverse problem, usually on soil cores. The experiments create specific situations during which it is possible to observe the state variables and with the aim of obtaining a model solution.

The upper and lower limits of the domain of each single parameter are obtained from: (1) literature if they are already evaluated. (2) specific analyses aimed at understanding the parameter itself. (3) information on typical values. (4) mathematical reasoning.

In addition coefficients and parameters can also come from:

- Literature survey (careful! Because even when belonging to the same class in some standard classification, seldom behave identically. Values found in the literature may be employed as first estimates [4])
- Laboratory experiments. They are usually carried out on relatively small samples (cores), and not always under undisturbed conditions.
- Small scale field experiments: pumping tests, slug tests, etc., as well as specially designed tests.

2.2.4 Sensitivity analysis

The sensitivity analysis, in the modelling context, is a tool used by the modeller to assess the impact of the input parameters uncertainty on the results predicted by the model. The objective of the analysis is to assess how sensitive are the predicted values to the variations of the model coefficients. Briefly, the influence that a variation of one of the input parameters has on the model output is evaluated. If this variation is significative, the parameter must be determined with a low uncertainty. Usually, in order to reduce the uncertainty of a parameter, it is necessary to invest more resources dedicated to acquiring more and more reliable data [4]. During the calibration phase 5.2.3., to evaluate the relative importance of a parameter uncertainty it must be assessed its influence on the residual error. The residual error is the output of the model (during the calibration process) and it is defined as the sum of the square of the difference between the measured values and the values obtained using the model. If a small variation of a parameter causes a large increase in the residual error, it is possible to say that the error is sensitive to that parameter. If, on the other hand, it causes only a small variation of the residual errors the calibration process is defined insensitive to that parameter and typically it is harder to calibrate it. When the calibration is insensitive to a certain parameter, it indicates that the acquired information on that parameter are of low quality and it implies a large quantity of data to improve the results.

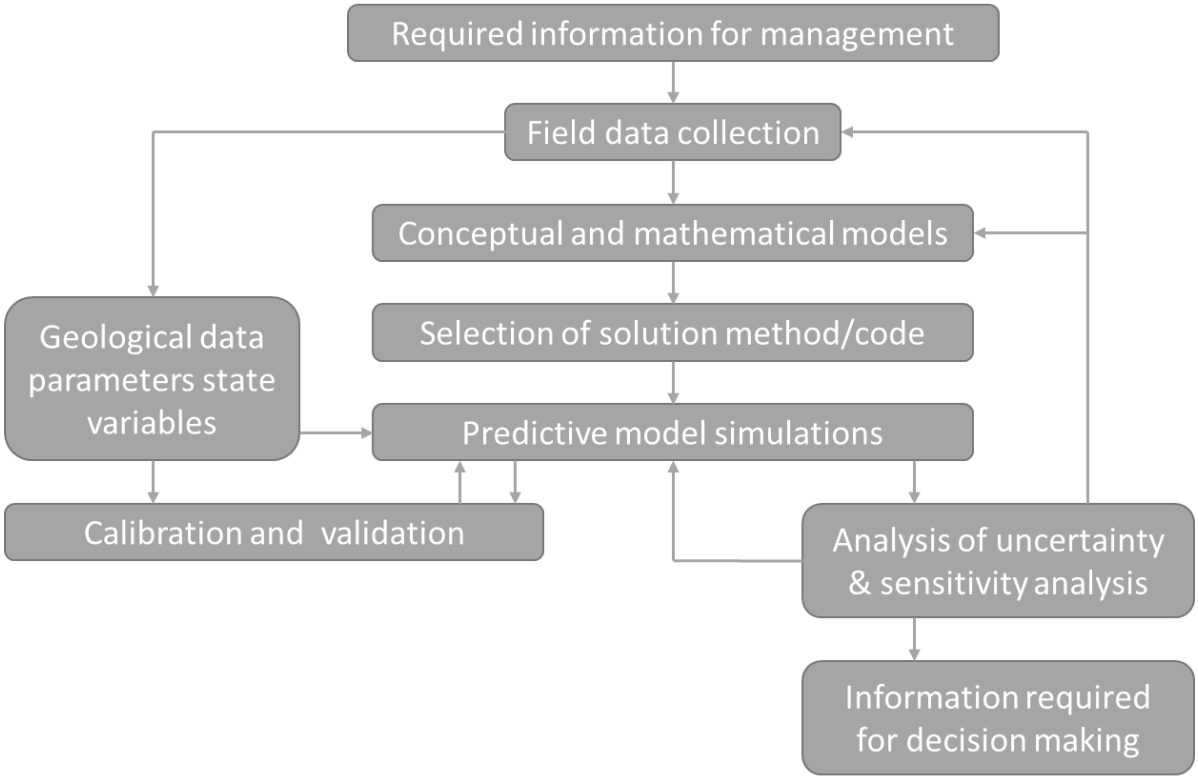

Figure 9: flow chart of the modelling process of a system with flows through a porous medium – Source: [4]

2.3 INVERSE PROBLEM

Numerical models for the simulation of flow and solute transport have been used by hydrologists and petroleum engineers ever since computers became widely available. However, simulated results will be accurate if, and only if, the computer model is close to the real system, at least with regards to the simulated variables, that are the output of the model. There are three types of requirements for the model to be close to the real system in terms of output. First, the model should include all the processes relevant to the simulation. Second, the structure of the model should resemble that of the real system. And third, the values assigned to the variables controlling the processes are similar to their real counterparts [6].

The modelling process is based on three main concepts: process identification, model structure identification and parameter estimation (aspect already treated in the subchapter 2.2).

Traditionally the inverse problem has been defined as the estimation of parameter from the measurement of the output [6].

2.3.1 Problem statement

The following discussion is a reworked and simplifies derivation of the inverse problem referring to a typical example of ground water problem from the detailed version proposed by Carrera (1988) [6].

The following example will refer to a flow and transport of a single non reacting specie:

- ground water flow equation:

$$\boldsymbol{\nabla} \cdot \left(\underline{\mathbf{k}} \cdot \boldsymbol{\nabla} \mathrm{h}\right) + \mathrm{f} = \mathrm{S_s} \frac{\partial \mathrm{h}}{\partial \mathrm{t}} \tag{2.17}$$

  Where $\underline{\mathbf{k}}$ is the permeability tensor (see chapter 2.1 for a more detailed definition), h is the hydraulic head, f represents the internal sink and sources and S_s is the specific storativity. The flow equation is subjected to initial condition $h = h_0$ in the spatial domain of the system and along the boundary it is subjected to

$$\underline{\mathbf{k}} \cdot \boldsymbol{\nabla} \mathrm{h} \cdot \mathbf{n} = \alpha(\mathrm{H} - \mathrm{h}) + \mathrm{q_b} \tag{2.18}$$

  in which **n** is the unit vector normal to the boundary, H is prescribed head on the boundary, q_b is the flux through the boundary, α is the weight of type of boundary condition.

- Transport equation:

$$\boldsymbol{\nabla} \cdot \left(\phi \underline{\mathbf{D}} \boldsymbol{\nabla} \mathrm{c} - \mathrm{q c_a}\right) + \mathrm{f_s} = \frac{\phi\, \partial \mathrm{c}}{\partial \mathrm{t}} \tag{2.19}$$

  where ϕ is the porosity, $\underline{\mathbf{D}}$ is the dispersion tensor, c is the concentration, $c_a$is the concentration do internal source, q is the Darcy's velocity and f_s is the sink source term. The transport equation is subjected to the initial conditions $c = c_0$ in the spatial domain of the system, and along the boundary

$$\left(\phi \underline{\mathbf{D}} \boldsymbol{\nabla} \mathrm{c} - \mathrm{q c}\right) \cdot \mathbf{n} = -\beta(\mathrm{c} - \mathrm{C}) + \mathrm{G} \tag{2.20}$$

  in which **n** is the unit vector normal to the boundary, C is prescribed concentration on the boundary, G is the internal and boundary solute source, β is the weight of type of boundary condition.

In order to be able to find the solution of the flow and transport equation is necessary to determine the parameters $\underline{\mathbf{k}}$, s_s, q, H, q_b, α, $\underline{\mathbf{D}}$, ϕ, C_a, β, C and G over the whole domain including the boundary. Those just mentioned are called physical parameters. The solution of the transport and flow equation is obtained numerically, it is also needed to know the parameters values over the sub regions in which the system is discretised. Those sub regions are called cells element or voxel (3D).

The number of parameters to be determine, thanks to the discretization, is not anymore infinite as in a continuous domain but it may remain a high number. So, it is of interest to express the discrete value of the parameters as function of as few variables as possible. This process is called 'parametrization'. The latter mentioned variables are called model

parameters. The reduction of the model parameters, in addition to simplify the problem understanding, increase the stability.

Parametrization is a problem by itself. Generally, the parameters reduction is performed using correlations that relate a parameter to some of the others (even all if it is possible). Alternative methods are [7]:

- Zonation: all the parameters of the model are determined univocally in a sub-domains(zones) in which the domain is subdivided. This method is appreciated for its simplicity.
- Finite elements: the parameter is determined using a polynomial relationship with the same parameters of the other nodal point of which the grid is formed, (its generalization is called spline)
- Kriging: it is the best linear unbiased estimation method. It is a parameter linear interpolation of a discrete set of point of the same parameter. The weights are estimated with the kriging method.
- Discretization: is the case in which all the discrete values of physical parameters are taken as model parameters.

Referring to the example problem, an implicit scheme can be set for the flow and transport equation obtaining a non-differential equation function of the model parameters and the prior information (in the flow equation example the head measurement). It can now be stated the inverse problem. Using the prior information obtained by a measurement campaign (in the flow equation example the head measurement), the parameters are modified in order to find the best match between the computed model output (the head estimation) and the measurements. Different formulation to inverse problem can be obtained depending on the nature of the measurement and the prior information.

It is common in literature [6] to find the classification of the inverse problem as: direct or indirect approach.

The indirect approach consist of seeks the minimum of the residual; referring to the example followed so far:

$$\epsilon_h = h_m - h_m^* \tag{2.21}$$

where the ϵ_h is the head residual, h_m is the computed head at measurement point, h_m^* is the measured head. Usually to minimize the objective function, let say $J(\epsilon, \dots)$, that lead to a sort of minimum ϵ_h.

On the other hand, the direct approach treats the parameter to be estimated as unknown and substitute the known measurement in the equation. The problem can be solved directly in a non-iterative manner. This method quickly leads to a solution, but it has a limited applicability at the problems that had e number of unknown parameters minors of the measurements. The main problem of this approach is that the solution is generally unstable.

2.3.2 Ill-posedness

A well-posed mathematical problem must respect the following characteristics: a solution must exist, it must be unique and a small variation on the data do not lead to large variation on the solution (stability). The inverse problem may fail to satisfy one or more of the just mentioned conditions.

An inverse problem solution is unique if do not exist more than one set of parameters that satisfy the condition to be the solution. It is possible, for some formulation, that more than one set of parameters satisfy the solution. One common example is the presence of plateau in a neighbourhood of the minimum of the objective function. The parameter is called non-identifiable because the model output is not sensible to it. It means that the result will be obtained regardless the value assigned to that parameter. The situation where all the parameters are identifiable but the solution is not unique is called discrete non-uniqueness.

The need to distinguish between non-identifiability and discrete non-uniqueness arises because the latter condition cannot be ever assessed.

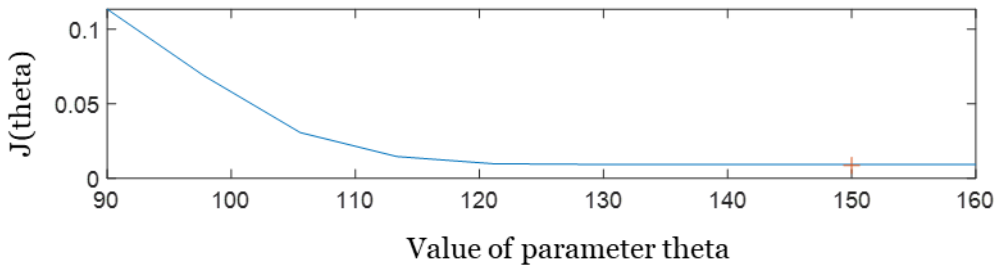

Figure 10:Example of a non-identifiable parameter, graph taken from the results of sensitivity analysis (appendix B)

In the picture is reported a plateau in the objective function and in red it is reported the real solution. All the values of the parameter reported in the graph greater than 120 satisfy the condition to be the solution.

Instability slow down the convergence rate of the iterative algorithm. It also may lead to stop the optimization algorithm at different solution characterized by local minima. There exist in literature many methods with the purpose of improve the stability. Some of them try to restrict the upper and lower limit to reduce the oscillations, while some others use smoothness criteria. The application of those methods is related to the parameters' prior information owned by the modeller. It must be considered that the greater is the number of model parameters the higher is the instability of the objective function. Many methods Aimed at increasing the stability of the model are reported or mentioned in Carrera 1988 [6].

2.3.3 Direct and indirect approaches

It is first briefly treated the direct approach.

If the head measurements are known in all the relevant points, the example's flow and momentum equation viewed in section 2.3.1. are first order partial differential equations. So, with the appropriate boundary conditions the problem can be solved analytically. The

first attempts to solve the invers problem has used these approaches in the early '60 [6]. But it has been faced the problem of instability in estimating the system parameters. This problem has led to the reduction of the dimension of the parameters space. And successively it has driven to no longer solve the problem exactly but rather to minimize some function of the residual equation.

In order to solve directly the inverse problem introduced as example in section 2.3.1. it is necessary to obtain the hydraulic head values at all nodes for each time step. Therefore, it could be necessary to interpolate the existing measures onto the nodes. The most used methods are:

- Hand contouring. It is the most intuitive method and it also allows to include subjective information.
- Spline interpolation and polynomial fitting, those methods gives smoothness in the variable interpolated.
- Kriging, it includes statistical considerations of the error introduced by interpolation.

Once to each node has been assigned a head value the objective function must be optimized in order to find the wanted parameters. In literature are present many different objective function [6]. When one of these objective functions is optimized, the residual parameters are somehow minimized as a result of the optimization. Usually objective functions, together with residues expressed in some form, may also contain prior information and other helpful tips.

The main problem of the direct method to solve the inverse problem is the instability. Possible solutions to instability have been already mentioned in section 2.3.2. Due to the just mentioned problem the direct approach is not frequently used, so in the thesis it is not treated in detail.

The basic idea behind the indirect approach is significatively different from that of the direct-one. In the indirect method the residuals to minimize are the ones referred to the difference between the measured and the computed values (in the followed example the hydraulic head). It is common to set relationship that contains non-linear components; in these cases, the indirect approach is right because it is iterative by nature.

In literature exist many indirect methods apt to minimize the residual:

- Empirical methods. The solution, obtained iteratively as for all the indirect methods, is found changing the parameter at every iteration using some empirical rule. Some of the methods modify the parameters in order to obtain a gradient equal to the measured-one.
- Extended Kalman filter. In this method the classical Kalman filter is used including both estimated values and model parameters. For further detail Wilson et al. 1978 [8] .
- Minimization of the objective function. It is the most used method to solve the inverse problem. It consists in defining an objective function that express in some way how much the results simulated (in the example the head values) differ from the measured values. It is intuitive that the smaller the objective function value, the better model representation of the system.

There exist many objective functions in literature, all of them can be written in general form as:

$$J = J_h + \lambda_p J_p \tag{2.22}$$

where the subscript h is referred to the head value (measured and simulated), the subscript p refers to parameters and λ_p is the weight given to the regularization term.
So, $J_h = (\mathbf{h} - \mathbf{h}^*)^\top \underline{\mathbf{W_h}} (\mathbf{h} - \mathbf{h}^*)$ is called model match, and $J_p = (\mathbf{p} - \mathbf{p}^*)^\top \underline{\mathbf{W_p}} (\mathbf{p} - \mathbf{p}^*)$ is called regularization term with **h** and **h*** that are vectors that contains all the nodal values (in the example head) , **p** and **p*** that are vectors that contain all the parameters, $\mathbf{W_h}$ and $\underline{\mathbf{W_p}}$ that are weighting matrices.
If no prior information is available and $\mathbf{W_h}$ is the identity matrix, the objective function become the square of the difference of the residual of h. It means that the problem reduces at the classical least square method, that consists in minimizing the function:

$$J_h = \sum_i^{n_{nodes}} (h_i - h_i^*)^2 \tag{2.23}$$

The choice of the values of $\underline{\mathbf{W_h}}$ and $\underline{\mathbf{W_p}}$ affect the relevance of the parameters, the ill-posedness and the convergence of the problem. Also λ_p is relevant. Namely, on one hand if the regularization term is present the instability may be mitigated, but on the other hand if its importance is too high the prior information may have a too small significance.
The problem, however, become the minimization of the objective function. In literature exists many methods. The most famous are the Gauss-Newton and the Gradient methods. More recently the artificial intelligence and advanced simulations have allowed the application of new algorithms simplifying the minimization process. The main problem of the gradient method is the evaluation of the derivate of the objective function. It may not be easy to be evaluated or even impossible. On the other hand, Gauss-Newton method do not require the evaluation of the derivate, but it has large computational cost. Many of the artificial intelligence methods do not require the evaluation of the derivate. The latter have introduced many other advantages in term of computational cost, applicability, evaluation time and stability (see chapter 2.4).

The measurements are affected by errors. Remember that the objective of the inverse problem is not only to find the minimum of the residuals, but it is to obtain meaningful parameters. Joining the last two statements, the statistical formulation of the inverse problem is naturally explained. Most of the statistical approach are based on:

- least square regression
- Bayesian inference
- maximum likelihood estimation

2.3.3.1 Weighted least squares estimation:

This method has been largely used and a very detailed information of it is available in literature [6]. The method consists in minimizing the function

$$J = J_h + \lambda_p J_p \tag{2.24}$$

where the model match component (J_h) is evaluated to filter outs the measurement error and the regularization term (J_p) is used to mitigate the instability problems. In absence of prior information, the reliability of parameter estimated can be measured by the approximate covariance matrix define as:

$$\mathbf{c}_p = \frac{J_h}{N - m}(\underline{\mathbf{J}}^\top \underline{\mathbf{J}})^{-1} \tag{2.25}$$

where N is the number of observations, m is the number of parameters, J_h is the sum squared residual (eq. 2.23), and $\underline{\mathbf{J}}$ is the Jacobian matrix $\underline{\mathbf{J}} = \partial \mathbf{h_m} / \partial \mathbf{p}$ ($\mathbf{h_m}$ is the vector of measured head). $\underline{\mathbf{J}}$ expresses the real covariance only if the assumption on linearity between the model parameter is respected. Usually this relation is nonlinear, however the covariance tends to be larger.

2.3.3.2 Bayesian estimation:

It is defined the vector $\boldsymbol{\beta}$ that contains all the parameters of the model and the, eventually present, statistical parameters. Jointly it is defined the vector $\mathbf{Z}$ that contains all the measured variables (i.e. heads and parameters observable). The method assumes that a probability distribution function $f = f(\boldsymbol{\beta}, \mathbf{Z})$ can represent jointly $\boldsymbol{\beta}$ and $\mathbf{Z}$. Applying the Bayes theorem it is It is possible to obtain the posterior probability as $f(\boldsymbol{\beta}/\mathbf{Z})$. Two approaches are now possible to solve the Bayesian estimation: (1) minimizing the conditional Bayes risk which requires the definition of a loss function. (2) Maximum a posteriori method whose goal is the maximization of $f(\boldsymbol{\beta}/\mathbf{Z})$ leading to the most probable parameter.

It is reasonable to assume that prior errors follow a gaussian probability distribution function (p.d.f.) with zero mean. It is also rational take them as independent in space. Thanks to the just explained statements it is possible to justify the use of a Gaussian p.d.f to represent jointly head and model parameters. If the latter are linearly related, the maximum posteriori and the Bayes risk with a quadratic loss function lead to a formulation of the form:

$$J = (\mathbf{h} - \mathbf{h}^*)^\top \underline{\mathbf{W_h}} (\mathbf{h} - \mathbf{h}^*) + \lambda_p (\mathbf{p} - \mathbf{p}^*)^\top \underline{\mathbf{W_p}} (\mathbf{p} - \mathbf{p}^*) \tag{2.26}$$

where $\underline{\mathbf{W_h}}$ and $\underline{\mathbf{W_p}}$ are the inverse of the covariance matrices respectively of measurement and prior information. In practices the Bayesian estimation allowed to naturally incorporate the prior information. It is possible to notice that the method is similar to the last square estimation because they are basically based on the same hypotesis of linearity and normal p.d.f. of the errors. Those last two hypotesis are the critical aspect of the two just mentioned methods.

2.3.3.3 Maximum likelihood estimation:

The meaning of the word likelihood is similar to the meaning of the word probability. In inverse problems, the probability allows to predict an outcome based on parameters. Oppositely, the likelihood enables to estimate the unknown parameter starting from the outcome.

The likelihood under some hypothesis regarding the value of $\boldsymbol{\beta}$ given $\mathbf{Z}$ and a specific model structure is defined as proportional to $f(\mathbf{Z}/\boldsymbol{\beta})$. The latter is the probability density that $\mathbf{Z}$ (observed) are estimated starting form parameters of the vector $\boldsymbol{\beta}$. The likelihood can be used to compare two sets of parameters. Practically the set of parameters $\boldsymbol{\beta}_i$ that gives a greater likelihood are the ones that give a better estimation of the observed value. To directly compare two sets of parameters is commonly used the likelihood ratio, which is defined as: $L(\boldsymbol{\beta}_1/\mathbf{Z})/L(\boldsymbol{\beta}_2/\mathbf{Z})$. It means that the maximum of the likelihood function is given by the set of parameters that estimates the head values that are most similar to the measured.

The main pros of likelihood method are:

- The objective is not to find the set of parameters that make the model able to reproduce the system exactly. The parameters selected as the solution are called most likely. This make natural to think about a criterion to compare the validity of different models.
- The approach is deterministic because it considers $\boldsymbol{\beta}$ as unknown but fixed, differently form the Bayesian that consider it randomly. This view allows to include prior information about parameter values based on their p.d.f. in a simple and strategic manner.

Usually the optimization algorithms are designed to minimize the function. So, in practical applications it is not maximized the likelihood but it is minimized minus the logarithm of the likelihood (also called negative log likelihood NLL). Under the assumption of Gaussian distribution of prior's errors is possible to obtain a formulation similar to the general form of the objective function already mentioned. Formally:

Applying the Bayes theorem, the likelihood is proportional to the probability to having observed $\mathbf{Z}$ giving $\boldsymbol{\beta}$.

$$L(\boldsymbol{\beta}/\mathbf{Z}) \propto f(\mathbf{Z}/\boldsymbol{\beta}) \tag{2.27}$$

Remembering the assumption of Gaussian distribution of prior's errors,

$$f(\mathbf{Z}/\boldsymbol{\beta}) = \frac{1}{\sqrt{(2\pi)^N |\underline{\mathbf{C}}_z|}} \exp\left[\frac{1}{2}(\mathbf{Z}-\mathbf{z})^T \underline{\mathbf{C}}_z^{-1}(\mathbf{Z}-\mathbf{z})\right] \tag{2.28}$$

where $\mathbf{z}$ is the estimated vector with $\boldsymbol{\beta}$, N is the sum of number of measurements (N_h) and number of model parameters (N_p) and $\underline{\mathbf{C}}_z$ is the covariance matrix of prior errors.

$$\underline{\mathbf{C}}_z = \begin{bmatrix} \mathbf{C_h} & 0 \\ 0 & \mathbf{C_p} \end{bmatrix} \tag{2.29}$$

So, the negative log likelihood is

$$\mathrm{NLL} = -2\ln[\mathrm{L}(\boldsymbol{\beta}/\mathbf{Z})] \tag{2.30}$$

$$\begin{aligned}\mathrm{NLL} = (\mathbf{h}^* - \mathbf{h})^{\mathrm{T}}\underline{\mathbf{C}}_{\mathrm{h}}^{-1}(\mathbf{h}^* - \mathbf{h}) + (\mathbf{P}^* - \mathbf{P})^{\mathrm{T}}\underline{\mathbf{C}}_{\mathrm{p}}^{-1}(\mathbf{P}^* - \mathbf{P}) + \ln|\mathbf{V_h}| \\ + \ln|\mathbf{V}_{\mathrm{p}}| + \mathrm{N_h}\ln\sigma_{\mathrm{h}}^2 + \mathrm{N_p}\ln\sigma_{\mathrm{p}}^2 + (\mathrm{N_h} + \mathrm{N_p})\ln 2\pi\end{aligned} \tag{2.31}$$

if σ_h^2 and σ_p^2 are constant NLL reduces to the general form of the objective function (eq. 2.24). It remains to be determined the relative weight of the prior information. It is equal to $\lambda_{\mathrm{p}} = \frac{\sigma_{\mathrm{h}}^2}{\sigma_{\mathrm{p}}^2}$. This approach penalizes the component with the grater variance. If a component has a greater variance, it means that the values are more distributed and so the measurement errors are larger. In literature are available other criteria to determine lambda [6].

2.3.4 Inverse problem issues

The main problem is the ill-posedness (see section 2.3.2). To eliminate this problem a necessary condition (not sufficient) is to acquire good data in term of quantity and quality. It means not only with a small measurement error but also in the right location and with a proper timing of sampling. The measurements have to provide as much information as possible about the relevant features of the system. One possible example could be the use of a higher sampling frequency during the main part of the transition and a lower frequency during the final stabilization. It is also relevant to have more observed values where they are more sensitive to the model parameters. There is various information in literature about the criteria to individuate the best number and location of sampling. The objectives remain to guarantee the uniqueness and to improve the stability.

Another important problem is the model structure identification. Which refers to the definition of the system conceptualization in terms of model parameters. It includes the geometry definition, the boundary condition identification and setting, the parametrization scheme and the parameters correlation etc. An example is when the number of parameters become too large that the problem becomes unstable. In order to mitigate the problem of structure identification there exists basically three methods. The first consist in selecting the model structure that reduces as much as possible the residual on the measured quantity maintaining the stability. In order to be able to achieve this goal, the inverse problem is solved using the least square error approach. Hence, the quality of the set of parameters is expressed by the sum of the squared errors between the model's estimated values and the measured values and by the covariance of the estimated parameters. The first is used for evaluating the model performance and the second is used to assess the degree of stability. In literature are available methods that allow to combine the information of covariance with the ones given by the residual and to automatically individuate the best parameterization [6]. The cons of this method are that the lest square errors method does not include prior's information. The second method consist of a discrimination procedure. It compares, on statistical base, pairs of models privileging the simplest model that is consistent with the available data. The third is the comparing approach. It defines criteria to compare different models. The idea is that using just the likelihood function for evaluating the model, the number of parameters may be too high

leading to an instable condition. Below are reported some examples of quantitative evaluation criteria:

- (Akaike. 1974 [9]) This method combines linearly the value obtained by the negative log likelihood with the number of parameters (M). The model that has the lowest AIC value is the best. In this way are preferred the models, which, in addition to minimize the function, are composed by the smaller number of parameters.

$$\mathrm{AIC}(\boldsymbol{\beta}/\mathbf{Z}) = \mathrm{NLL}(\boldsymbol{\beta}/\mathbf{Z}) + 2\mathrm{M} \tag{2.32}$$

- Similarly in (Akaike, 1977 [10]) has been proposed an updated evaluation criterion. The only difference with the previous method is the weight given to the number of parameters (M) component. The weight is proportional to the natural logarithm of the number of available data(N).

$$BIC(\boldsymbol{\beta}/\mathbf{Z}) = NLL(\boldsymbol{\beta}/\mathbf{Z}) + M\ln\, N \tag{2.33}$$

- (Kashyap, 1982 [11]) propose a further update that introduce in the 'quality criterion' the covariance matrix ($\underline{\boldsymbol{\Sigma}}$). The covariance matrix, as already explained above, include information about the degree of stability.

$$KIC(\boldsymbol{\beta}/\mathbf{Z}) = NLL(\boldsymbol{\beta}/\mathbf{Z}) + M\ln\,(N/2\pi) - \ln\,|\underline{\boldsymbol{\Sigma}}| \tag{2.34}$$

All the just reported criteria privilege the models defined by the lower number of parameters (M). The idea is to maintain the model as simple as possible. It means that all the relevant processes and characteristics of the system must be represented requiring the least number of parameters. In some papers it is called the parsimony principle [12].

A too complex model may perfectly represent the measured data, but it does not mean that the model is perfect. The data ever contains some measurement errors. It means that a too accurate data estimation will include a model of the measurement error. So, it is not representing just the system. [7]

2.4 OPTIMIZATION ALGORITHM

One of the main parts of the inverse problem is the detection of the parameters of the system. It can be resolved through optimization. As mentioned in the previous chapters, the original problem is transformed into an equivalent function minimization or maximization problem. The mathematical property of the objective function heavily influences the difficulty to solve the problem. There exist some rare cases where the optimization problem may be resolved analytically. Unfortunately, it is not common. Usually the optimization problem searches the solution for complex system that are modelled as function of many parameters. The latter observation implies that the optimal solution is searched in large multi-dimensional spaces that further complicate the problem. Fortunately, the current computer technology allows the solution of such complex optimization processes thanks to smart algorithm procedure. Using computers as means to solve optimization problems, the solution obtained is an approximate numerical solution [13].

Nowadays many optimization algorithms are available. These algorithms can have very different characteristics, which lead to very different mathematical properties. These properties are exploited in specific applications depending on the type of optimization problem to be solved. Historically, algorithms have been developed that take advantage of the differentiability of the objective function. The most famous between these methods is the gradient descendent [14] [15].

Unfortunately, these types of problems are often characterized by discontinuity, by lack of analytical representability of the objective function and by the presence of noises. Due to the above-mentioned problems, the applicability of classical methods such as gradient descent is limited. It is therefore necessary to develop different methods. The most obvious attempt is that of random sampling in space. It is evident, however, that this method loses its effectiveness when the domain of the optimal of the objective function becomes more complicated and the dimensions increase.

Inspired by some simple natural phenomena, able to bring the natural system in a sort of optimum condition, new algorithms have been developed. The historically most famous algorithms inspired by natural phenomena, are the evolutionary algorithms. The evolutionary algorithms are based on Darwinian biological evolutionary theory. It is based on the combination of the properties of a population by crossing the characteristics of the individuals with the objective of obtaining a new population in which the individuals with a lower performance are eliminated. The basic idea is to maintain and combine the best features and discard the worst ones. Following this principle, a series of algorithms, called evolutionary algorithms, have been developed. The most famous among these are the genetic algorithm and the differential evolution algorithm (widely used during the thesis). Nature has inspired researchers not only by looking at the world of genetics. In fact, algorithms based on the macroscopic behaviour of organized social groups have been developed. The most common examples are those of hierarchical organization of groups of animals such as flocks of birds, schools of fish and groups of insects such as bees or ants. These examples are interesting because these groups of animals are able to achieve objectives without an organised decision-making structure. The dynamics of these systems have been studied and modelled in a simplified manner. Exploiting the similarity with particle physics and using the probability theory and the stochastic processes, it was possible to understand and study the basic theory. This category of algorithms is called ‘swarm intelligence’. [16]

2.4.1 History

The history of evolutionary algorithms has very ancient origins. About 5 centuries B.C. Pythagoras has claimed 'the principles of mathematics were the principles of all things'. This principle hypothesize that it is possible to represent anything through a mathematical model. Even the principle of optimization of mathematical abstractions has very ancient origins. In fact, it is attributed to Euclid a few centuries after Pythagoras. The optimization was applied, among other things, by Euclid, for the determination of the minimum length between a point and a circumference and other geometry’s problems. A central concept of optimization is algebra which consists of studying of rules to manipulate mathematical symbols. Algebra is credited to the Persian mathematician al-Khwārizmī (790-850CE). In addition, algebra introduce Arabic numerals including zero. The word algorithm is derived from the Latin translation of the pronunciation of the name al-Khwārizmī.

The next steps to arrive at today's definition of optimisation problem introduced in the 17th century:

- The definition of coordinates for a multidimensional space introduced by René Descartes.
- The use of derivatives for the identification of the optimum introduced by Pierrede Fermat.
- the concept of 'calculus', namely the continuous change introduced by Gottfried Wilhelm Leibniz and Sir Isaac Newton

The first numerical algorithms have been developed since the second half of the twentieth century with the appearance of the first electronic computers. Thanks to them it has become possible to apply the optimization to a larger variety of problems. It has been firstly presented a formulation for linear programming and the algorithms to solve them. Later on, more and more efficient algorithms have been presented. Further developments lead to the definition of dynamic programming, which consists in reducing a complex problem into simpler sub-problems. The acquired experience has led to increasingly complex engineering and large-scale modelling. In addition to this, systems based on artificial intelligence have been recently designed. The potential of artificial intelligence systems has been amply demonstrated. Some curious examples in chronological order are:

- In 1996 IBM's Deep Blue has beaten the then world chess champion by optimizing its moves by evaluating millions of possible scenarios.
- In 2011 IBM's Watson has played Jeopardy! and it has won, against the champion in charge, the highest prize, optimizing his answers using probabilistic inference of 200 million pages of acquired data.
- In 2017 Google's AlphaGo has beaten the world champion of Go. The system has used artificial neural networks with millions of parameters to optimize combined information from observing matches between humans and self-generated for learning.

For a more detailed version of the history refers to (X.-S.Yang 2010 [17])

2.4.2 Basics optimization problem setting and critical points

A general example of optimization consists in the determination of the vector $\mathbf{x}$ that as input to the function $F(\mathbf{x})$ that returns the minimum value of the function. $\mathbf{x}$ is a designed point belonging to the domain χ; it is a vector composed by a number of component equal to the dimension of the domain in which the solution is searched. Every component refers to a designed variable and all the coordinates combined indicate a single point in the n-dimensional space.

$$\mathbf{x} = [x_1, x_2, \cdots, x_i, \dots, x_n] \tag{2.35}$$

where the x_i is the i-th designed variable of the objective function $F(\mathbf{x})$. The elements of the vector $\mathbf{x}$ are adjusted to minimize $F(\mathbf{x})$. Any value of $\mathbf{x}$ in the domain χ that minimize the objective function is called solution or minimizer.

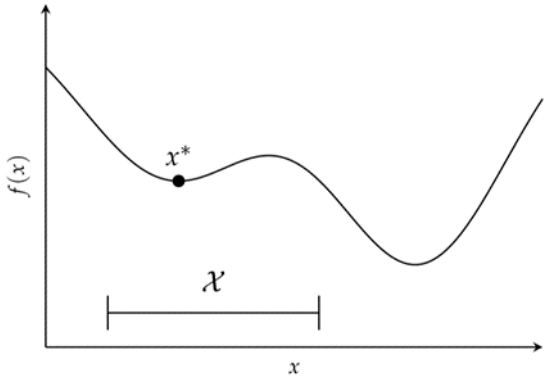

Figure 11:Mono-dimensional example of solution identified within the domain - Source: [16]

Many problems are constrained. By combining all constraints, the domain χ where the solution can be found is defined. Typically, the constraints are expressed as upper and/or lower limit for a i-th variable x_i. There are also constraints for some combinations of parameters that further reduce the objective function domain. It speeds up the convergence rate. A simple two-dimensional domain is reported:

Minimize

$$f(x_1, x_2), \tag{2.36}$$

subjected to

$$x_1 \geq 0$$
$$x_2 \geq 0$$
$$x_1 + x_2 \leq 1$$

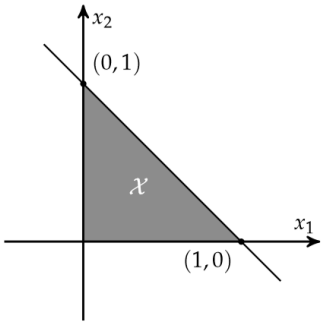

Figure 12:example of limits imposed in a two-dimensional space - Source : [16]

It is extremely important to determine the limits. On one hand if the limit is too restrictive it is possible that the real solution is excluded, on the other hand if the limit is too large the convergence rate reduces. It is responsibility of the modeller to find a domain as small as possible without excluding any possible solution. He must choose the limits based on the information derived from the literature, so according to the physics of the problem. It is common that limits are imposed following intuition, which is one of the main causes of error in setting an optimization problem [16].

Usually the objective of an optimization problem is to determine the global minimum of the objective function. It could happen that the optimization algorithm is deceived by some characteristics of the objective function and determines as a solution a point that is not the real solution of the problem. Usually these critical points are characterized by a derivate equal to zero. Unfortunately, it is generally hard to determine if a point is really the global minimum of an objective function. The first check that is done is to ascertain if the point is a local minimum.

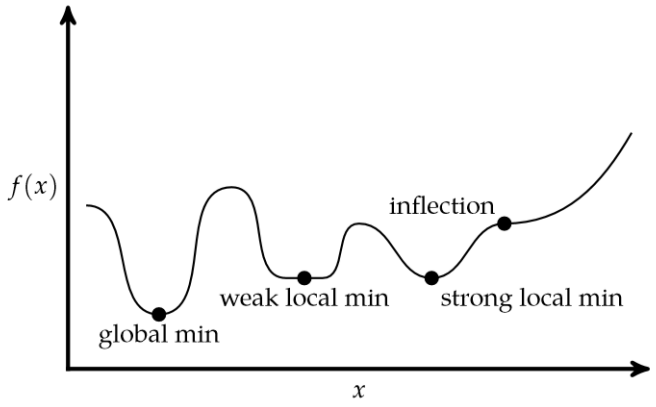

Figure 13:two-dimensional example containing some critical points - Source: [16]

The figure shows some of the most common critical points that can mislead the optimization algorithm. A strong local minimizer is a point that minimizes the objective function f($\mathbf{x}^*$) with respect to a neighbourhood. Formally **x*** is a strong local minimizer if exist a $\delta > 0$ such that f($\mathbf{x}^*$) < f($\mathbf{x}$) for every $x^* \neq x$ in a neighbourhood defined as $\| \mathbf{x} - \mathbf{x}^* \| < \delta$ (the definition is expressed in general form for a multivariate problem). The derivative of the objective function equal to zero often characterizes both the local minimum and the global minimum. Having a zero derivative is a necessary condition to have a minimum point for a continuous and derivable objective function, but it is not a sufficient condition because a point of inflection has derived equal to zero but is not a minimum (global or local). For non-derivative and non-continuous functions there may be local minima that do not have the first derivative equal to zero. In the first case the derivative does not exist, so it cannot be equal to zero, in the second case it is possible that the minimum point corresponds to a discontinuity point and therefore its first derivative could be different to zero. A discontinuity may be given by a boundary condition as shown in the example below or for a zonal definition of the objective function.

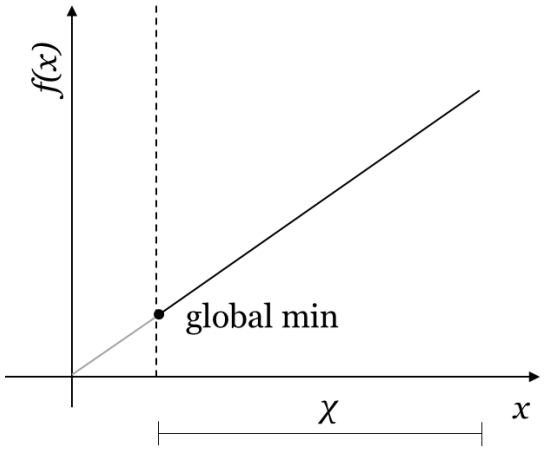

Figure 14:univariate example of point of minimum within the domain with derivative different from zero - Source: [16]

2.4.3 Methods overview

In this paragraph the five categories into which optimization methods are usually divided [16] are presented in a generic way. These categories are:

- First-order methods
- Second-order methods
- Direct method
- Stochastic methods
- Population methods

Below there is a brief description of the most famous categories and algorithms. Some of these algorithms will also be covered extensively in later chapters.

First-order methods are methods that use the first order approximation, first derivative or gradient, of the objective function to detect a direction towards the minimum of the objective function. The most famous methods that belong to this category are:

- The gradient descendent that detects the direction to go to the minimum using the gradient of the objective function veiled at a specific point. The convergence takes place in steps. The direction as previously mentioned is that of the gradient and the step with which the assessments move can vary and is set in various ways. The method continues to evaluate new points of the objective function following the method just explained until it reaches convergence in the nearest local minimum. (A detailed explanation of the method is given in the chapter 2.4.4)
- The conjugate gradient is a gradient descendent based method. It seldom self-adjusts the direction when it reaches narrow valleys where the gradient descendent perform poorly.

There are several methods in the literature that are derived from the above-mentioned methods which accelerate the convergence rate and/or increase their robustness. For a complete discussion of the above methods and several optimized methods examples please refer to chapter 5 of Algorithm for Optimization book [16].

Second-order methods use a second-order approximation utilizing second-order derivate or Hessian matrix (in the case of multi-varied analysis) to direct the search. This method makes possible to combine the information present in a first-order derivative with that obtained from a second-order derivative. The most famous methods are:

- Newton's method that uses second-order information, weighing it appropriately, to quickly converge to the local minimum. Specifically, the information derived from the second order derivative of the objective function is used to determine the length of the step to be applied to a method similar to the descending gradient.
- The secant method and the quasi-Newton method which are approximations of the just described Newton method. In these methods the second order information is not directly needed. This feature makes these methods more attractive in cases where the calculation of the second derivative is complex.

Direct methods do not require objective function derivative evaluation. In fact, these methods are also called zero order, black box, or derivative free methods. The direct methods are able to direct themselves toward the local minimum and to identify whether the observed point is the minimum without any derivative information. The most famous methods are:

- Cyclic coordinate search which optimizes one coordinate at a time by applying a linear research.
- Powell's model. It, similarly to Cyclic coordinate, searches for the optimum in one direction at a time, but in this case the directions do not have to be orthogonal to each other and are optimized according to the characteristics of the objective function. It is done to achieve faster convergence [18].
- Hooke-Jeeves. It evaluates the objective function at an equal distance, usually small, in all coordinate directions from a given point. The point that has a lower value is chosen as starting point to repeat the search in all directions in a similar way to the one already done. If none of the valued points has a lower value than the centre points, the distance of the evaluation is restricted [19].
- Generalized Pattern Search. The idea is similar to that of the just seen method, the main difference is that in this algorithm the search is not made along the main coordinates but follow a pattern defined by the modeller [20].
- Nelder-Mead simplex. it is similar to the Hooke-Jeeves method, but instead of evaluating the objective function equidistantly from a centre in the directions of the main coordinates, the objective function is evaluated at the vertices of a simplex built around this point. The vertex with the minimum value is taken as the new centre point for the next iteration. The skewness of the triangle and its dimensions are customized by the modeller.

Stochastic methods use strategic randomization sampling to explore the space in which the minimum is located. The concept of random motion can be useful to avoid getting stuck in local minima and to achieve the global minimum. Pseudo-random number generators are used to ensure repeatability. A completely random process would be useless because it would not be possible to use information previously acquired randomly, making the optimization process very slow. Below are reported some optimization methods that exploit the concept of randomness:

- The Noisy Descent method is an updating of the gradient descendent method. It adds a random component to avoid the stuck in local minima. Specifically, when the point of the next iteration is evaluated, a Gaussian noise is added:

$$\mathbf{x}^{(k+1)} \leftarrow \mathbf{x}^{(k)} + \alpha \mathbf{g}^{(k)} + \mathbf{e}^{(k)} \tag{2.37}$$

  where α is the step $\mathbf{g}$ is the gradient vector, $\mathbf{e}$ is the gaussian noise and k is the iteration number [21].
- Mesh Adaptive Direct Search. This method is a modification of the Generalized Pattern Search. The difference between the two methods is that in the second method the point pattern in which the function is evaluated is selected through a random process. The point random selection process may vary depending on the type of problem.
- the Simulated Annealing method is inspired by metallurgical processes in which the temperature gradually decreases. The degree of stochasticity gradually decreases as the temperature decreases during a cooling process characterized by a good thermal inertia. The sampling is similar to the previous method. The difference is that in this method stochasticity decreases as explained.
- Cross-Entropy Method. This the method consists in the definition of a probability distribution with its parameters (momentum of 1st, 2nd, ... order). The points at which the objective function is evaluated are randomly sampled following the just defined distribution. The parameters of the distribution are modified to fit the best results of the objective function. The procedure is repeated until the minimum of

the objective function is obtained. This method is particularly effective for objective functions with many local minima.
- Similarly to the cross-entropy methods, the natural evolution and covariance matrix method exist. All of these methods have the objective of identifying the best distribution for the type of optimization. They differ from the previous method in the way they identify the fitting. These methods are often more robust than the Cross-Entropy Method [16].

The population methods, differently from all the methods previously seen, instead of having only one point moving towards the objective, exploit a population of points whose objective function is evaluated at each iteration. The points that form a population are called individuals. The evaluation of many individuals scattered in the space for each iteration avoids to getting stuck in local minima. The information acquired by the individuals at each iteration is shared among the individuals in order to globally optimize the objective function. Many of the methods have stochastic bases. In addition, it is often possible to parallelize the evaluations during each iteration because the individuals are independent from each other.

Population methods require the definition of an initial population which is a set of points distributed in space that will be evaluated during the first iteration. The initial population must be well distributed throughout space in order to increase the probability of identifying the best region. There are several methods in the literature for the determination of the initial population. The most trivial method consists in random sampling from a uniform distribution in all the coordinates. There also exist methods that sample the initial population from a normal multi-variated distribution. It is also possible to have information on the objective function that makes possible to create specially selected initial populations. The most popular methods are:

- Genetic algorithm. it takes inspiration from biological evolution. The algorithm is based on the same logical principle of gene conservation in Darwinian evolutionary theory. The idea is to combine genes that have more promising characteristics with the hope of obtaining next generations with better and better characteristics. In population-based methods the chromosomes are represented by the individuals, the characteristics are the values of the objective function and the genes are represented by variables that define the objective function. The various chromosomes are combined and create a new generation. The processes that take place are the crossover process in which the genes of the various chromosomes are combined to obtain the chromosomes of the next generation and the mutation process in which some of the genes are modified. Mutations also allow to explore conditions that are not present in the genes of the initial population, otherwise some areas of space would never be evaluated. Mutations can also help to avoid getting stuck in local minima [22].
- The differential evolution tries to improve all individuals in the population by combining them with other individuals. A simple formula is used for the re-combination. The basic concept is not too far from the one on which the genetic algorithm is based. In this case the combination happens between three components of the population through a crossover process. A complete discussion of the method is reported in the following chapters.
- Particle swarm optimization is a method inspired by the movement of insect swarms or more generically of a group of animals that move together such as fish and birds. Each individual of the population is considered as one of the animals that form the group. The direction that each member of the population takes in

order to bring themselves to the point of optimum depends on: (1) a component of inertia, following the direction of the previous step, (2) the direction of the point in which the particle has detected its best value, a sort of memory of the best visited by itself (3) the direction of the point where the best value of the objective function is obtained among all iterations. A full discussion of this algorithm is also proposed in the following sections.

- The firefly algorithm is inspired by the behaviour of fireflies. Fireflies are attracted to the lights emitted by other insects of their species. The idea behind the algorithm is that the individuals in the population behave like fireflies. They are attracted to the light of the other members of the group. The brighter a component is, the better is the value of its objective function, the more attractive it is to other individuals. So, the other individuals will move towards him more strongly.
- The cuckoo search is a method inspired by the cuckoo's bird behaviour. It is a bird that lays its eggs inside the nests of other birds. The other birds, when they find a foreign egg in their nest, can have three different reactions: (1) they can destroy the foreign egg (2) they can choose to leave in a new nest (3) they can accept the egg and raise it. In case of an optimization problem, the nests are the points where the objective function is evaluated. In case the value of the objective function is good it is considered as if the egg has been accepted and therefore the individual of the population is maintained. Otherwise the remaining options are two: that point is eliminated and will not be part of the population in subsequent evaluations (the egg is destroyed) or other points are created where the evaluation can be carried out, the hosting bird leaves and creates another nest.

Usually population methods are able to avoid getting stuck in local minima. Actually, with these methods it is easy to find the best region. Unfortunately, these methods are not as preforming as the descending methods in local research. Therefore, many hybrid methods have been developed [16]. These techniques are able to combine the characteristics of the various methods. In fact, many extended population methods have been developed and they also show characteristics of the descending methods. The result is a significant increase in performance in local research.

In the following sections some of the presented algorithms are treated in depth. specifically, the gradient descendent method will be treated as it is the most famous algorithm, and two population algorithms that have been used in the workflow for the determination of the parameters.

2.4.4 Gradient descent method

The gradient descent method is a non-linear optimization algorithm. It is realized to find, iteratively, the minimum of a of first order differentiable function. In order to be able to find the local minima of a function a point is sampled in the domain of the objective function. This point is chosen thanks to prior information on the objective function or is sampled randomly. The gradient of the function is evaluated at that point and the next point is identified by moving through the search space in the objective function gradient direction with a defined step. In the new point, the gradient calculation is repeated, and the next point is found in the same way. This operation is repeated until the local minimum or a good approximation of the local minimum is determined. To determine whether a point is a minimum of the objective function, many methods are available in literature. If the point is considered as the minimum, or its proximity, the algorithm is

stopped, otherwise the next point is determined [15]. Below a brief formal mathematical discussion of the algorithm is reported.

It is considered a multi-variable differentiable function $F(\mathbf{x})$. Firstly, a point $\mathbf{x_0}$ is sampled in the domain. The point is chosen randomly or it is imposed by the modeller thanks to prior information that place it in a position that is probably the solution. So $\mathbf{x_1}$, the next iteration point, is determined as:

$$\mathbf{x}_1 = \mathbf{x}_0 - \gamma_0 \nabla F(\mathbf{x}_0) \tag{2.38}$$

The operation is repeated until $\mathbf{x_n}$ is the minimum, or an approximation of it, as:

$$\mathbf{x}_{n+1} = \mathbf{x_n} - \gamma_n \nabla F(\mathbf{x}_n), n \geq 0 \tag{2.39}$$

with γ_i that is the step size that can change at every iteration. One example of step selection is given by the Barzilai–Borwein method [23]:

$$\gamma_n = \frac{|(\mathbf{x_n} - \mathbf{x_{n-1}})^T [\nabla F(\mathbf{x_n}) - \nabla F(\mathbf{x_{n-1}})]|}{\| \nabla F(\mathbf{x_n}) - \nabla F(\mathbf{x_{n-1}}) \|^2} \tag{2.40}$$

Convergence, the identification of a set of parameters as a minimum, can be established as:

$$|\mathbf{x_n} - \mathbf{x_{n-1}}| < \text{small value} \tag{2.41}$$

Or as (or combined with)

$$\nabla F(\mathbf{x}_n) = 0 \tag{2.42}$$

If it is a convergence condition $\boldsymbol{x}_n$ is the solution of the problem otherwise another point $\boldsymbol{x}_{n+1}$ is evaluated.

The last two methods unfortunately do not avoid the problem of critical points presented in section 2.4.2

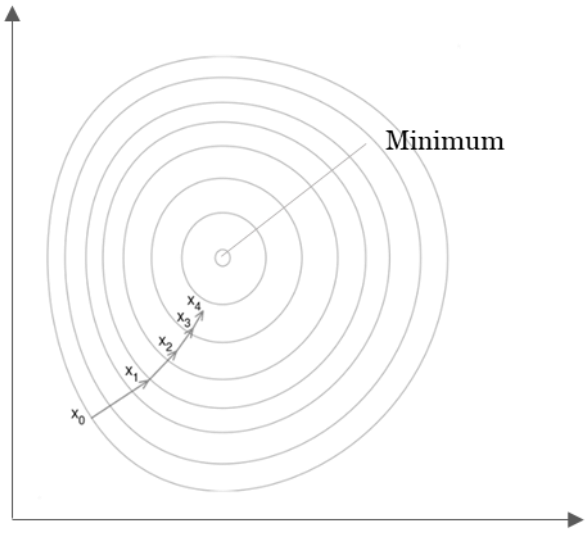

Figure 15: Example of application of the gradient descendent method in a two-dimensional domain, the closed lines represent the isolines of the objective function value - Source: https://en.wikipedia.org/wiki/Gradient_descent

These methods guarantee excellent convergence rates but in practice they are hardly applicable because of the hypothesis on which they are based, e.g. the differentiability of the objective function which is rarely encountered.

2.4.5 Differential evolution

Differential Evolution (D.E.) is a recent algorithm compared to most of the algorithms seen in section 2.4.3.. It is an evolutionary algorithm. It was created with the aim of meeting the main requirements in the field of optimization problems. The algorithm is able to handle non-differentiable, non-linear, and multi-modal objective functions. In addition to being a population method, DE is designed to perform direct stochastic research. Direct research methods have the advantage of being easily applicable to objective functions based on physics. This type of objective functions is therefore those derived from physical experiments. Computers using parallel processors are commonly used, nowadays even mobile devices use parallel processors. It is therefore a fundamental characteristic for an optimization algorithm to be able to carry out calculations in parallel using all the processors. Often the simulations of experiments take minutes or hours; considering that an optimization algorithm must carry out many simulations, the parallel calculation is of fundamental importance. The DE allows to evaluate the components of a population independently using multicore processors. Another property required to an optimization algorithm is the simple setting through a few simple variables to choose. Lastly, an optimization algorithm requires also good convergence properties. Extensive tests are available in the literature with excellent results for DE [24].

As already described, the DE is a direct parallel method of research. Each generation (G) is composed of NP individuals. Given an objective function dependent on D-parameters, the search is conducted in a D-dimensional space, so the parameters are expressed with D-dimensional vectors

$$\mathbf{x}_{i,G}, i = 1,2, \dots, NP \tag{2.43}$$

The number of individuals is equal in each generation. The initial population (G=1) is chosen randomly and must be able to cover the whole space. DE generates a new vector of parameters by adding, in a weighted way, the difference between two vectors, randomly chosen from the existing population, to a third vector. This last operation is the previously described mutation of the evolutionary algorithm. For each vector of the current generation $\mathbf{x}_{i,G}, i = 1,2,3, \dots, NP$, also called target vectors, it is generated a vector

$$\mathbf{v}_{iG+1} = \mathbf{x}_{r_1,G} + F \cdot (\mathbf{x}_{r_2,G} - \mathbf{x}_{r_3,G}) \tag{2.44}$$

Where $r_1, r_2, r_3 \in \{1,2, \dots, NP\}$ are random vector indexes of the current generation and F is a positive weight for the difference of two of three random selected vectors when it summed with the third random vector. r_1, r_2 and r_3 must be different to each other and from the index i of the target vector.

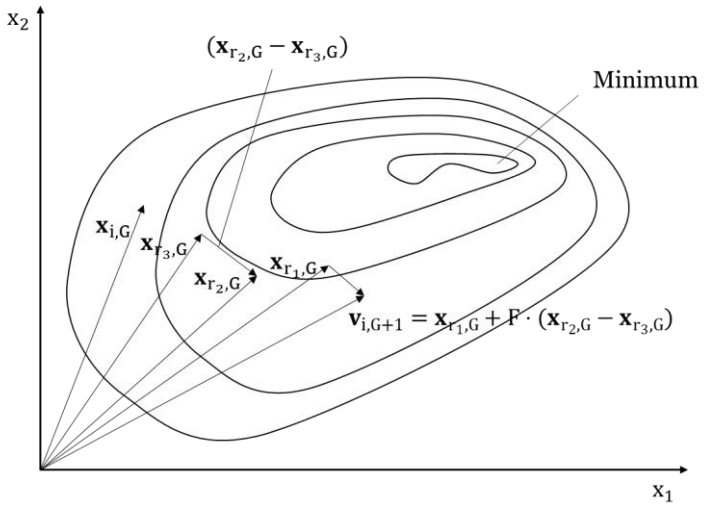

Figure 16: example of application of the differential evolution algorithm in a two-dimensional domain – Source: [24]

The parameters of the mutated vector are then combined with the parameters of the target vector. The mixing of parameters is the crossover operation of the evolutionary algorithms. The crossover operation is carried out to increase the whole diversity of the perturbed parameter vectors. The trial vector is obtained:

$$u_{i,G+1} = (u_{1i,G+1}, u_{2i,G+1}, \dots, u_{Di,G+1}) \tag{2.45}$$

For each parameter, a random value is sampled from a uniform distribution between zero and one. If this value does not exceed the CR parameter imposed by the modeller than the trial vector parameter is equal to the parameter of the mutated vector otherwise the parameter remains equal to the parameter of the target vector. Formally:

$$u_{ji,G+1} = \begin{cases} v_{ji,G+1} & \text{if } (\text{rand b}(j) \leq CR) \\ x_{ji,G} & \text{if } (\text{rand b}(j) > CR) \end{cases} \quad \forall j \mid j = 1,2,\dots,D \tag{2.46}$$

where j is the index of the variable that compose the vectors.

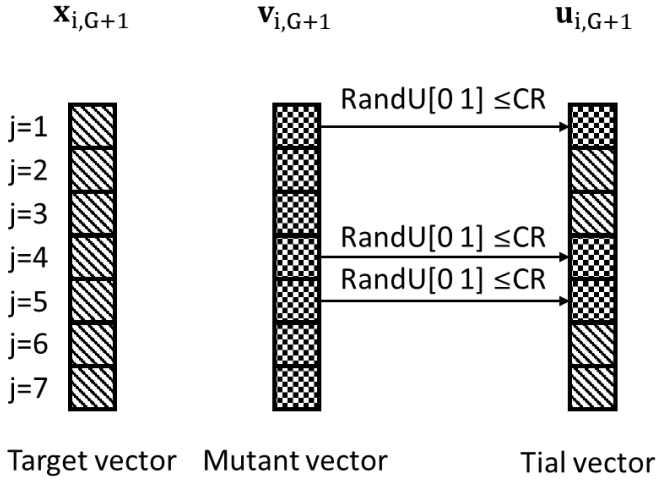

Figure 17: seven-dimensional example of combination of the target vector with the mutant vector. – Source: [24]

Finally, it is evaluated which vector, combination of parameters, allows to obtain the best value of objective function. The vector that returned a better value is kept in the next generation while the other is discarded; in this way the population has always the same number of individuals. This operation is called selection.

The choice of the parameters that characterize the optimization algorithm strongly influences the performance of the algorithm and, sometimes, the identification of the solution of the problem can be compromised. The selection of the number of populations depends strictly on the variables to be determined, and therefore on the size of the research space. For a good space exploration, a recommended value is NP between 5*D and 10*D. For parameter F a value around 0.5 has shown to be a good initial choice [24]. In case of premature convergence by the population it is recommended to increase this parameter. Very small values or values above 1 have shown to be rarely effective. For the Crossover Rate (CR) a very small value of this parameter (e.g. 0.1) shows very good reliability, on the other hand, a CR equal to 0.9, very high, speeds up the convergence rate [24]. The parameter must be selected in an intermediate way to find a good compromise between reliability and convergence rate.

2.4.6 Particle swarm optimization

Particle swarm optimization was discovered by simulating simplified social models. The social models from which it is inspired are those of flocks of birds and schools of fish. The observation and study of these social groups has led to understand the dynamics of social information sharing to coordinate the group movement and provide benefits to the whole group [25]. The primary objective was to simulate the behaviour of a flock of birds. After several development it has been possible to model the flock component in a realistic way if their movement was guided by an objective, in this case a food source. It was easy to understand how the model of the flock was an objective research with exchange of information between particles. The next step is constituted in the simple extension to multi-dimensional problems. The algorithm has shown good properties in optimization problems [25]. The first step of the algorithm is the definition of the initial population. The initial population is composed of a large number of individuals representing the birds of a flock. Given an objective function dependent on D parameters the space in which the optimal is searched is D-dimensional. Each individual is defined by a vector $\mathbf{x}_i$ of D components, each of which represents a coordinate in the D-dimensional space. Each individual is univocally defined by a set of parameters. The initial population must be able to identify the best region so it must be sufficiently large and well distributed. There are several methods to identify the initial population; for example, it can be randomly sampled or evenly distributed throughout space. The first iteration starts with the evaluation of the objective function for all particles $F(\mathbf{x}_i)$. The values obtained are then compared with the stored values and between each other. It is then defined for each point ($\mathbf{x}_i$) if:

- the evaluated value is the best absolute among all iterations and all particles; if it is true the value is stored in memory as best absolute $\mathbf{P}_g$.
- the value is the best ever obtained for that particle; if it is true the value is stored as best personal of the i-th $\mathbf{P}_i$ particle.

The so-called velocity vector is then defined using the information previously acquired. The velocity vector defines the direction and displacement steps of a particle. All particles move. The velocity vector is the weighted sum of three components:

- the inertia component which is the velocity vector of the previous iteration
- the best history value component which is directed towards the historical optimal point of the particle $\mathbf{P}_i$
- the best global component which is directed towards the direction of the absolute optimal $\mathbf{P}_g$.

Lastly, it is summed the velocity vector of the particle with the current position of the particle to obtain the next iteration position.

Formally:

$$\begin{cases} \mathbf{v}_\mathrm{i} = \mathrm{w}\mathbf{v}_\mathrm{i} + \mathrm{c}_1\mathbf{U}(0,1) \otimes (\mathbf{P}_\mathrm{i} - \mathbf{x}_\mathrm{i}) + \mathrm{c}_2\mathbf{U}(0,1) \otimes (\mathbf{P}_\mathrm{g} - \mathbf{x}_\mathrm{i}) \\ \mathbf{x}_\mathrm{i} = \mathbf{x}_\mathrm{i} + \mathbf{v}_\mathrm{i} \end{cases} \tag{2.47}$$

Where w, $\mathrm{c}_1$and c_2 are the weight of the direction relatively of inertia, best history value and best global value and $\mathbf{U}(0,1)$ represent a sample number from a uniform distribution between 0 an 1.

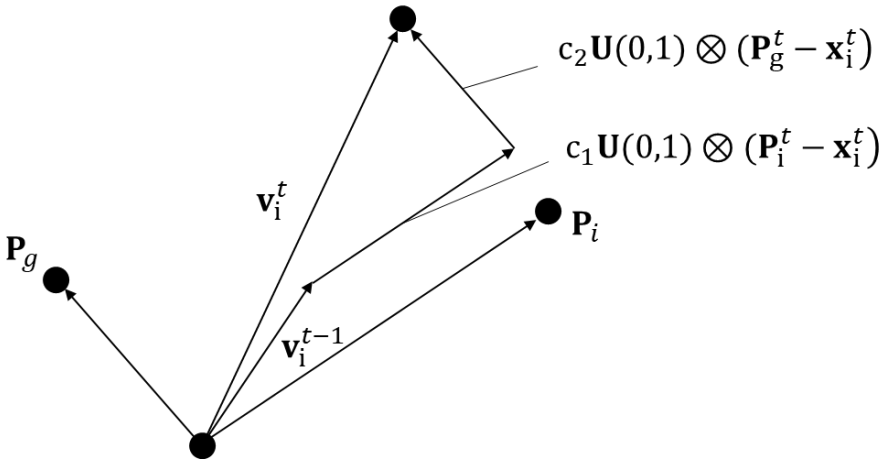

Figure 18: Example of combination of the components to obtain the speed vector – Source: https://medium.com/analytics-vidhya/implementing-particle-swarm-optimization-pso-algorithm-in-python-9efc2eb179a6

The procedure is repeated until a convergence criterion stops the loop and returns an $\mathbf{x}_i$ vector as a minimum point.

The modeller may vary the relative weights of the velocity vector components. Giving too much weight to the global optimum direction may cause the algorithm to fall into a local minimum speeding up too much convergence; on the other hand a too small value may never make the algorithm converge or converge very slowly. In contrast if the other two components are multiplied by a too large coefficient the convergence could be slowed down resulting in a very dispersive behaviour of the swarm. If the just mentioned coefficients value is too small, the best global component becomes very important, returning to the condition of very rapid convergence towards local minima [25].

2.5 HISTORY OF SUBSURFACE FLOW MODEL PARAMETER ESTIMATION

Due to the interest of the topic, in the literature there are several articles dealing with new methods for the determination of parameters characterizing multi-phase flows in sub-surface systems.

The estimation of the reserve model parameters from data is a process that has an ancient history. In the 1960s, Sheldon et al. [26] and Jacquard [27] calibrated flow simulation models manually until they obtained a good correspondence between the real data and the model simulation. These methods were soon abandoned because they were very time-consuming and incompatible with the increasing complexity of the flow simulation models. In 1972 Thomas et. al [28] presented the first automatic attempt to determine the parameters of a flow model in a porous medium; for the first time the problem of parameter determination was considered as an optimization problem. The first optimization attempts used gradient based methods, Monte Carlo methods and Kalman filter-based methods. Later on, Kulkarni [29] and Liu et al. [30] started to consider the determination of the relative permeability and capillary pressure trends as the key aspect in oil production models. This is particularly true when considering multiphase systems where traditional models struggle to accurately find the parameters necessary to determine the trends of the variables of interest. Usually the determination of the relative permeability is obtained from water flooding experiments on core samples [31] and the capillary pressures with other experiments [32] [33]. In 1992 Chardaire-Rivieresd [34] were able to derive relative permeability and capillary pressure by combining pressure drop and saturation (1D). Sun and Mohanty 2005 [35] showed that it is preferable to determine the capillary pressure and the relative permeability simultaneously. They also noted that the increasing complexity of flow simulation models led to abandon the use of gradient-based methods in favour of population methods. Specifically, they used the genetic algorithm for the estimation of the parameters needed for the flow model. In the literature there are many examples of population based method applications to identify the sub surface flow model parameters, such as the particle swarm optimization (PSO) [36] (2009), the ant colony optimization [37](2011) and the differential evolution (DE) [38] (2010). In 2012 Zhang et al. [39] presented a methodology for the simultaneous estimation of relative permeability and capillary pressure. They used power-law models to determine the relative permeability curves in water flooding experiments. They performed a model validation on a synthetic mono-dimensional dataset simulating a water flooding experiment on a core sample.

One of the improvements on which research is active today is the hybridisation of the optimisation algorithms to simplify the determination of the algorithm's parameters. Santhosh et al. [40] have proposed a comparison between the hybrid differential evolution algorithm and the traditional differential evolution applied in the sub-surface flow model parameter estimation. They have determined with high accuracy the parameters of the 3D model of a benchmark reserve using the hybridized method. The methodology that uses a hybrid algorithm has led to results more similar to the exact ones but on the other hand has required a longer calculation time than the traditional algorithm. Another field of active research is the combination of artificial intelligence methods (such as optimization algorithms) with machine learning and artificial neural networks. Ahmadi end Chen in 2018 presented a method able to exploit machine learning to estimate permeability from petro-physical logs. Aliouane et al. presented a method of artificial neural network to detect permeability. The publications that report methodologies for the determination of

permeability that combine artificial neural networks with optimization algorithms [41] [42] are even more recent (2020). The Artificial neural network are multivariate, nonlinear interpolators techniques capable of reconstructing the complex relationship between input (parameters) and output by combining multiple simple functions [43]. One of the main advantages of these methods is that they are able to automatically calibrate the parameters through a training phase based on the available input/output data. On the other hand, the reason why this aspect was not explored in depth during the project is the difficulty of interpreting the physical model that characterizes the phenomena. This feature may lead the inability to capture all the information available from core sample experiments.

3 EXPERIMENT AND MODEL

The ideas on which the project is based are: firstly, to create a synthetic dataset that simulates a real experiment and secondly to create a calibration process able to identify in a reasonable time and with a high accuracy the parameters used to generate the dataset. The model must be able to create a synthetic dataset that simulates a real experiment and must be applicable in the inverse problem. The obtained algorithms must be adaptable for future projects on real datasets. In order to simulate some real experiments carried out by ENI, whose results are available for research purposes, a specific model has been developed by a research group of the Department of Civil and Environmental Engineering of Politecnico di Milano. The model is able to perform calculation and obtain results but is not yet in its final version. In fact, during the whole project several updates and improvements have been made available. This model has been developed using the already existing and open source models of the Matlab MRST toolbox.

3.1 EXPERIMENT ON CORE SAMPLE

The reference experiments for the dataset generation have consisted in the analysis of a cylindrical rock samples, extracted within an oil reserve, into which a fluid has been injected. The experiment has been conducted in a controlled environment. The available information is referred to a specific test. The test has been carried out on a cylindrical rock sample. In the sample has been injected brine from the bottom side and it has been kept the pressure constant in the upper side reproducing a waterflood condition. The synthetic dataset has been generated simulating a condition similar to the experiment.

3.1.1 Materials properties and Testing condition

For the experiment the rock that has been used is a Berea sandstone in which layers has been identified by visual analysis and through more in-depth x-ray analysis. The identified layers are not perpendicular to the axis of the core sample cylinder. The presence of layers indicates that the sample is not isotopic and is non-homogeneous at all the scales. The core has a height of 19.8 centimetres and a diameter of 3.81 centimetres that results in a total volume of 0.226 litres. The porosity has been measured at x-ray and it is 20% resulting in a total pore volume of 45 millilitres.

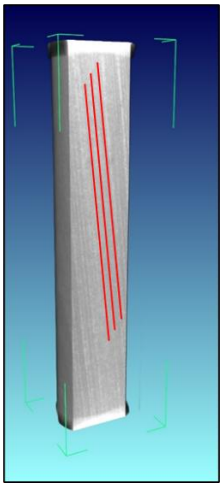

Core properties	
Core	Berea Sandstone
Length (cm)	19.8
Diameter (cm)	3.81
Porosity (%)	20 %
Pore Volume (mL)	45

Figure 19: image of the sample on which the Eni experiment has been carried out. Section of the core sample with diagonal layers clearly visible and highlighted in red. – Source: Eni

Table 1: summary table of core sample properties

The experiment has been conducted in a controlled environment. The temperature has been kept constant and equal to 90°C which is the estimated temperature of the sample extraction point (reservoir temperature). The temperature is higher than the ambient temperature because, often, going deep underground the temperature increases. This phenomenon happens because the reservoir is closer, only slightly, to the hot core of the earth.

The test has consisted in the injection of a constant flow of salty water from the bottom face of the just descripted core sample. The water that has been injected is synthetic sea water with a salt concentration of 40 g/kg. The choice to inject a salty water has been made to simulate conditions similar to the real ones, because in practical cases in the reservoir is injected water already available from the sea or water that come from the reserve and that is extracted with hydrocarbons. Both these waters contain a high concentration of salts. The oil that has been used during the experiment is the one initially found throughout the sample. It is the hydrocarbon contained in the reserve from where the core comes from. The main properties of the fluids that have been used during the experiment are shown in the tables below:

Fluid properties	
SSW Density (g/mL)	0.99
SSW Viscosity (cP)	0.3
Oil Density (g/mL)	0.94
Oil Viscosity (cP)	20

(i)

SSW Composition	
Salt	**Concentration (g/Kg)**
NaCl	28.76
$CaCl_2$	1.35
KCl	1.411
$MgCl_2$	7.130
Na_2SO_4	4.289

(ii)

Table 2: (i) Summary table of the properties of the fluids used in the experiment (SSW synthetic salty water) (ii) Synthetic salty water composition summary table – Source: Eni

The multi-phase flow has been thermographically monitored by x-ray during a transient injection process where the oil, naturally placed inside the sample, has been displaced. X-ray tomography uses x-rays to create a virtual three-dimensional model of the analysed object. The instrument that has been used for the experimentation has a static x-ray generator and a static detector; it is the sample that rotates inside the machine allowing the development of the three-dimensional model. Thanks to this type of analysis it has been possible to obtain the local porosity of each elementary volume in which the geometry has been discretized. These values have been obtained independently from the experiment. Indeed, it has been obtained from a static analysis of the sample. Instead, during the experiment, the average saturation of all the elementary volumes has been evaluated thanks to the images of the inside of the rock obtained by x-ray equipment. The instrumentation has returned a vector containing all the average saturation values inside the voxels for each time step in which the whole experiment has been discretised.

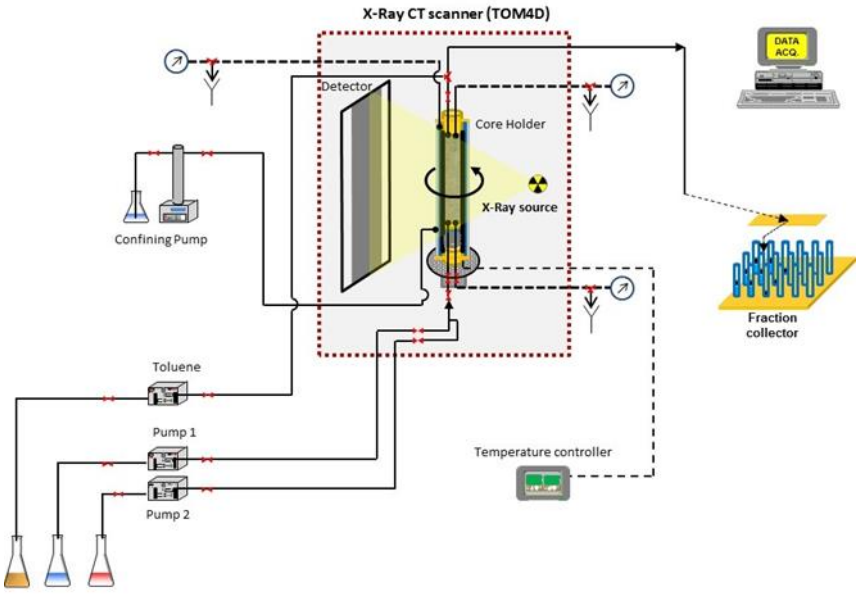

Figure 20: Scheme of the core sample experiment equipment – Source: Eni

The pressure at the outlet of the porous medium is kept constant and equal to the ambient pressure. The difference in pressure between the head and the bottom of the sample has been also constantly measured. This measurement adds information for a possible calibration process, and it can increase its stability if properly used. Finally, the output flow was collected and analysed to assess the amount of oil extracted.

3.2 CORE EXPERIMENT MODELLING

Once the typology and dynamics of the experiment has been understood and analysed, the model has been subjected to a series of preliminary investigations by the research group. The model has been realized to be applicable in the inverse problem in order to identify the parameters of the reserve starting from the results of the experiments. The thesis project is inserted within this macro project and has the purpose to make an inverse problem using a synthetic dataset. Therefore, the model that has been used is the same and it has benefited of all the updates that the research group has made to enhance the inversion properties. Some of the updates that will be encountered in the next chapters have the purpose to consider the dependence between some of the parameters that characterize the model. This upgrade has been aimed to increasing the optimization algorithms stability during the inversion process (even with the synthetic dataset).

The open source MATLAB MRST (MATLAB Reservoir Simulation Toolbox) has been used to create the grid and to perform the simulations. The toolbox has been developed by the Computational Geosciences group in the mathematics and cybernetics department at SINTEF digital. The software includes modules developed externally by research groups at Heriot-Watt University, NTNU, University of Bergen, TNO, and TU Delft. MRST is not primarily a simulator but has been developed as a research tool for rapid prototyping and demonstration of new simulation methods in reservoir simulations [44]. The software offers a wide range of data structures and computational methods that can be combined by the modeler with the aim of creating a customized model of the system that has to be analysed. In the case of the thesis, the core sample grid and model have been realized using MRST functions by the research group and kindly updated and provided to me.

3.2.1 Geometry discretization

To numerically solve a continuum problem, it is necessary to convert the continuum itself into a set of finite points. The determination of points is done by defining a grid of space discretization. The choice of the grid in simple problems is often made a priori because they do not require attention at points where complex phenomena (e.g. turbulent) occur and the geometry is simple. In the case of a simple problem, the grid is just adapted to the geometry of the domain to be discretized. Otherwise, special measures must be taken, e.g. refinements that do not distort too much the elements that compose the grid in the regions of particular interest. For more complex cases there are methods for self-adapting the grid. Unfortunately, even if these methods are well implemented, it is always necessary a verification a posteriori by the modeller. The modeller has the task of checking the quality of the grid and checking that the refining has been carried out accurately and in the correct place. Once the geometry has been discretised, the equations must also be discretized to be solved [45].

There are two approaches to discretize a geometry: (1) unstructured grid and (2) structured grid.

In the first case the grid adapts better to the geometry but introduces more significant discretization errors due to the deformation of the elements of which the grid is composed (cells). Unstructured grids can be hybrid or not. A hybrid grid is a grid that contains elements with different geometry (e.g. composed of tetrahedra and hexahedra). In unstructured meshes it is not easy to make a rational numbering of nodes. However, these grids allow to better reproduce more complex geometries due to their flexibility. For this reason, these grids are the most used for structural calculations. A short approach to this type of mesh has been carried out in the final part of the thesis and is left as a possible development to increase the applicability of the method (Appendix D).

The second type of grid is composed of two families of lines belonging to certain Cartesian or curvilinear coordinate systems. For this type of grid, obtaining a rational numbering of nodes is simple. Most of the studies carried out during the thesis were based on models using Cartesian structured grids.

The simulation of the experiment that has been described above has been carried out using Cartesian structured grids. The grids have been realized with rectangular prismoid cells with rectangular base with different resolutions. In principle, a very fine grid composed of a large number of cells has been created. Since the data provided (saturation and porosity) are regular in space, the basic idea has been to create a grid capable of using one datum per cell. The measuring instrument has used a sufficient resolution to obtain a three-dimensional grid composed of 313992 elements. The grid has been created using the function dedicated to the creation of structured cartesian grids by simply giving as input the number of subdivisions for each side. In order for x, y and z equal to 42 42 and 178 respectively. The MRST function that has been used is `cartGrid(x y z)`. Being the problem non-steady-state, it has been also necessary to perform simulations for each temporal instant. The sampling frequency must be sufficient to characterize the whole phenomenon. This has meant that a very fine grid must be solved at different temporal instants requiring a really high computational cost. Indeed, the realization of a coarser versions of the grid has been one of the proposed updates (it will be discus in the next chapters).

The three-dimensional model created by the measuring instrument has also evaluated the saturation in the areas outside the sample. Therefore, the number of cells used in the simulations is reduced eliminating the void space cells. Immiscible incompressible flow equation and solver

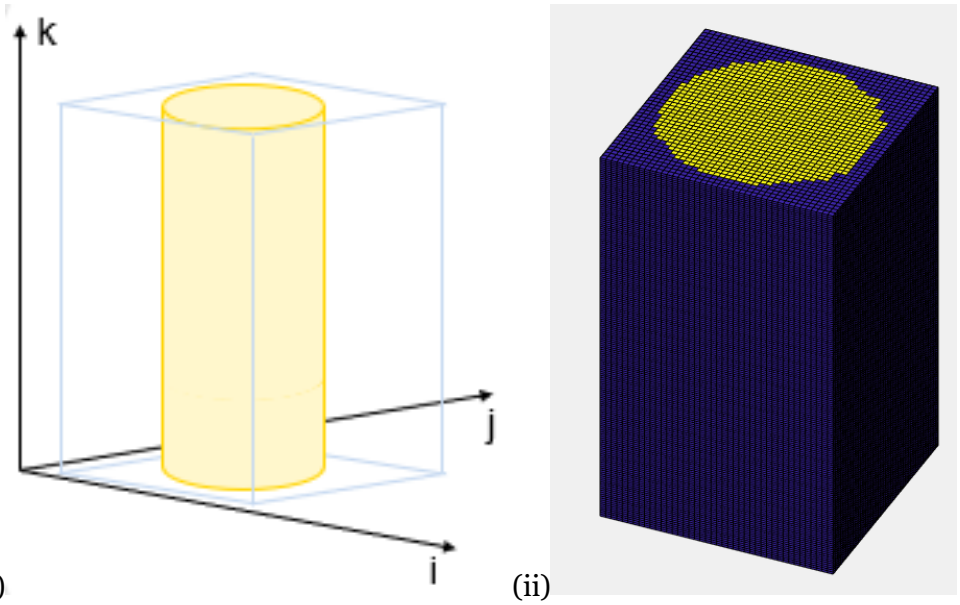

Figure 21: (i) Sampling volume of the instrument with the volume occupied by the sample highlighted, (ii) discretization sampling volume at the measuring points

In hydrocarbon extraction processes, with or without injection, pressure differentials cause the mono or multiphase flow. The motion is characterized by viscous advection. Pressure waves in this type of problems propagate at a speed much higher than the flow rate; this combined with the difficulties of modelling mono and multiphase flows seen in chapter 2.1. make the solution of the problem very complicated. The experiment carried out on the sample simulates an extraction process where a two-phase immiscible flow occurs, so the model is made using the same equations and codes. The developed model is based on the assumption of incompressible fluid, which is a reasonable hypothesis because the problem involves only liquid phases with low velocities (largely sub sonic) and small pressure variations. In addition, the thermodynamic conditions under which the experiment takes place are far above the situation of phase transition.

Having introduced in chapter 2.1 the key phenomena of the immiscible multi-phase flows and the parameters commonly used to describe them, it is possible to develop a mathematical model able to describe the multi-phase flow. The generic equations describing the multi-phase flow have been set resulting in a system with more unknowns than equations. The problem will therefore require constitutive equations that relate the various quantities and the introduction of boundary conditions and source term. The used correlations will be discussed in datil in section 3.2.3

The system of multi-phase flow equations was developed starting from the fundamental principle of mass conservation. The equation of mass conservation for each immiscible phase (α) is:

$$\frac{\partial}{\partial t}(\phi \rho_\alpha S_\alpha) + \boldsymbol{\nabla} \cdot (\rho_\alpha \mathbf{q}_\alpha) = f_\alpha \qquad (3.1)$$

where ϕ is the porosity, ρ_α is the density of the phase, S_α is the saturation, $\mathbf{q}_\alpha$ is the specific flux and f_α includes source and sink terms.

Each phase can contain several chemical species, but it has been considered as if the flow has a single component since there is no species transmission between phases during all the experiment. The main constitutive relationship is the extension of the Darcy's law for multi-phase flows. The equation 2.15 can be extended with the gravity term obtaining:

$$\mathbf{q}_\alpha = -\frac{\underline{\mathbf{k}}k_{r\alpha}}{\mu_\alpha}(\boldsymbol{\nabla} p_\alpha - g\rho_\alpha \boldsymbol{\nabla} z) \tag{3.2}$$

Most of the commercial models calculate an approximate solution by inserting Darcy's law for multiphase flows into equation 3.1 [46]. Functional relationships must also be introduced for capillary pressure and phase pressure with porosity ϕ and density ρ_α.

The fully implicit discretization of the equation 3.1 e 3.2 for the phase (α) are:

$$\frac{(\phi S_\alpha \rho_\alpha)^{n+1} - (\phi S_\alpha \rho_\alpha)^n}{\Delta t^n} + \text{div}\,(\rho \mathbf{q})_\alpha^{n+1} = (f)_\alpha^{n+1} \tag{3.3}$$

$$\mathbf{q}_\alpha^{n+1} = -\frac{\underline{\mathbf{k}}k_{r\alpha}}{\mu_\alpha^{n+1}}[\text{grad}\,(p_\alpha^{n+1}) - g\rho_\alpha^{n+1}\text{grad}\,(z)] \tag{3.4}$$

where p_α is the partial pressure of the phase α (all the other components have been already introduced in the previous chapters). It must be noticed that porosity, saturation and pressure values are expressed for each cell and the fluxes are expressed per face. The script Δt stands for the time step in which the whole process has been discretized. The difficulty in solving the system depends on the coupling between the two equations and the non-linearities that are present in all the other equations.

Discrete differential operators for divergence and gradient must be introduced. They have to represent their continuous counterparts. These discrete operators must be able to incorporate the information about grid geometry. The structure of a grid is composed of face cells and nodes. Each cell is delimited by a set of faces which are limited by the contours which are determined by a pair of nodes. The geometric properties (volume, areas, centroids) have been evaluated for all the objects. The MRST's function `computeGeometry` has been used to automatically evaluate all the properties of the grid objects.

The divergence operator 'div' is a linear mapping from the faces to the cell and it is applied to a discrete flow $\mathbf{q}$ evaluated on the face f. The orientation of the flow is assumed from C1(f) to C2(f) referring to face f according to the table in figure 22. Therefore, the total quantity leaving the cell c is given by the sum of the outgoing flows minus the incoming flows:

$$\text{div}(\mathbf{q})\,[c] = \sum_{f \in F(c)} \mathbf{q}[f]\mathbf{1}_{\{c=C_1(f)\}} - \sum_{f \in F(c)} \mathbf{q}[f]\mathbf{1}_{\{c=C_2(f)\}} \tag{3.5}$$

Where the logical vector $\mathbf{1}_{\{c=C_1(f)\}}$is equal to one if cell c is near face f and it is equal to zero in the other case.

The discrete differential operator grad is defined as:

$$\text{grad}\,(\boldsymbol{p})[f] = \boldsymbol{p}[C_2(f)] - \boldsymbol{p}[C_1(f)] \tag{3.6}$$

It is just the difference of a quantity in the cell centre C1 and C2 adjacent to the face f.

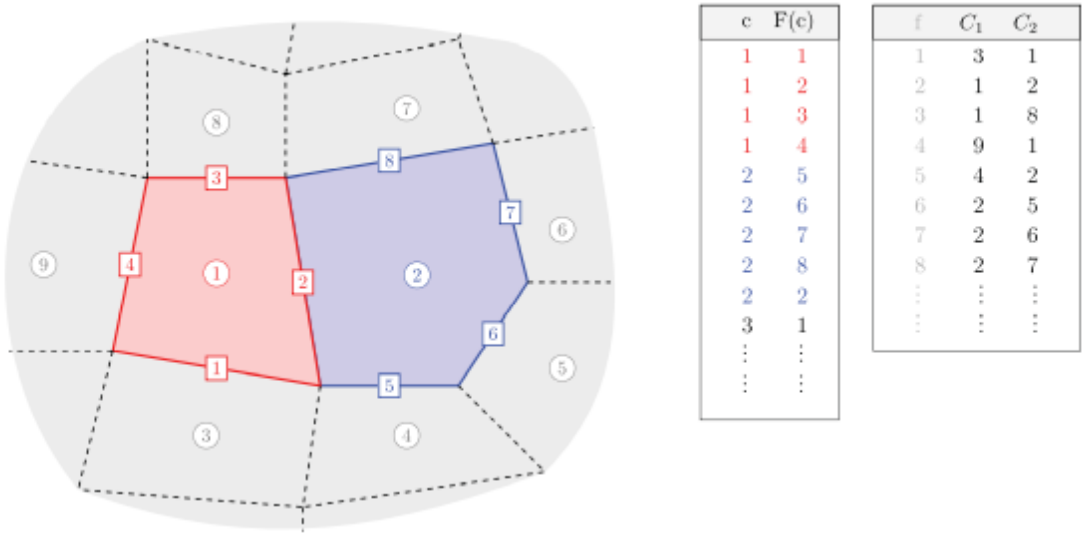

Figure 22 Two-dimensional example of the numbering of grid objects. the circled numbers are the numbers of the cell centroids the squared values belong to the numbering of the faces. On the right are reported the reference tables, where c stands for centroid, F(c) stands for face relative to the centroid.- Source: [46]

In the case of a two-phase immiscible flow, using the previously introduced equation with the notation 'w' for the wetting and 'nw' for non-wetting phase, the system is simplified to:

$$\frac{\partial}{\partial t}(\phi S_w \rho_w) + \nabla \cdot (\rho_w \mathbf{q}_w) = f_w \tag{3.7}$$

$$\frac{\partial}{\partial t}(\phi S_{nw} \rho_{nw}) + \nabla \cdot (\rho_{nw} \mathbf{q}_{nw}) = f_{nw} \tag{3.8}$$

Starting from this formulation of the problem, the missing equations of closures necessary to make the problem well posed and to find a solution will be introduced in the next chapter.

The combination of a sequential solution of the equations with an incompressible model is commonly used in research, since it is able to well represent multi-phase phenomena by returning a model with equations that are easier to analyse and develop. In the standard sequential solution, the system, composed of the mass conservation equations and the extension of Darcy's law for multi-phase flows in a two-phase system, requires the definition of temporal step Δt. Starting from an instant of time t in which the values of s_α, p and $\mathbf{q}$ are known, the solution is evaluated at time $t + \Delta t$. In the first iteration of the solution at time instant $t + \Delta t$,the values $s_\alpha$used is the one of the previous time step (t). In this way all the components in the Darcy's equation remain only a function of the position excluding p_α. Once obtained the solution of the equation 3.4 the values of p_α and $\mathbf{q}$ are updated for the current time step. Then the equation 3.3 is solved keeping constant the values of $\mathbf{q}$ and $p_\alpha$obtaining the new values of s_α at the current time instant. The operation is repeated for the same time step starting from the value of s_α just obtained until convergence is reached. Then it is possible to pass to the next time step. The starting point is usually the initial time (t=0) in which the values of the initial conditions must be provided in order to solve the whole problem. Both equations to solve the problem are solved iteratively because they are implicit. So, within the iterative cycle of the coupled

solution of the time step there are iterative cycles for the solution of the single equations. They are called inner cycles.

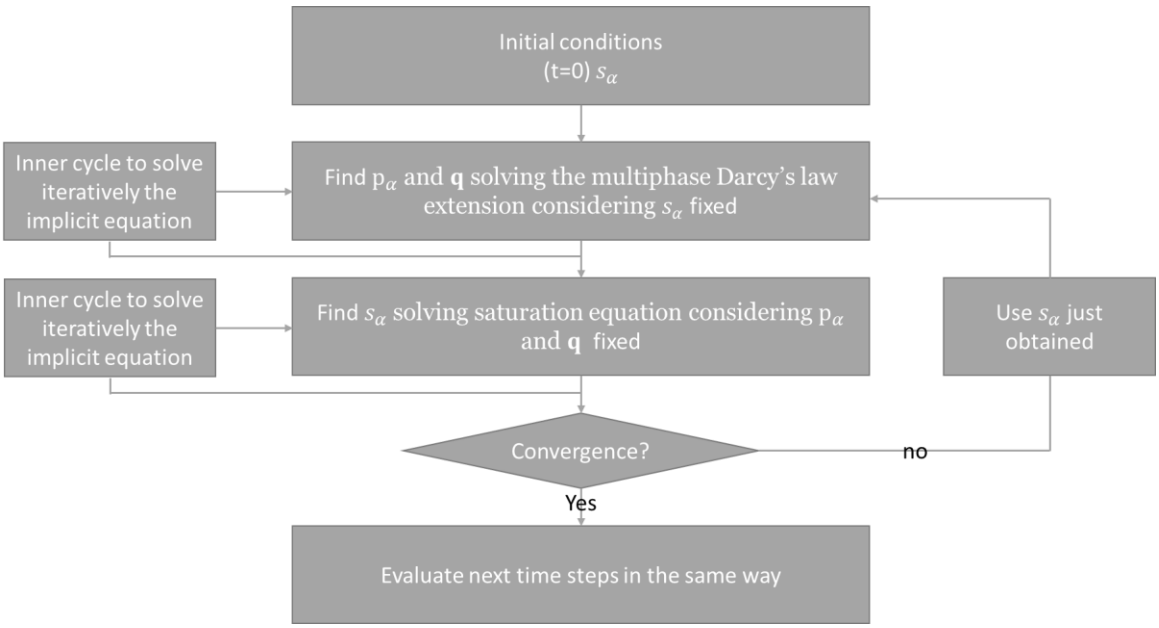

Figure 23: Summary flow chart of the coupled solution of equations (with implicit scheme).

The solution of the problem is implemented in the MRST `implicitTransport` function. It uses an implicit discretization of the transport equation. In space a first-order upstream mobility-weighted discretization and a backward Euler discretization in time are used. The transport equation is solved calling the function '`twophaseJacobian`' to build a function that calculates the residues and the Jacobian matrix; the function '`newtonRaphson2ph`' is used to update the solution during the iterations of the Newton-Raphson algorithm, and it contains logical updates that intervenes in case of non-convergence of the algorithm. The function in input requires:

- The data from the grid that discretize the system in which the evaluation must be performed, i.e. the core sample.
- The final time of the transient interval to be evaluated. The beginning of the calculation is automatically set at t=0 in which the initial conditions are imposed.
- The properties of the rock, i.e. porosity and in the presence of gravity, as in the experiment, the permeability values for each cell.
- The properties of the fluid, i.e. viscosity and density.
- The boundary conditions.

3.2.2 Closure equations

As already anticipated in the previous chapter, in order to obtain a number of equations equal to the number of unknowns, some closure models that relate the quantities and properties that characterize the system must be introduce. In this section are reported the correlations that has been used in the first version of the model.

3.2.2.1 Brooks-Corey model

An important parameter in porous flow problems is the relative permeability. There exist many models in the literature that relate the relative permeability with other reservoir properties [47]. One of the most used models is the Corey model that relates relative permeability to saturation. The Corey model has also been included in the core sample model used in the thesis. Corey [48] has shown that there is a correlation between the relative permeabilities of a two-phase system. Observing the trend of the experimental capillary pressure vs saturation curves and using the already existing equation that links the capillary pressures and relative permeabilities, Corey has shown that there is a correlation between the relative permeability and the saturations of both phases.

$$K_{ro} = \left(\frac{S_o - S_{or}}{1 - S_{or}}\right)^4 \text{ and } K_{rg} = \left[1 - \left(\frac{S_o - S_{or}}{S_m - S_{or}}\right)\right]^2 \left[1 - \left(\frac{S_o - S_{or}}{1 - S_{or}}\right)^2\right] \quad (3.9)$$

The above equations are those derived from Corey and reported in the original paper of 1954 [48]. The equations were developed for a two-phase model composed of gas (g) and oil (o). The equations developed by Corey have been subsequently extended by Brooks and Corey [49] to obtain a "power-law" model used to describe the relative permeabilities of oil, water and gas obtaining:

$$k_{ro} = k_{ro,max}\left(\frac{S_o - S_{or}}{1 - S_{or} - S_{wirr} - S_{gc}}\right)^{N_o} \quad (3.10)$$

$$k_{rw} = k_{rw,max}\left(\frac{S_w - S_{wirr}}{1 - S_{or} - S_{wirr} - S_{gc}}\right)^{N_w} \quad (3.11)$$

$$k_{rg} = k_{rg,max}\left(\frac{S_g - S_{gc}}{1 - S_{or} - S_{wirr} - S_{gc}}\right)^{N_g} \quad (3.12)$$

Only the relative permeability of the water that has been injected and that of the oil already present in the sample are of interest for the model that has been used for the simulations. The thermodynamic conditions of the sample has been far from the bubble point and there hasn't been inert gases in significant quantities in the system, therefore it is possible to simplify the equations by eliminating the gas saturation components because they are constant and equal to zero during the whole experiment. It has been also possible to eliminate the equation that has been used to obtain the relative permeability of gas because it would be useless. So, the equations have been reduced to:

$$k_{rw}(s_w) = k_{rw,max} S_{wn}^{N_w} \quad (3.13)$$

$$k_{ro}(s_w) = k_{ro,max}(1 - S_{nw})^{N_o} \quad (3.14)$$

with

$$S_{wn} = \frac{S_w - S_{wirr}}{1 - S_{wirr} - S_{orw}} \quad (3.15)$$

$$k_{rw,max} = k_{rw}(S_{orw}) \quad (3.16)$$

$$k_{ro,max} = k_{ro}(S_{wirr}) \quad (3.17)$$

where S_{wirr} is the irreducible water saturation (minimum obtainable), S_{orw} is the maximum water saturation obtainable, $k_{rw,max}$ and $k_{ro,max}$ are the maximum relative permeabilities of water and oil, N_w and N_o are constant exponents. The exponents are two parameters to be determined for the specific problem. From the numerous tests present in the literature of Corey's model it is known that N_w and N_o are between 1 and 6 [47]. The other constant parameters present in Corey's model are the maximum relative permeabilities $k_{rw,max}$ and $k_{ro,max}$. They must be determined for every specific case, intuitively their range is between 0 and 1. The figure 8 has been obtained using Corey's model. The parameters have been selected to obtain characteristic trends of rocks with different wettability. The characteristic trends are described in Blunt 2017 [3].

3.2.2.2 Skjaeveland capillary pressure model

The Skjaeveland model is a generic correlation for capillary pressure. This correlation is able to cover a wide range of problems such as primary drainage, primary imbibition, secondary drainage and secondary imbibition and it is also able to consider the hysteresis effects. The applicability of the correlation has been widely demonstrated by Skjaeveland et al. [50] with numerous experimental tests, carried out under different physical conditions and using different materials, or fitting dataset from reserves.

The equation has been developed starting from the correlation of Brooks-Corey [49], mentioned in the previous section, developed for primary drainage in mixed wet rocks. To facilitate its extension the classical expression for water wet media is rewritten as:

$$P_{cd} = \frac{c_{wd}}{\left(\frac{S_w - S_{wirr}}{1 - S_{wR}}\right)^{a_{wd}}} \tag{3.18}$$

where c_{wd} is the entry pressure and $1/a_{wd}$is the pore size distribution index. Since the equation 3.18 is valid for water wet systems, an equal counterpart for oil-wet porous media has been created. In order to represent all the cases that are in the middle of these two extremes, a correlation that is able to represent the intermediate conditions has been created by linearly combining the two equations. It has been obtained a general equation as:

$$P_c = \frac{c_w}{\left(\frac{S_w - S_{wirr}}{1 - S_{wirr}}\right)^{a_w}} + \frac{c_o}{\left(\frac{S_o - S_{or}}{1 - S_{or}}\right)^{a_o}} \tag{3.19}$$

or expressed only as a function of $S_w (S_w = 1 - S_o)$

$$P_c = \frac{c_w}{\left(\frac{S_w - S_{wirr}}{1 - S_{wirr}}\right)^{a_w}} + \frac{c_o}{\left(\frac{1 - S_w - S_{owr}}{1 - S_{orw}}\right)^{a_o}} \tag{3.20}$$

where a_w , a_o , c_w and c_o are constants. The constants just mentioned are different depending on the problem, e.g. in a forced imbibition problem, the coefficients are different from those of a drainage process. The parameters a_w, a_o and C_w are positive parameters while C_o is negative. In the code implementation, the C_o coefficient has also been imposed positive by modifying the equation in order to simplify the post processing procedures and have only positive parameters.

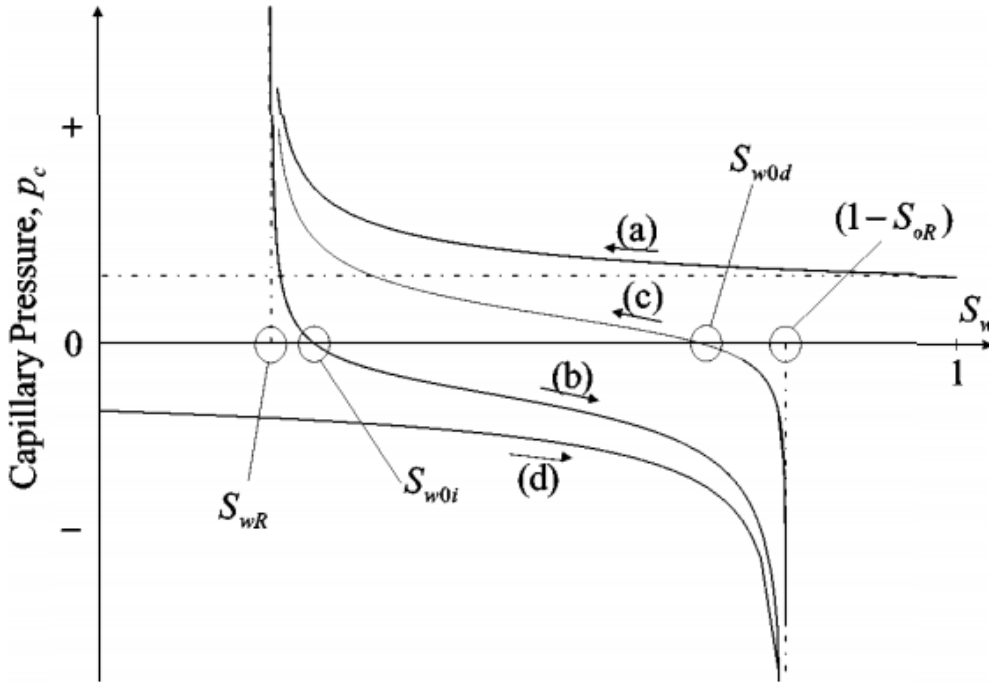

Figure 24:Capillary pressure curves as function of the water saturation for different phenomena – Source: [50]

In figure 24 four characteristic curves that represent the typical trends of the four possible phenomena are represented. The capillary pressure curve (a) represents the primary drainage. During the primary drainage, the saturation goes from $S_w = 1$, which is the initial condition, towards S_{wirr} where the capillary pressure has a positive vertical asymptotic behaviour. This curve is obtained by imposing $C_o = 0$ and C_w equal to the entry pressure (as already presented by Brook and Corey [49]).The curve (d) represents the phenomenon of primary imbibition. The initial conditions start from a water saturation equal to zero which increases as the process progresses. The curve has an asymptotic downward trend for the maximum achievable water saturation. The curves (b) and (c) represent the cases of secondary drainage and secondary imbibition respectively. The drainage process goes from right to left of the graph, while the imbibition goes in reverse. In these two cases all the parameters have to be calibrated for the specific problem. The different wettability conditions make the curve shape vary; specifically, for a more water-wet porous medium, the saturation value in which the capillary pressure (p_c) is equal to zero is closer to the maximum water saturation and C_o tends to 0. It is also evident from the figure 24 how well the concept of hysteresis is represented by the model.

3.2.2.3 Porosity- absolute permeability relationship

Absolute permeability appears within Darcy's law and in previous chapters it has already been explained how knowledge of this parameter is important in order to model oil and water flows within a porous medium.

The determination of permeability usually is done thanks to tests carried out on core samples. Unfortunately, since the core sample represents only a minute part of the entire reserve, it is necessary to use techniques that extend the information acquired in the laboratory to the entire domain of interest. So, this information is integrated with measurements of various types that are often carried out with different instruments in all the domain. In the present case study, the determination of permeability must carry out in the cells with which the core sample has been discretized and therefore all the necessary measurements are available in the entire space. Due to the impossibility of dividing the sample into pieces of the cell size and for each cell to experimentally determine the absolute permeability value, it is necessary to use empirical correlations. Empirical estimates based only on permeability value are based on logarithmic-logarithmic relationships for carbonate rocks, or on logarithmic-linear relationships for sandstone [51].

$$\mathrm{Log}_{10}\, k = m \log_{10} \phi + q \tag{3.21}$$

$$\log_{10} k = m\phi + q \tag{3.22}$$

where m and q are parameters to be calibrate case by case. From the sensitivity analyses of the model that the research group (that has realized the model) has carried out it had been identified how the parameter q is not very significant and a constant value equal to -16 can be imposed without being calibrated.

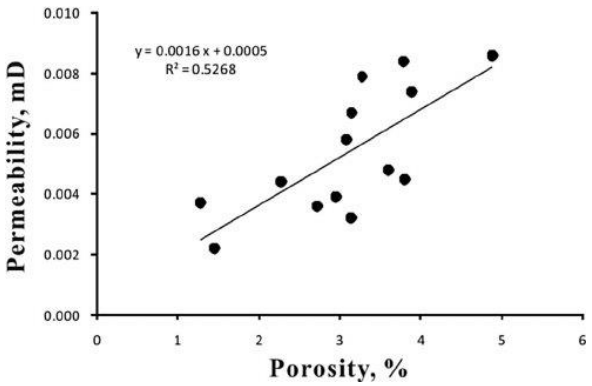

Figure 25: Example of linear relation – Source: [52]

Unfortunately, the correlations linking absolute permeability to porosity are not highly accurate. In the updates that has been proposed during the thesis, it has been proposed a technique to alleviate this problem.

3.3 FORWARD PROBLEM

The first simulations carried out had the objective to practice with the model described in the previous chapter and learn how to treat and understand the output. Then, the model has been set up to represent the drainage experiment conducted by Eni. So, the initial conditions and boundary conditions has been imposed and the temporal discretization was set. Later on, a forward problem was carried out. i.e. a simulation with the parameters imposed by the modeller and the results were displayed and briefly analysed. Finally, some coarser grids have been realized and simulations have been performed to verify if the simulations conducted with those grids were simpler and yet sufficiently accurate.

3.3.1 Boundary and initial conditions

In addition to the closure equations, in order to make the simulation problem a well-posed problem, it has been necessary to impose all the boundary conditions. Since the simulation problem of the experiment has been a non-stationary problem, it has been also necessary to impose some initial conditions from which the model has started to obtain all the solutions of the following time steps.

3.3.1.1 Boundary conditions and porosity

Given the purpose of the experiment to simulate the circumstances of a reserve drainage, the conditions under which the experiment took place have simulated the reserve environment and the injected salty water flow. The boundary conditions of the model were imposed to faithfully represent the conditions imposed during the experiment. The temperature during the test has been kept constant and equal to 90°C which is the temperature of the reserve at the core sample extraction point. It is important to consider the correct temperature because the properties of the fluids are strictly dependent on the thermodynamic conditions. The temperature boundary conditions have not been imposed automatically by the software, but they have been taken into account during the fluid properties estimation. All the properties are reported in the materials section. The fluids, with their properties, have been initialised using the `initSimpleADIFluid` function of the MATLAB MRST toolbox to be used as solver input.

It has been set the ambient pressure at the out-flow point of the sample (the top side). The outflow boundary condition is commonly chosen as constant ambient pressure because imposing different boundary conditions may cause complications, e.g. it may require a continuous flow or pressure measurement which in addition needs a dataset treatment in order to impose the boundary conditions to the model. Moreover, keeping the pressure constant and equal to the ambient pressure during the experiment is technically simple. The entry-flow boundary condition at the bottom side in the core sample has been imposed. A salty water flow of $4.167*10^{-9}$ m3/s has been set. The flow has been kept constant as during the experiment. The flow and the pressure boundary conditions at the lower and upper faces of the sample, discretized with a Cartesian structured grid, has been imposed using the functions `fluxside` and `pside` of the MATLAB MRST toolbox.

	Values	U.o.m.	S.I.	S.I. u.o.m.
Pressure (top side)	ambient		101325	pa
Temperature	90	°C	363,15	K
Perpendicular flux at bottom			4,167	m3/s

Table 3: Boundary condition summary table

The flow boundary condition equal to 0 along the entire lateral surface has been automatically set by the software. The gravity force has also been imposed throughout all the domain to consider the potential energy component within the flow equation.

Finally, the parameter values of porosity have been assigned for each cell. Thanks to the analyses that has been carried out on the sample before the experiment, it has been possible to obtain the porosity field distribution with a resolution sufficient to compute an average value for each voxel. The porosity data have been provided already scaled on the grid presented in section 3.2.1.

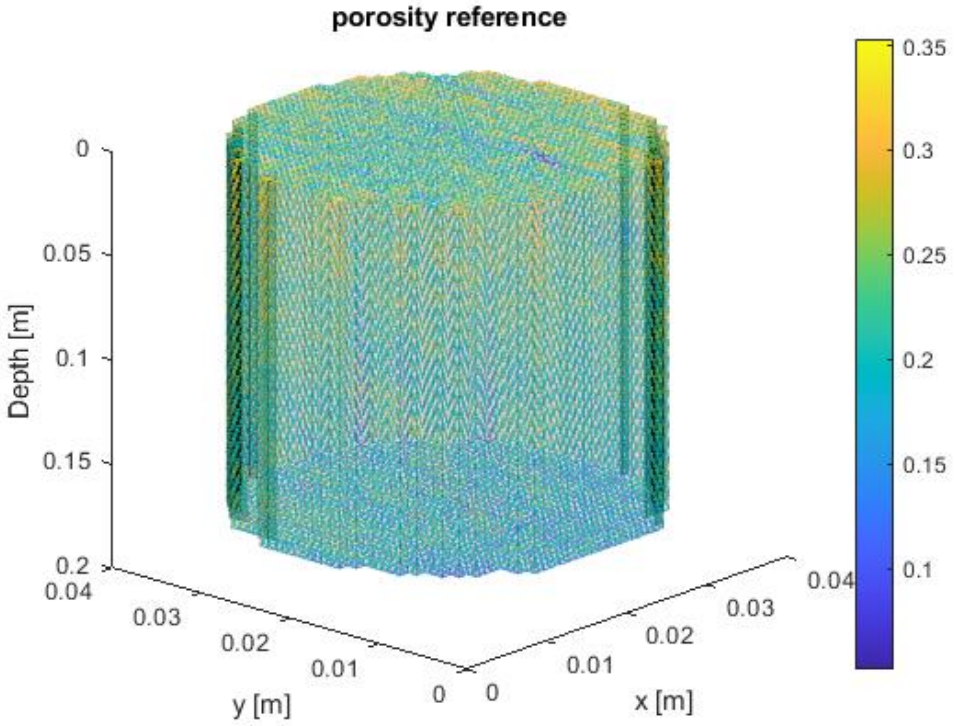

Figure 26: Discretised core sample with the measured porosity values assigned to each cell.

In the figure the highest porosity values are yellow, and the lowest porosity values are blue, the other colours are the intermediate values as shown in the lateral colorbar.

3.3.1.2 Initial conditions

Since the model is able to return the values of pressure drop present between the inlet and outlet point and the values of average saturation within the voxels at all the time steps, the initial conditions must provide starting values of those two quantity. Similarly to the porosity measurement, the initial values of saturation have been obtained during a

primary x-ray's examination of the core sample. The average saturation values have been computed for all the cells of which the grid presented in section 3.2.1 is composed.

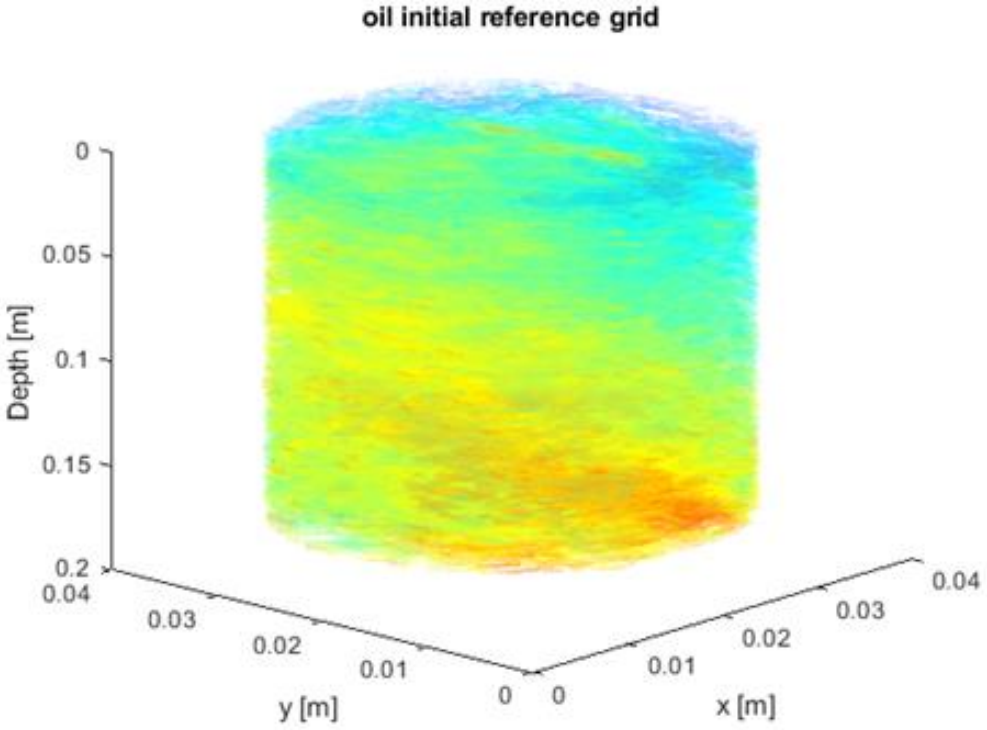

Figure 27: Initial saturation values measured within the sample

In the figure the highest oil saturation values are red, and the lowest oil saturation values are blue, the other colours are the intermediate values.

The initial pressure difference between the top and the bottom of the core sample must be also set. It has been chosen a pressure drop of 14500 Pa. This value is equal to the one that has been measured before the start of the experiment.

3.3.2 Grid refinement

At a first analysis, the grid realized as described in section 3.2.1. has been tried. The calculations of the first part of the thesis have been performed using an HP laptop with an intel core i7 5500U CPU @ 2.40 GHz and 8 GB of ram memory. As the data to be handled by the processor has exceeded its potential, the goal has become to find more manageable dataset. Since, as seen in the dedicated sections, the optimization algorithms require hundreds or thousands of evaluations of the objective function, which require the performance of as many simulations, the grid has been classified as not applicable for the thesis purposes. Fortunately, the research group had already realized a less fine grid that is more manageable. The quality of the results obtained from the model using the coarse grid has been verified by comparing its results with those obtained on the original grid, using a powerful computer made available by the Politecnico di Milano. The less refined grid was taken as the starting point for the generation of the synthetic dataset and consequently all the analyses carried out during the project.

This grid will be called during the whole thesis 'coarse grid'. In addition, in order to carry out an additional check, a grid has been built with an intermediate number of cells between the two previously mentioned grids. This grid will be referred to as a 'medium grid'.

Dimensions						
Grid name	**x**	**y**	**z**	**Cell tot**		**Refinement ratio**
Fine	42	42	178	313992	**f-c**	71,36182
Med	20,62236	20,62236	87,39951	37169,41	**f-m**	8,447592
Coarse	10	10	44	4400	**m-c**	8,447592

Table 4: Summary of all the information of the used grids. The refinement ratios between the various grids available are also shown in the left side of the table.

The choice of the medium grid size has been made on the basis of the refinement ratio. The refinement ratio between the original (fine) grid and the coarse grid has been obtained as $N_{cells,fine}/N_{cells,coarse}$ with a value of about 71. The refinement ratio of the average fine grid has been chosen intermediate and then evaluated as $\sqrt{\text{Refinement Ratio}_{F-C}}$. The obtained refinement ratio is equal if considered between the fine and medium grid or between the medium and coarse grid. For the choice of the intervals in which the grid is divided in the different directions it has been maintained the proportions of the original grid.

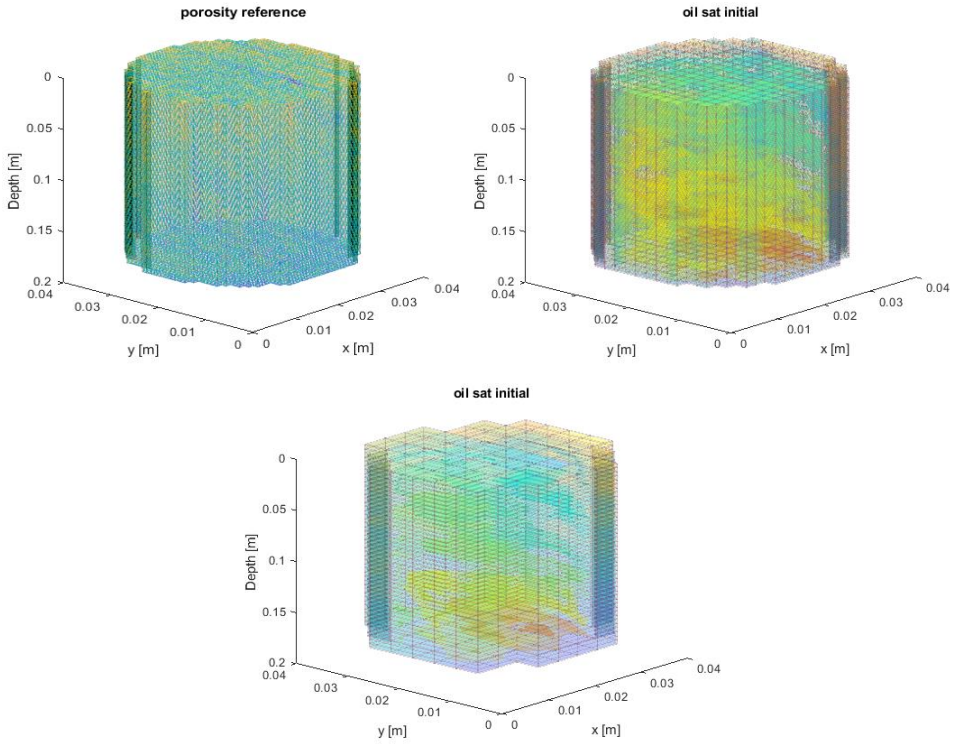

Figure 28: the three grid refinements from the finest to the coarsest, the graphs do not represent the same quantity, they are useful to give a graphic idea of the different discretization

It can be seen from the figure (in the one above) how the refining has led to a deformation of the initial geometry, but nevertheless the coarse grid is still able to represent the features of saturation.

3.3.3 Simulation results

After the grids has been created, the simulations have been performed and their results have been analysed and compared. A set of parameters have been imposed on the model, the same for both grids so that the results can be compared. The parameters have been kindly provided by the research group. They have obtained the parameters from the first attempt solution of an inverse problem carried using as input the real data of the experiment.

PARAMETERS		
	Values	**Brief description**
$\mathbf{S_{w,in}}$	0,96	initial water saturation (Corey + Skjaeveland)
$\mathbf{S_{w,irr}}$	0,01	irreducible water saturation (Corey + Skjaeveland)
$\mathbf{k_{ro}}$ **(Swirr)**	0,78	max oil perm (Corey)
$\mathbf{S_{o,r}}$	0,04	residual oil saturation (Corey + Skjaeveland)
$\mathbf{k_{rw}}$**(S_or)**	0,05	max water permeability (Corey)
$\mathbf{N_w}$	2	Brooks-Corey exponent
$\mathbf{N_o}$	8,7	Brooks-Corey exponent
$\mathbf{c_w}$	0,016	Skjaeveland model coefficient
$\mathbf{a_w}$	1,08	Skjaeveland model coefficient
$\mathbf{c_o}$	0,6	Skjaeveland model coefficient
$\mathbf{a_O}$	1,7	Skjaeveland model coefficient
m	15,05	Porosity- absolute permeability relationship
q	-16	Porosity- absolute permeability relationship
k	1,02E-13	Porosity- absolute permeability relationship

Table 5:Summary table of the model parameters with a brief description for each parameter

Of the coefficients reported, it has been verified that the curves obtained from the Skjaeveland and Corey models had shapes consistent with wettability.

The model simulates a transient phenomenon for sixty-six minutes. The total interval has been divided into 80 equal time intervals. The execution times were very different between the two simulations. On one hand the medium grid has taken about 600 seconds to perform the entire simulation, on the other hand the coarse grid has taken a tenth of the time completing the calculations in just one minute. It has been immediately clear that the medium grid cannot be used for calibration. The coarse grid could also create problems because the solution of an inverse problem with this grid could take days and several simulations of this type may be needed to properly set the optimization algorithm.

The results that have been obtained from the simulation with the coarse grid are:

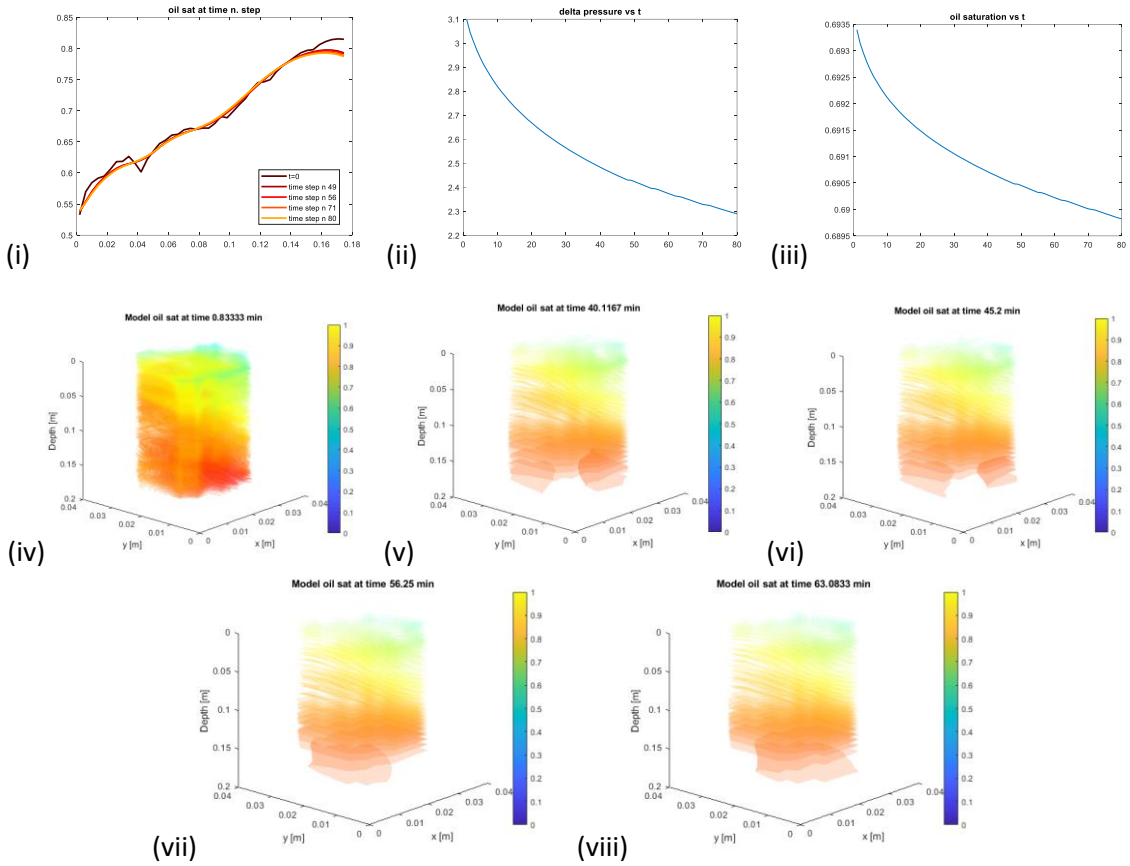

Figure 29: The image includes all the results obtained with the simulation carried out with the coarse grid. (i) saturation vs. height of the sample (the different colours represented different time steps which are 5 and are equidistant), (ii) pressure drop at the ends of the sample at the variation of the 80 time steps, (iii) average oil saturation at the variation of the time steps (80), (iv) oil saturation distribution after 0.83 minutes from the start of water injection (v) oil saturation distribution after 40. 11 minutes from the start of water injection (vi) oil saturation distribution after 45.20 minutes from the start of water injection (vii) oil saturation distribution after 56.25 minutes from the start of water injection (viii) oil saturation distribution after 63.08 minutes from the start of water injection

The results that have been obtained from the simulation with the medium grid are:

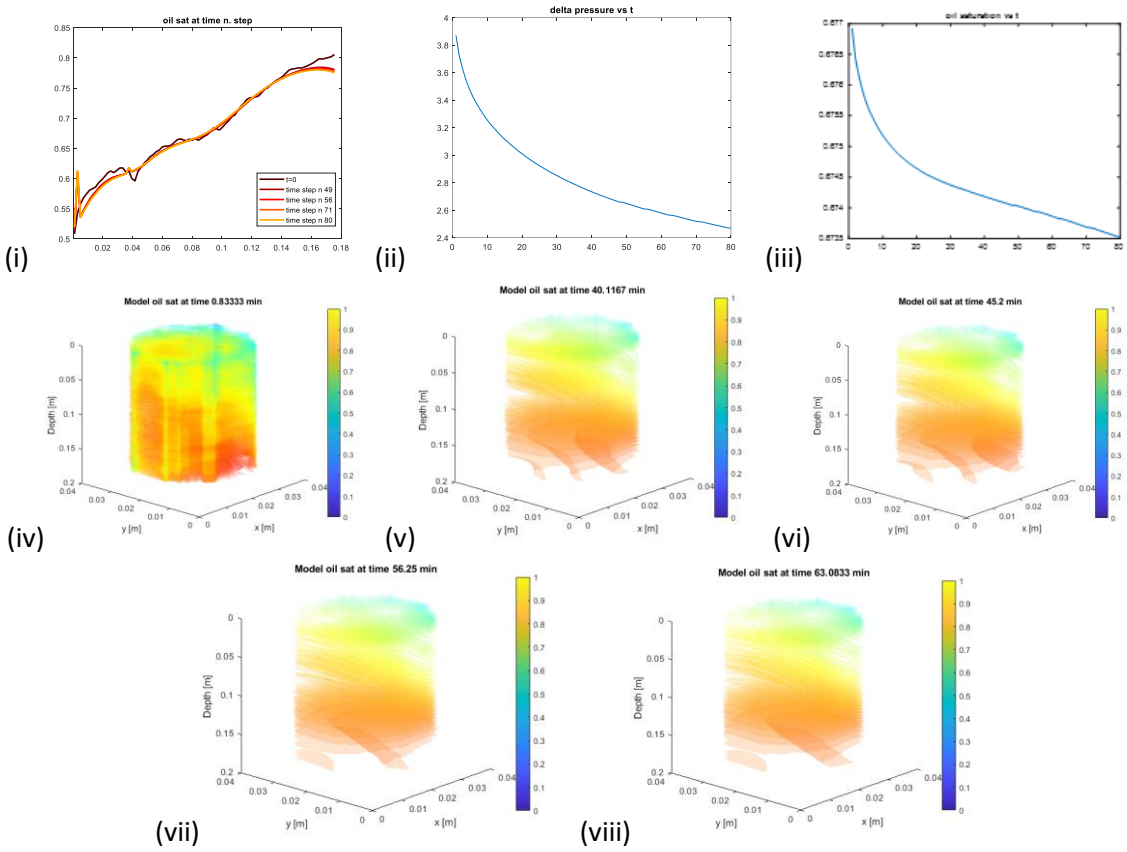

Figure 30: The image includes all the results obtained with the simulation carried out with the coarse grid. (i) saturation vs. height of the sample (the different colours represented different time steps which are 5 and are equidistant), (ii) pressure drop at the ends of the sample at the variation of the 80 time steps, (iii) average oil saturation at the variation of the time steps (80), (iv) oil saturation distribution after 0.83 minutes from the start of water injection (v) oil saturation distribution after 40.11 minutes from the start of water injection (vi) oil saturation distribution after 45.20 minutes from the start of water injection (vii) oil saturation distribution after 56.25 minutes from the start of water injection (viii) oil saturation distribution after 63.08 minutes from the start of water injection

From both results it has been possible to notice that: the pressure difference at the ends of the core sample has decreased as the injected water has increased and the oil saturation has decreased as it has been displaced by the water. It has been also possible to notice that the problem towards the end is approaching a steady state condition, so all the main features of the transient process have been captured by the simulation. The average oil saturation has decreased abruptly at the beginning of the transient and then the decreasing has been reduced as time goes by (as the injected water has increased). By carrying out an analysis of the saturation trend in the various layers at different core sample heights it has been possible to notice that the oil saturation decreases in all layers following the average saturation trend. Exceptions have been the higher layers that had a saturation value already low in the initial conditions and through which the oil displaced from the lower layers has passed. In addition, an anomalous trend of the average saturation over time curve has been identified in one of the lowest layers in the midium refined solution. The cause has been attributed to numerical errors during the calculation. The Comparison of the two solutions has shown that the grid refinement hasn't led to large differences between the two results. Despite the curves on the coarse grid has been smoother than those of the solution that has been obtained with the medium grid, the solution has been

accurate in both simulations. All the curves obtained have been very similar confirming that the coarse grid is better for the inverse problem due to the much more convenient computation time. Observing the coarse grid, however, it is evident that the horizontal layers that have been noticed by a visual and x-ray analysis in section 3.1.1. are not detectable and therefore it has been modeled an average behavior.

4 SYNTHETIC DATASET GENERATION

The synthetic data generation corresponds to the production of data applicable to a given situation where the data are not obtained from direct measures [53]. Synthetic datasets have various uses in different fields. The creation of synthetic datasets may have the purpose to anonymise sensible data or, as seen in the chapter of optimisation processes section 2.4.1., to train artificial intelligence by simulating real situations. For the thesis project the synthetic dataset has been used to test the model and create an effective optimisation algorithm for applications with real datasets. The use of the synthetic dataset allowed to directly assess whether the calibration of the parameters was successful. It has been possible because the solution parameters must be the same used to generate the dataset itself. The idea behind synthetic datasets is to create specific conditions that may not be encountered in the original datasets (real measured data). In fact, they can be applied in the design phases of any type of system. Thanks to the artificial generation of data, it is possible to create unexpected situations in the real case; it is done to verify the robustness of the designed algorithms or models [54]. The generation of the first synthetic data set is due to Rubin in 1993 [55], who developed synthetic data generation methods for the anonymisation of census data in order to guaranteeing privacy and to simplifying the census operation. In the following years, it has been developed methods that simulate real sampling (as carried out in the project) and some methods for the treatment of dataset with missing data.

4.1 DATASET ALTERATION

A synthetic dataset has been created to simulate the data from the experiment described in Chapter 3.1. The main exploited advantages of the synthetic dataset are:

- the knowledge of the parameters that characterize the system and therefore the a priori knowledge of the solution of the inverse problem
- the possibility to create data that simulate different wettability conditions by verifying the robustness of the developed inversion problem algorithm.

The data has been generated starting from the solutions obtained from the forward problem (see chapter 3.3.3.). The solution obtained in the forward problem represents the exact solution of the model. In reality the measurements are never exact but always contain a so-called measurement error. Indeed, the models of the physical problems do not represent the data in a perfect way but have the objective of representing the physical phenomena of interest. However, in the synthetic data, the measurement error must be introduced since the objective has been to obtain a dataset as similar as possible to one derived from a real experiment. The measurement uncertainty is the degree of uncertainty with which the value of a measured quantity is obtained, the measurement result is not a single value, but a set of values derived from the measurement of the quantity [56]. In the simplest cases it can be assumed that the error is equal to the uncertainty of the instrument [56].

4.1.1 coefficient of variance of one percent to modify the oil saturation results

The first synthetic dataset has been generated by altering only the saturation values, the result of the problem of chapter 3.

Unfortunately, there has not been detailed information available about the measuring instrument, so the measurement uncertainty values have not been provided. It has been decided to insert a noise in the dataset that simulates a possible error made by an instrument and/or an error made during the experimentation. Due to the lack of information, it has been reasonable to assume that a measurement error could be described with a Gaussian distribution function [7]. The global description of a Gaussian distribution is done by defining the parameters mean (μ) and standard deviation (σ). It has been therefore assumed that the measured value of the average saturation in a cell is around the exact value, and the probability of the value is described by a Gaussian distribution defined with:

- μ which has been the average saturation value of each Voxel. It is the value obtained in the forward simulation of the problem and it is available for each cell at each time step.
- σ which is the standard deviation. It has been derived from a coefficient of variation σ* of 1 % (subsequently for the generation of other datasets it has been increased to 5 %). Then the coefficient of variation has been multiplied with the oil saturation in order to obtain a σ value for each voxel in each time step.

Once the distributions in each cell were defined for each moment of time, it was necessary to replace the exact values of the solution with values randomly sampled from the just defined distributions.

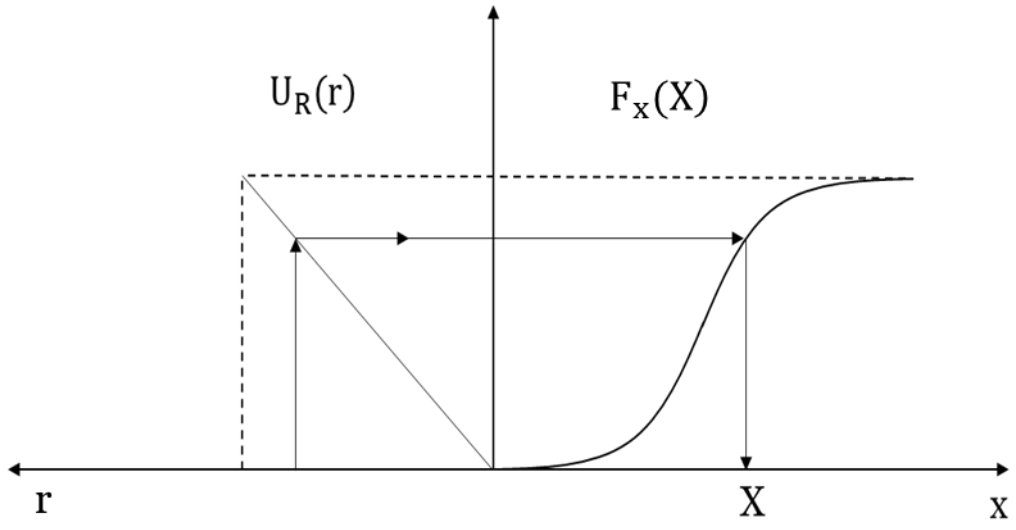

Figure 31: Random sampling, Fx(X) is the distribution function, Ur= is the uniform distribution between 0 and 1.- Source: [43]

$U_R(r)$ is a uniform distribution between 0 and 1 and the $F_x(X)$ that has been used is a

Gaussian cumulative distribution function, formally:

$$F_x(X) = \frac{1}{2}\left(1 + \text{erf}\frac{x - \mu}{\sigma\sqrt{2}}\right) \tag{4.1}$$

The Matlab function `normrdn(μ,σ)` has been used to perform random sampling. The function requires in input only the μ and σ of the Gauss distribution.

Since the Gaussian distribution has a domain ranging from - ∞ to + ∞ it is possible that during random sampling some saturation values is negative. Negative saturation values make no physical sense so if the value is negative it must be resampled until it become positive.

In order to do all the operations described above, a MATLAB function has been realized. It receives in input the complete dataset of all the saturation values in space and time (result of the forward simulation) and the chosen coefficient of variation returns the synthetic dataset in its final version (without negative values). The generated synthetic dataset simulates a real dataset after being pre-processed.

In real cases the datasets often are very distorted and sometimes negative values are present even if they do not make sense. Usually the data receives a pre-treatment that detects and corrects these problems. On method to fix the dataset may be a filtering process (e.g. median filter). An example of a dataset correction procedure is the MATLAB `filmissing` function [57].

4.1.2 A single variance value for all the cells

As a first approach σ has been obtained multiplying the coefficient of variation (σ*) by the average saturation value in each Voxel (the one defined above as μ); it has been noticed that it may leads to uncoherent situation. In order to understand the just mentioned criticality, it is necessary to first define the synthetic measurement error.

$$e(i,t) = S_{i,t} - S^*_{i,t} \tag{4.2}$$

where $S_{i,t}$ is the saturation evaluated with the forward problem in the i-th cell at the time step t and $S^*_{i,t}$ is the saturation in the synthetic data referred to the same cell and at same time step.

By displaying the synthetic measurement error, it has been noticed that the error was position dependent. This is because the saturation varies as the Z coordinate changes. Since the white error caused by the measuring instrument is not dependent on the saturation value or on the position it has been chosen a single σ valid for all the cells. A mean saturation value over time and space has been computed and this obtained value has been multiplied by the coefficient of variation chosen by the modeller to obtain the value of σ valid for all the cells. At this point the synthetic dataset has been recalculated using the same values for μ but changing the value of σ (which has been kept constant and equal for all the values.)

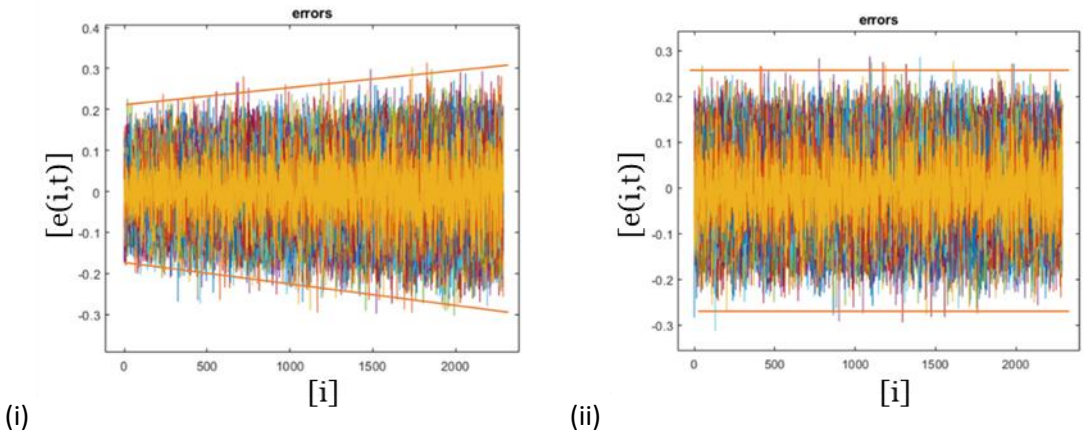

(i) (ii)

Figure 32: With different colours shows the synthetic measurement errors for each instant in time. The errors are shown in order from the cell at the bottom left of the grid to the cell at the top right of the grid. (i) shows the synthetic measurement error before correction. (ii) shows the synthetic measurement error after correction for variance evaluation. In order to make more appreciable the phenomena the graphs have been done with a coefficient of variance equal to 10%

In the images are reported the synthetic measurement error values. The different colours represent the different time steps. On the left in the graph are reported the saturation values of the top side of the sample while on the right are reported the values of the bottom side. Form the first graph it has been noticed that the trend is present at all the time steps. The second graph reports the same measurement error for the same grid after the correction. It is possible to appreciate that no trends are anymore present.

A second synthetic dataset has been subsequently generated with the same criteria with, as the only difference, the coefficient of variation equal to 5%.

4.1.3 Alteration of oil saturation and pressure drop dataset using variance coefficients of 1% and 5%:

Finally, two synthetic datasets have been generated which, in addition to creating the oil saturation random variation as described in the previous section, create a random variation of the value of pressure drop through the core.

The variation for the pressure drop has been made following a criterion similar to that used for oil saturation. The only difference has been that the pressure drop value is one at each time step, so the coefficient of variation has been multiplied by the time average of the pressure drop values in order to obtain σ. A single synthetic value has been obtained for each time step. In these datasets it has been considered that pressure drop values can also be affected by measurement errors.

The previously defined MATLAB function has been updated to calculate the synthetic values of the pressure drop. The function has been modified to receive in input the pressure data, the saturation data, the coefficient of variation for the pressure drop values and the coefficients of variation for the saturation.

4.2 SYNTHETIC DATASET CONCLUSIONS

The function for creating the synthetic datasets has been used throughout all the thesis project whenever the parameters of the simulation model has been changed. It has been easy to modify the parameters of the problem forward and, using the function to alter the data, it has been extremely fast and cheap to obtain new data useful to test the optimization algorithms and for other purposes. Modifying the parameters, it has been simple to create different wettability situations without having to carry out special and expensive experiments. Therefore, all the synthetic datasets used have been created with the criteria described in the previous sections.

The synthetic dataset is the input used for the inverse problem.

5 INVERSE PROBLEM

The inverse problem workflow setting is the core of the project. The current chapter shows how the workflow has been built to calibrate the model (described in chapter 3) starting from the artificially generated datasets (described in chapter 4). All the obtained results from different configurations of the proposed calibration methodology have been reported. At the beginning many comparisons between different workflow settings have been used to choose the best calibration methodology. In the second part the workflow has been tested under different conditions changing the settings of the main components of the proposed method. Finally, the applicability of the method has been tested for some key situations.

5.1 A WORKFLOW FOR MODEL CALIBRATION

Thanks to the synthetic dataset that has been generated following the indications in chapter 4 a real condition has been simulated, i.e. the objective has been to determine the model parameters owning only the data available from measurements. This subchapter deals with the creation of the calibration workflow which includes the choice of the optimization algorithm, the definition of an effective objective function and the parameters domain. The second part of the subchapter describes the improvements added to the numerical model, the sensitivity analysis and all the evaluation criteria used to choose the best methodology.

5.1.1 Objective function, parameters and limits

The process of identifying the simulation model parameters is included in the part of the inverse problem called calibration. Mainly there exist two methods to perform the calibration: the direct method and the inverse method. The direct method can be performed mainly in two ways: analytically if the direct problem is composed of equations that can be easily inverted or by optimizing an objective function. The first way (the analytical) has the advantage of being very fast once the inversion of the equations has been done. Thanks to the model description covered in the chapter 3 it is easy to understand the complexity of the model and the impossibility to invert the equations. Therefore, the possibility of identifying analytically the solution has been discarded a priori. Moreover, the direct method that implies the solution of an objective function has been abandoned because it is known from the literature that this type of solving methods are usually unstable and practically not used (for further details refer to section 2.3.3) . In order to find the solution of the inverse problem, the indirect method has been chosen. This method requires the definition of the objective function; in fact, the indirect solution of the inverse problem has been found by optimizing the objective function. Two of the most frequently used objective functions are likelihood and least square. The method of optimizing the objective function using the likelihood function consists of minimizing the opposite of the logarithm of the likelihood function. The least square method, in a simpler way, minimizes the square of the differences between the estimated and the measured values. Below the equivalence between the two objective functions in the current inverse problem is demonstrated.

Firstly, the likelihood function has been defined as:

$$\mathbf{L}(\boldsymbol{\beta}/\mathbf{z}^{*}) \tag{5.1}$$

Where: $\boldsymbol{\beta} = (\mathbf{P}, \boldsymbol{\theta})^{\top}$ is a vector that contains all the parameters of the model to be determined in the vector **P** and a vector with all the unknown statistical parameters characterizing the prior error $\boldsymbol{\theta} = (\sigma_{i}^{2}, \dots)$. $\mathbf{z}^{*} = (\mathbf{h}^{\star}, \mathbf{p}^{\star})^{\top}$ are all the observations values; specifically, $\mathbf{h}^{\star}$ are all the measures (in the thesis are the synthetic data) and $\mathbf{p}^{*}$ are all the parameters prior information.

In the simulation of the core sample experiment there has not been prior information on the parameters to be determined, moreover it has been reasonable to assume that the measurement error can be described by a Gaussian distribution with constant variance. This last assumption is perfectly in line with the observations made to generate the dataset in chapter 3. During the generation of the synthetic dataset the variance has been kept constant, so this hypothesis has been certainly respected. Thanks to the two just mentioned observations it is possible to demonstrate that the likelihood is equivalent to the least square regression as follows:

The optimization algorithms generically are designed to minimize the objective function so in practice instead of maximizing the likelihood function it is minimized the opposite of its logarithm

$$\min\{\mathrm{NLL}\} = \min\{-2\ln[\mathrm{L}(\boldsymbol{\beta}|\mathbf{z}^{\star})]\} \tag{5.2}$$

Applying the Bayes theorem and the Gaussian distribution hypothesis for the measurement errors it is possible to obtain the following formulation for the likelihood

$$\mathbf{L}(\boldsymbol{\beta}/\mathbf{z}^{*}) \propto \mathbf{f}(\mathbf{z}^{*}/\boldsymbol{\beta}) = \frac{1}{\sqrt{(2\pi)^{\mathrm{N}}|\mathbf{C}_{\mathbf{z}}|}} \exp\left[\frac{1}{2}(\mathbf{z}^{*} - \mathbf{z})^{\mathrm{T}}\mathbf{C}_{\mathbf{z}}^{-1}(\mathbf{z}^{*} - \mathbf{z})\right] \tag{5.3}$$

combining the equation 5.3 with the equation 5.2 is obtained

$$\begin{aligned}\mathrm{NLL} = (\mathbf{h}^{*} - \mathbf{h})^{\mathrm{T}}\mathbf{C}_{\mathrm{s}}^{-1}(\mathbf{h}^{*} - \mathbf{h}) + (\mathbf{P}^{*} - \mathbf{P})^{\mathrm{T}}\mathbf{C}_{\mathrm{p}}^{-1}(\mathbf{P}^{*} - \mathbf{P}) + \ln|\mathbf{V}_{\mathbf{h}}| + \ln|\mathbf{V}_{\mathrm{p}}| \\ + \mathrm{N_h}\ln\sigma_{\mathrm{h}}^{2} + \mathrm{N_p}\ln\sigma_{\mathrm{p}}^{2} + (\mathrm{N_h} + \mathrm{N_p})\ln\ 2\pi\end{aligned} \tag{5.4}$$

without prior information and applying the constant variance hypothesis it becomes similar to the least square regression objective function. Specifically, the maximization of the likelihood (equation 5.1) is equivalent to

$$\min\left\{\frac{\sum_{\mathrm{i}}^{\mathrm{N_{time\ step}}}\sum_{\mathrm{j}}^{\mathrm{N_{celle}}}\left(\mathrm{h}_{\mathrm{ij}}^{*} - \mathrm{h}_{\mathrm{ij}}\right)^{2}}{\mathrm{N_{time\ step}} * \mathrm{N_{celle}}}\right\} \tag{5.5}$$

A more detailed discussion of the analogy between the two optimization methods can be found in the section 2.3.3.

It has been therefore chosen the least square error method (and with it the maximum likelihood due to its equivalence in this problem) for the calibration process for its simplicity.

Therefore, in the specific case the objective function to be minimized has been defined as:

$$f_{obj} = \frac{\sum_{i}^{N_{time\ step}} \sum_{j}^{N_{celle}} \left(s_{ij}^{*} - s_{ij}\right)^2}{N_{time\ step} * N_{celle}} + \frac{\sum_{i}^{N_{time\ step}} (\Delta Pn_{i}^{*} - \Delta Pn_{i})^2}{N_{time\ step}} \quad (5.6)$$

where s_{ij}^{*} is the sampled saturation value (of the synthetic dataset) and s_{ij} is the saturation value obtained from the simulation done by the optimization algorithm evaluated in j-th cells at i-th time step; ΔPn_i^* is the measured pressure drop value (of the synthetic dataset) between the upper and the lower surfaces of the core sample and ΔPn_i is the pressure drop value obtained from the simulation for the i-th time step.

Since the parameters are 11 the solution is searched in a 11-dimensional space. In order to be able to perform the optimization in a reasonable time, it has become necessary to define a reduced domain. This has been done by introducing the upper and lower limits for all the parameters to be determined. For some of the parameters the limits have already been discussed (see section 3.2.3.). For the parameters of which no information about the range is present, the values reported as common for a sandstone rock have been taken and wide ranges have been created around these values.

	Dataset parameter	Upper limit	lower limit
n_w	2	1	10
n_o	8,7	1	10
S_{wirr}	0,01	0,0077	0,56
S_{oi}	0,04	0	0,1476
k_{roMax}	0,78	0,01	1
k_{rwMax}	0,05	0,01	1
m	15,05	11	21
C_w	0,16	0	0,5
A_w	1,08	0,5	1,5
C_o	0,4	0	0,5
A_o	1,4	0,5	1,5

Table 6: In green are reported the parameters values to generate the synthetic dataset and in black are reported the search domain limits for each parameter (upper and lower)

The table 6 shows in green the parameters used to generate the synthetic dataset and the upper and lower limits for each parameter.

The narrower the limits around the exact value, the easier it is for the optimization algorithm to find the minimum of the objective function and therefore the exact solution. Since a real experiment has been simulated, the intervals have been chosen as if there was no information about the result and therefore wide enough to not exclude any possible solution.

5.1.2 Optimization algorithm

Once the objective function and the domain boundaries have been defined, the appropriate minimization algorithm must be identified. It is evident, from the description of the model made in chapter 3, that the function is not derivable so all methods that require the calculation of the derivatives have been excluded a priori. Among the other categories of methods for optimization, the population methods have been recognized as the most appropriate; because they are suitable for problems where the objective function requires long evaluation times and for functions that may have critical points.

5.1.2.1 Particle Swarm Optimization

As a first approach to optimization the particle swarm optimization algorithm has been used. The algorithm implemented in the `particleswarm` function of the MATLAB Global optimization toolbox has been chosen. The function is based on the algorithm developed by Kennedy and Eberhat [25] and is described in detail in section 2.4.6.. The complete guide that includes all the added refinements of the function is reported in the Particle Swarm Optimization Algorithm section of the MATLAB Help Centre [58]. The function requires in input the objective function previously described, the limits for each variable defined in the previous section, the number of variables that must be calibrated and additional options. The main available additional options are:

- the stop criterion (default: no stopping criteria)
- the number of individuals in the population (default: 10 x (number of parameter))
- the results display options (default: no display)
- the parallelization of the calculation in the case of multicore processor (default: no parallelization)
- the minimum limit of the objective function (if known; default: 0)
- the weights of the various components of the speed vector (see Equation 2.47, default: c1=1.49 c2=1.49)

No automatic stopping criteria has been selected, but the software has been stopped manually if a situation requiring intervention has occurred (such as convergence or other). For each iteration it is necessary to evaluate the objective function for each individual. Since a simulation with the coarse grid takes about one minute (as already shown in section 3), a population of 20 individuals has been selected to carry out the calibration in a reasonable time. As a first approach, hybridization of the algorithm has not been deemed necessary. The calculations of the first simulations have not been parallelized because neither the used HP laptop nor the MATLAB student licence have allowed it. Since the objective has been to simulate the real dataset conditions, the value of zero for the absolute minimum of the objective function has been left. The weights for the various components of the velocity vector have not been modified from the default values.

Unfortunately, a numerical problem, that caused the flow calculation program to get stuck within a cycle, has been found and it has not been possible to continue with the PSO iterations. The same problem has been documented in the application of the PSO algorithm in an inverse problem based on the set of experimental data. Given the problems encountered in carrying out simulations with some sets of parameters, the goal has become the identification of which set of parameters led the simulation in stuck. The problem has occurred during the evaluation of the objective function in the first iterations of the

optimization algorithm (during the second or third iteration). Fortunately, the programme problem occurred in a short time, so it has been launched multiple times to save the combinations of parameters that has caused the block in the evaluation.

This allowed to identify several combinations of parameters causing the problems. It has been noted, again with a trial & error approach, that the program has get stuck calculating the flow solution in points at the limit of the searching domain. Specifically, one or more of the model parameter values were equal to the limit values (both upper and lower).

	n_w	n_o	S_{wirr}	S_{oirr}	k_{roMax}	k_{rwMax}	m	C_w	A_w	C_o	A_o
1	1	3,638	0,035	0,079	0	0	16,900	0,337	0,5	0,5	1,102
2	10	7,149	0,044	0,029	0,807	0	21	0	1,5	0,5	1,5
3	4,820	10	0,027	0,032	0	0	20,231	0,201	0,5	0	0,640
4	1,576	5,3687	0,029	0,063	1	0	20,446	0	1,5	0,500	0,5
5	1	1	0,05	0,117	0,942	0	18,411	0,208	0,831	0,125	0,5
6	1	10	0,05	0,022	0	0	11	0,2142	1,5	0,5	1,233

Table 7: Six set of parameters that has led the flow simulation program to be blocked

It is known that the behaviour of the PSO, due to the swarm logic on which it is based, in the first iterations causes a significant dispersion of the points to be evaluated within the domain. This phenomenon can lead one or more particles to the edges of the domain. A more detailed description of the behaviour of the algorithm is available in section 2.4.6..

5.1.2.2 Differential Evolution

The solution that has been proposed is to replace the particle swarm optimization algorithm with an evolutionary algorithm. The differential evolution has been chosen because it includes the required properties (further details are available in section 2.4.5.).

A MATLAB package containing the functions for the identification of the optimal solution using the differential evolution algorithm has been acquired [59]. The package's functions are realized to identify the parameters of a model starting from the measurements. They can minimize the objective function without calculating its derivative. The package of functions allows:

- the implementation of a code able to evaluate in parallel the objective function.
- to save all intermediate results that may be useful in the post-processing.
- to show the intermediate and final results in the user's preferred ways.
- to select different stop conditions
- to recover the intermediate results in case of simulation code crash and restart the computation form the previous iteration.

For a detailed explanation of all the function present in the package refers to the File Exchange section of the MATLAB web site [59].

It has been chosen the `differentialevolution` function from the just described package.

As input the code requires the objective function, the number of parameters and the limits of the search domain. The inputs that have been used are the same already used for the particle swarm optimization. In the algorithm options the only thing that has remained

constant is the number of individuals of the population. The other options required by the code are the F parameter and the CR parameter (Crossover Rate) (see section 2.4.5.). For the F parameter a value close to 0.5 is recommended by the literature (section 2.4.5). Considering that the objective has been to reduce the dispersive behaviour in space to avoid the model valuation of the points at the edges of the search domain, F has been reduced to 0.3 which is a value that has proved to be effective even with complex functions (for more details refers to appendix A). As a first approach it has been chosen to be conservative. In order to allow the algorithm to converge, at the expense of its speed, a parameter CR equal to 0.4 has been chosen.

Thanks to the change in the optimization algorithm it has become possible to evaluate 100 iterations of the optimization algorithm (2000 evaluations of the objective function) without any flow simulation program issue.

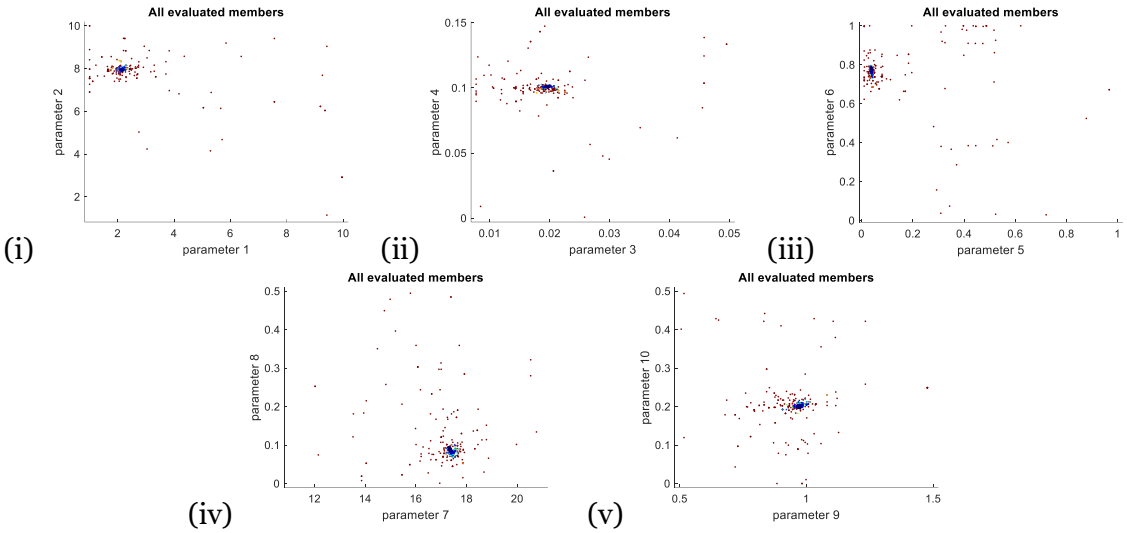

Figure 33: The figure shows in pairs the values of the parameters that have been used as input in the simulations carried out by the optimization algorithm. In blue are represented the values of the parameters evaluated in the last generations, in red the value of the parameters evaluated in the first generations

From the obtained results (figure 33) it has been noticed that the points evaluated in the first iterations (in red) were scattered in space while the ones evaluated in the last iterations (in blue) converged towards a single value for each parameter. Due to the high number of parameters to calibrate, the graphs of ten parameters have been shown in pairs. The work has led to an algorithm that does not stop due to numerical errors within the objective function. Thanks to the results obtained, the particle swarm optimization algorithm has been substituted by the differential evolution algorithm and the goal has become to determine more accurately all the parameters.

5.1.3 Improvement of the numerical model

In parallel with the analysis carried out on the optimization algorithm of the previous section a more robust solver to prevent possible effects on the numerical issues mentioned above has been tested.

The code for the evaluation of the flows has been modified. For this purpose, the ad-BlackOil module package available for MRST [44] has been used. The package has added models that implement the equations for the multiphase, miscible, compressible flow and

at the same time it has included a more updated versions of the MATLAB functions for the solution of immiscible and incompressible multiphase flows (as the one in the case study). Specifically, it has been used `TwoPhaseOilWaterModel` function to describe a two-phase oil/water system without dissolution. With the particle swarm optimization algorithm, this code has shown to be able to complete the simulation also with some combinations of parameters that blocked the flow model based on the `implicitTransport` function (described in Chapter 3).

A further improvement has concerned the expression of $S_{w,irr}$ and $S_{o,r}$ through documented relationship with permeability and wettability respectively.

Measurements of irreducible water saturation are nowadays easy to be obtained. These measurements have been accumulated to a number that has made possible to find for a correlation between the value of irreducible water saturation and the permeability in a specific reserve [60]. The idea on which the used correlations are based is that in a non-ideal system a low permeability is the result of an increase in non-uniformity of the porous structure caused by a gradation of particles rather than a reduction in particle scale. It is therefore expected that irreducible water saturation increases as permeability decreases. Empirical correlations can only be valid for a given formation. For formation with similar dependence of permeability with porous structure the correlation structure can be analogous. It has been chosen to use a simplified version of the Morris correlation [61] that defines S_{wirr} as a function of permeability (which in turn is obtained from an empirical relationship with porosity):

$$S_{wirr} = \frac{c}{k^d} \tag{5.7}$$

where c and d are constant to be determined. Typical values reported by Tarek A. are c= 0.362 and d= 0.132 [60].

Finally, to further increase the flow simulation code performance, an already existing trapping model has been used to determine the trapped oil saturation ($S_{o,r}$). From the point of view of the pore scale the effect of hysteresis has at least two causes: the hysteresis of the contact angle and the entrapment of the non-wetting phase. Indeed, the correlation was introduced by Spiteri et al. [62] to describe the phenomenon of hysteresis on relative permeabilities. From their observations they established that the saturation of trapped oil is related to the initial oil saturation value through a quadratic equation:

$$S_{or} = \alpha S_{oc} - \beta S_{oc}^2 \tag{5.8}$$

The α and β parameters correspond to the initial slope and curvature of the quadratic equation curve. The limits reported in the literature for these parameters are

$$0 \leq \alpha \leq 1, \quad \beta \geq 0 \tag{5.9}$$

The introduction of this correlation would have increased the number of parameters to be calibrated, affecting the quality of the optimization (for further details see section 2.3.3.3.). Fortunately, the two coefficients can be linked to the contact angle between the two phases (θ).

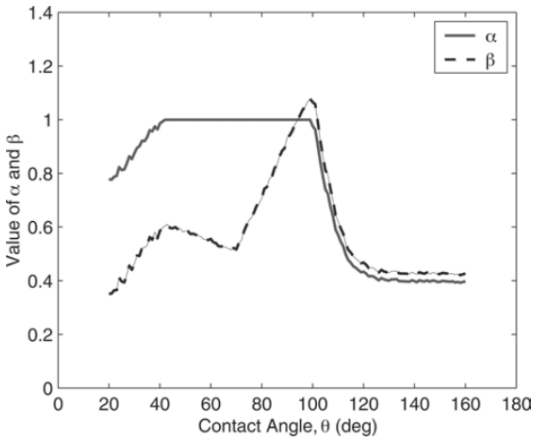

Figure 34: The graph shown in the figure represents the relationship of the theta parameter with the alpha parameter and with the beta parameter – Source: [62]

For the two curves, no interpolation functions have been derived, so their discrete point have been used. Giving theta the program automatically interpolates the graph and obtain alpha and beta. It has been important to notice that by varying the parameter θ for a value greater than 120 the Alpha and beta coefficients will not change and consequently the value of $S_{o,r}$ will remain constant. The values that the parameter θ can assume have been taken from the graph, so the range include values from 20 to 160 (degrees). The contact angle is strictly related to wettability; if theta is greater than 90 it represented a condition more oil-wet, instead a theta angle lower than 90 is consistent with more water-wet conditions. For further detail on wettability refers to section 2.1.5.

Different parameters define the new model; so, it has been created a new synthetic dataset. It has been generated following the procedures described in chapter 4. Therefore, a forward simulation has been carried out with a set of parameters consistent with the wettability and the type of rock selected. The dataset has been altered with the function defined in section 4.1.1. using the coefficients of variation equal to 1%. The limits for the new parameters to be calibrated c and d have been defined as wide ranges around the value previously reported as common, because no information about them possible values are available. For theta the range has been already provided.

	Exact solution	**Upper boundary**	**Lower boundary**
$\mathbf{n_w}$	2,2	2	5
$\mathbf{n_o}$	7,6	4	8
theta	150	90	160
c	0,08	0,01	0,5
d	0,08	0,01	0,5
$\mathbf{K_{rw,max}}$	0,1	0	0,2
$\mathbf{K_{ro,max}}$	0,8	0,5	1
m	15,05	11	21
$\mathbf{C_w}$	0,16	0	0,5
$\mathbf{A_w}$	1,08	0,9	1,5
$\mathbf{C_o}$	0,4	0	0,5
$\mathbf{A_o}$	1,4	0,9	1,5

Table 8: In green are reported the parameters values to generate the synthetic dataset and in black are reported the search domain limits for each parameter (upper and lower)

5.1.4. Sensitivity analysis

In order to understand the impact of the parameters to be calibrated on the objective function and on its two main components (the component linked to the residual of saturation in every cell and the component related to the residual of pressure drop), a local sensitivity analysis has been performed.

The sensitivity analysis is the study of how uncertainties in model input affect the output. One of the main purposes of the sensitivity analysis is the evaluation of how much an input contributes to the uncertainty on the output. This evaluation is carried out ordering by importance the relevance of each input, with an order determined by the variation it causes on the output [63]. In this way it is possible to find out the parameters whose value should be estimated better and those that have little influence on the solution. Since the aim has not been to identify the quality of the model with the relative probability distributions of uncertainties, but to understand the effect that a parameter has on the objective function, it has been chosen a one-at-a-time local sensitivity analysis. Mathematically, the local sensitivity analysis of the objective function with respect to certain parameters is similar to the calculation of the partial derivative of the function itself with respect to those parameters. The evaluation of the derivative for complicated functions, such as the one under examination, may be impossible. Therefore, the objective function has been evaluated several times in order to discreetly visualize its trend. The one-at-a-time approach analyses the effect of one parameter on the cost function at a time, keeping the other parameters fixed. This approach is one of the simplest and most used. The main drawback of this approach is that it does not provide insight about how the interactions between parameters influence the objective function. This approach is suitable only for a small portion of the space [64](in the project it has been explored only the defined interval table 8).

The local one-at-a-time sensitivity analysis has been carried out in the following way: the values of one parameter at a time have been varied, keeping the others equal to the exact value; each parameter has been varied 10 times and has assumed values equidistant between the lower and upper limits set in the calibration table 8.

The graphs containing the results of the sensitivity analysis are reported in appendix B.

From the local sensitivity analysis no critical points have been noted for most of the parameters, (no local minima and plateau). The exceptions have been the theta and m parameters that have presented plateau (that are critical points) that can create problems to the optimization algorithm (figure 54 and 59). The plateau for the parameter theta has been presented for values higher than 120 and it has been perfectly in line with the observations made on the Figure 34 in section 5.1.3.. Therefore, all the values between 120 and 160 of the theta parameter can equivalently be identified as the solution if the real value of theta is included in this range. The theta angle is not a fundamental characteristic in reserve analysis, but the dependent parameter S_{or} is important. Hence, a limit of the inverse problem carried out with this methodology has been recognized as the impossibility of univocally identifying the S_{or} value if the contact angle is higher than 120.

5.1.5. Performance evaluation criteria

Many methodology improvements have been proposed during the thesis project. In order to verify if a change has been able to improve the methodology, it has been necessary to introduce parameters that are easy and quick to understand. In addition, the latter have also proved to be very useful for assessing the applicability of the final version of the method. These evaluation parameters were able to evaluate how much a proposed solution has been different from the exact one (being the exact solution the set of parameters used as input in the flow simulation program to generate the synthetic dataset). Introducing a normalization criterion has been necessary to make the evaluation parameters comparable even if they referred to different flow simulation program parameters. The evaluation parameters that have been used are the nCE and the nCE* which differ in the normalization method.

The normalized calibration error (nCE) is defined as the difference between the value of the parameter that characterize synthetic dataset (P_{sd}) and the parameter of the particle ($P_{b,i}$) that the objective function has returned as the best value of the i-th generation (one generation for each iteration); this difference has been normalized dividing the error by P_{sd}:

$$nCE = \frac{P_{sd} - P_{b,i}}{P_{sd}} \tag{5.10}$$

The average nCE has also been defined as the average of the absolute value of the nCE of all the parameters at a given iteration. This parameter has been useful for a quicker understanding of the general performance of the method.

Instead, the nCE* considers how far the evaluated parameter is from the exact value in relation to its domain dimension (between the upper (UB) and the lower limit (LB)).

$$nCE^* = \frac{P_{sd} - P_{b,i}}{UB_p - LB_p} \tag{5.11}$$

The average nCE* has been useful for an easier understanding of the general quality of the calibration; it has been defined as the average, among all parameters, of the absolute values of the nCE*.

These last two parameters (nCE* and average nCE*) have been used only during the setting phase of the optimization algorithm. They are not appropriate for calibration evaluation, but they are suitable for the evaluation of the optimization algorithm behaviour.

Another important parameter, to understand the effectiveness of the optimisation algorithm and with it of the whole workflow, have been the minimum of the objective function for each iteration. It has been noted that there exists a minimum obtainable value for the objective function. This can be computed by evaluating the objective function between the synthetic dataset and a simulation made with the parameters expected as result (those used in order to generate the dataset itself). Of the objective function, the component due to the saturation residue and the component related to the pressure drop residue have been evaluated independently.

Saturation residues component of the objective function has been evaluated as:

$$f_{obj_{sat}} = \frac{\sum_{i}^{N_{time\ step}} \sum_{j}^{N_{celle}} \left(s_{ij}^{*} - s_{ij}\right)^2}{N_{time\ step} * N_{celle}} \tag{5.12}$$

The objective function component related to the pressure drop residues has been evaluated as

$$f_{obj_{\Delta P}} = \frac{\sum_{i}^{N_{time\ step}} (\Delta Pn_i^{*} - \Delta Pn_i)^2}{N_{time\ step}} \tag{5.13}$$

So, the minimum of the objective function obtainable in the calibration is the (weighted) sum of the two just mentioned components.

The last element used to compare the methodologies has been the overall time that they took to obtain the results. Given the long calculation times for each simulation carried out by the flow simulation program, an important aspect has been the choice of the workflow that gave good results in a reasonable time.

5.2 PRELIMINARY TESTS

As anticipated the algorithm used to perform the calibration has been the differential evolution. No stop criteria have been set as the solutions are monitored periodically. In case of convergence the program has been stopped manually. During the first attempts and during the comparisons, the algorithm has been stopped when the necessary information has been acquired. Indeed, during the applicability testing phase (section 5.3.2) of the methodology, the algorithm has been stopped observing the minimum obtained value of the objective function and in particular the variation that the minimum obtained value of the objective function makes with respect to the previous iteration (if any) and the frequency of these just mentioned variations.

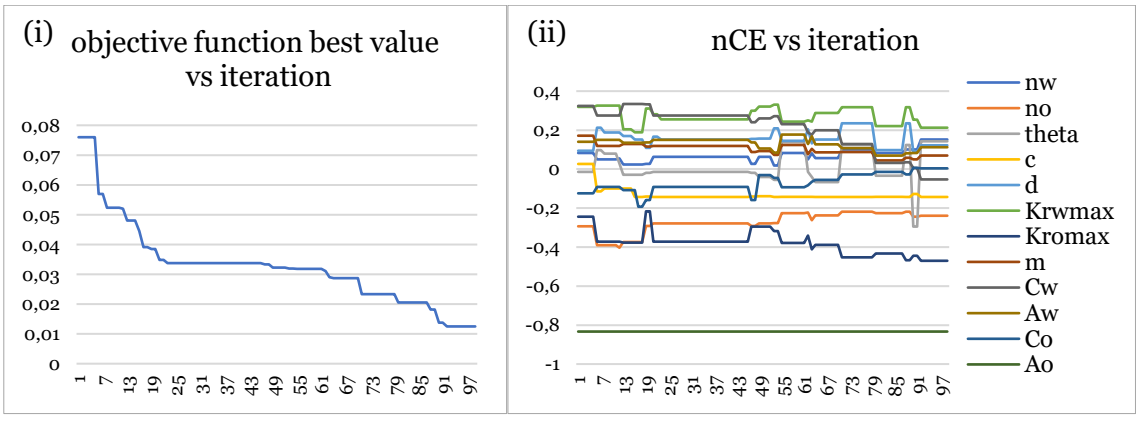

Figure 35: The graph (i) represents the best value obtained by evaluating the objective function during the iteration numbered on the horizontal axis. The graph (ii) represents the value of nCE for all the parameters of the simulation program that belong to the set of parameters that returned the best value of objective function shown in graph (i) for the same iterations.

From graph i) of figure 35 it can be seen that the objective function has been gradually reduced. From graph ii) it has been noted that after 100 iterations most of the parameters have a normalized error lower than 25%. The parameters that have shown the most difficulty in being detected are A_o and K_{roMax} (they have the greater nCE value).

The code has moved very slowly towards convergence, in fact it has taken more than twelve hours to perform 100 iterations. Moreover, the solution has not been satisfactory because the obtained values have not been sufficiently close to the exact ones.

Once the model has been updated and the appropriate optimization algorithm has been selected, it has become necessary to work to make the calibration process effective. Since performing a parameter optimization of the optimization algorithm is not possible in this case, a trial and error approach guided by a theoretical background has been used. A second important aspect that has been taken into account is the computational burden of the process. The optimization algorithm has taken more than 12 hours for perform just 100 iterations. This has been one of the main reasons for the rich acquisition of information from the literature which have been reported in Chapter 2.

5.2.1 Testing different objective function

Due to the insufficient quality obtained in the preliminary test, changes have been studied and applied to the new version of the methodology. One of the problems that has been observed in the preliminary tests is the difficulty of the optimization algorithm to identify the minimum of the objective function. Therefore, to simplify the optimum research, it has been chosen to perform the calibration on mono-dimensional data with regard to saturation. Hence, the dataset has been transformed into 1D before being altered. This transformation has been done evaluating the average saturation for each layer in which the core sample is divided along the Z axis (the vertical one); 44 values per time step have been thus obtained. The average saturation values have been altered with the function described in section 4.1.1 using a coefficient of variation of 1%. Afterwards, the objective function has been adapted to be able to compare the 1D dataset with the data of the simulations analysed by the optimization algorithm. So, even the solutions of the simulation done by the optimization algorithm has been analogously transformed into mono dimensional. The objective function has been transformed into:

$$f_{obj} = \frac{\sum_i^{N_{time\ step}} \sum_j^{N_{piani}} \left(\overline{s_{ij}^*} - \overline{s_{ij}}\right)^2}{N_{time\ step} * N_{piani}} + \frac{\sum_i^{N_{time\ step}} (\Delta Pn_i^* - \Delta Pn_i)^2}{N_{time\ step}} \qquad (5.14)$$

where $\overline{s_{ij}^*}$ is the, average on layer, sampled saturation value (of the synthetic dataset) and $\overline{s_{ij}}$ is the, average on layer, saturation value obtained from the simulation done by the optimization algorithm evaluated in j-th layer at i-th time step.

The input dataset to the calibration problem has been the one described in section 5.1.3, realized with the parameters available in the table 8.

The first applications of the methodology thus realized has led the optimization algorithm to converge at a point very far from the exact solution (a possible critical point) leading to an extremely high nCE (result not reported). The possible causes of a worsening in the results of the optimization algorithm has been studied. A thorough analysis of the workflow has been blamed on the methodology used to alter the data. In fact, by altering

the dataset after the average saturation calculation the measurement errors have been added not coherently with the reality. Therefore, in the next version of the methodology the dataset has been first altered and then the average saturation has been calculated.

The next calibration procedure has been set leaving the same objective function and keeping the domain limits reported in the table 8; in practices the only difference with respect to the previous workflow has been the new input dataset.

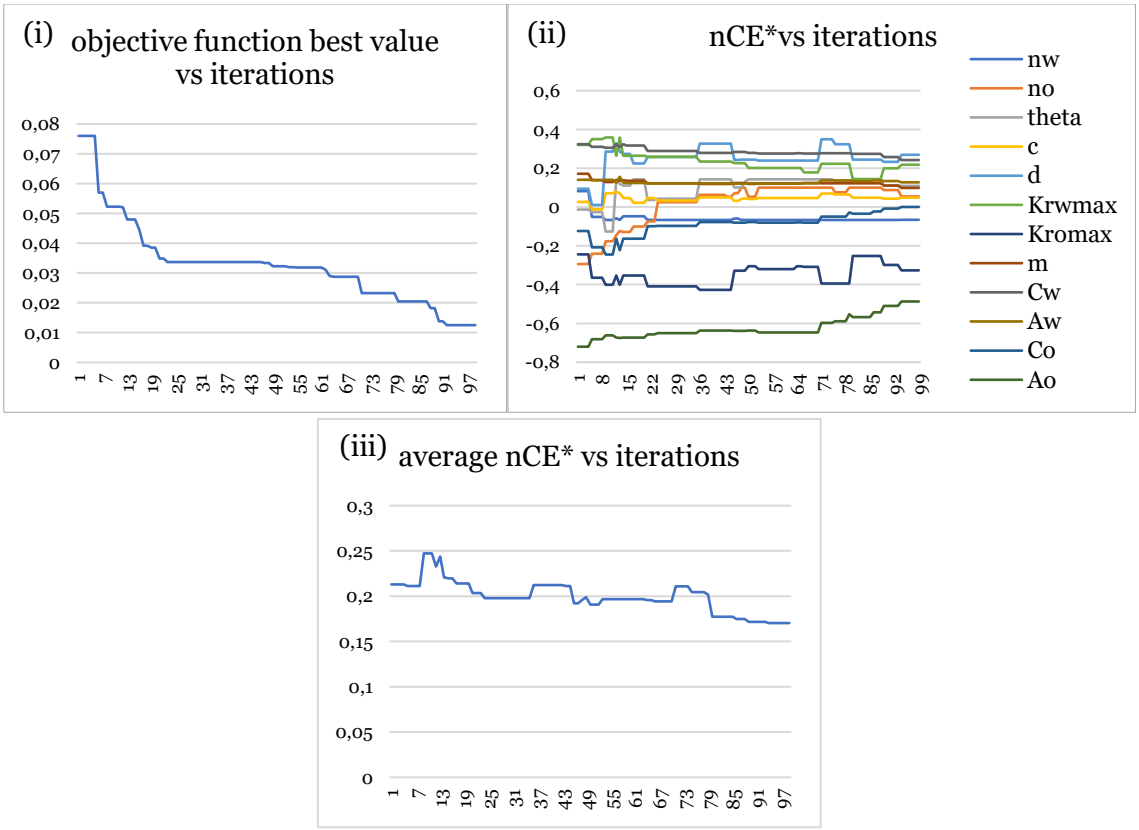

Figure 36: The graph (i) represents the best value obtained by evaluating the objective function during the iteration numbered on the horizontal axis. The graph (ii) represents the value of nCE for all the parameters of the simulation program that belong to the set of parameters that returned the best value of objective function shown in graph (i) for the same iterations, the graph (iii) represent the average among all the parameters nCE* represented in the graph (ii)*

With this methodology, it has been possible to identify a set of parameters that are more similar to the exact solution ones than those obtained in the preliminary test. The most critical parameters have been the A_o parameter of the Skjaeveland model and the maximum relative oil permeability. Since this evaluation has been done just to acquire information and since the objective has been to obtain better results than those obtained, this method has not been pursued, but the observations made on average values and critical parameters have been taken into account in the next updates; so, the next evaluations have used only a 3D dataset.

A second aspect that has been evaluated of the objective function has been the weight to be assigned to the two components of the objective function.

$$f_{obj} = w_{rs} \cdot \frac{\sum_i^{N_{time\ step}} \sum_j^{N_{celle}} \left(s_{ij}^* - s_{ij}\right)^2}{N_{time\ step} \cdot N_{celle}} + \frac{\sum_i^{N_{time\ step}} (\Delta Pn_i^* - \Delta Pn_i)^2}{N_{time\ step}} \qquad (5.13)$$

Since there are only two components, only one weight has been added to the saturation residue one (w_{rs}) to be able to choose the relative importance between them within the objective function. The choice of the relative weight has been made using the sensitivity analysis tool. For this purpose, various local sensitivity analyses have been carried out on different versions of the objective functions. Specifically, some functions that increased the weight of the two components have been compared to the objective function without added weights. The local sensitivity analysis has been carried out with the same methodology seen in section 5.1.4.. Thanks to this comparisons, it has been noted that the objective function that gives more importance to the saturation residue has increased the relative importance of some of the parameters of the Skjaeveland function (the one identified as critical in section 5.1.4.). Furthermore, tests with this objective function confirmed what has just been stated, obtaining lower average nCE* (figure 37). (the sensitivity analysis comparison is reported in appendix C)

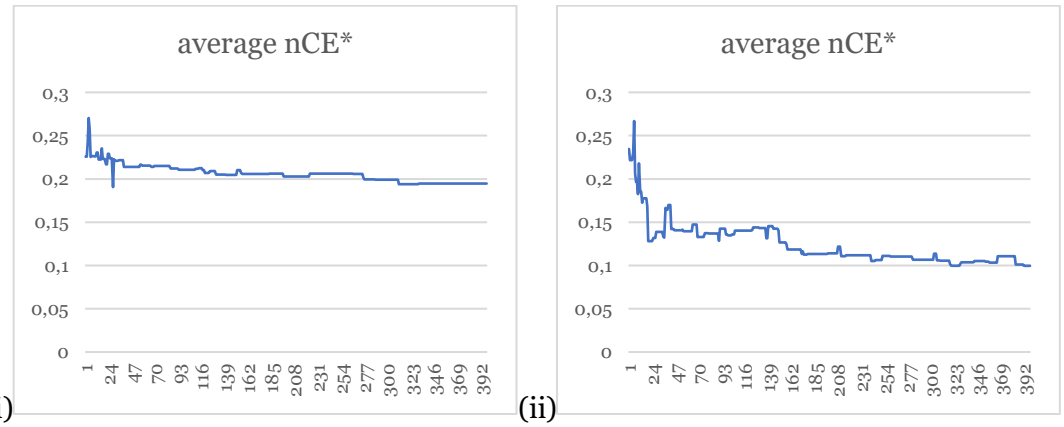

Figure 37:Two different simulation with the only different setting in the weight in the objective function (i) report the average nCE with Wrs =1 (ii) report average nCE* with Wrs=10*

5.2.2 Effect of the population size

Previous applications of genetic optimization algorithm [65] highlighted the importance of a proper choice of the number of individuals in the population: if the population is too small it is possible that the algorithm converges too fast not exploring well all the domain. The result may be that the residuals (and with them the value of the objective function) remain higher if the algorithm locks in local minima. If the population is too large the genetic algorithm could waste computational resources lengthening the waiting time. In the theoretical description of the MATLAB function [59] it is recommended, to avoid the just described problem, to use a population equal to ten times the number of parameters or at least equal to 100.

To investigate the effect of the population size, it has been necessary to take advantage of more powerful computational resources: the optimization algorithm was launched on a cluster available at Politecnico di Milano.

Two solutions of the inversion process have been compared: the first has been carried out with a population of twenty chromosomes (individual in genetic algorithm) and the second with a population of one hundred.

Population of 20

info			
algorithm	DE		
Population	20		
Stop	84	iter	
CR	0,3		
F	0,3		
Min objective function	0,008		
tot time	50400	S	14h

Population of 100

info			
algorithm	DE		
Population	100		
Stop	10	iter	
CR	0,3		
F	0,3		
Min objective function	0,008		
tot time	30000	S	8,3h

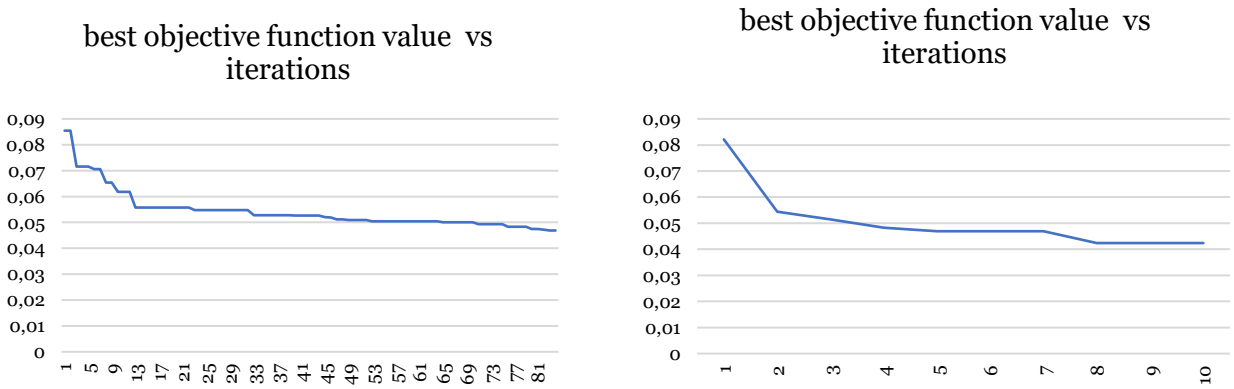

Figure 38:Comparison between the methodology with a population of 20 individuals in the optimization algorithm and the same methodology with a population of 100 individuals in the optimization algorithm.

From the graph has been noted that, as expected, the population of 100 individuals has led to better results. In a shorter time and with a very limited number of iterations a lower value of the objective function has been obtained. With a small number of iterations, the residuals have been very low, therefore the algorithm still had enough particle dispersion in the domain to explore the space in order to identify a better solution. The main problem has remained the computational cost. Unfortunately, every single simulation has needed long computational time. Therefore, having to estimate a so elevated number of members of the population for every iteration has led to a very long time for the overall process.

Due to the improvements observed from the increase of the numerousness of the population, a simulation with a population of 40 individuals has been carried out. The parameters to individuate and the imposed limits have been those described in table 8 and the objective function used is the function 5.2.1. In order to have a sufficient speed of convergence the CR has been set to 0.35. The optimization algorithm parameters and the results are reported below.

Algorithm,	DE
Population	40
CR	0,35
F	0,3

Table 9:Summary table of the settings of the optimization algorithm

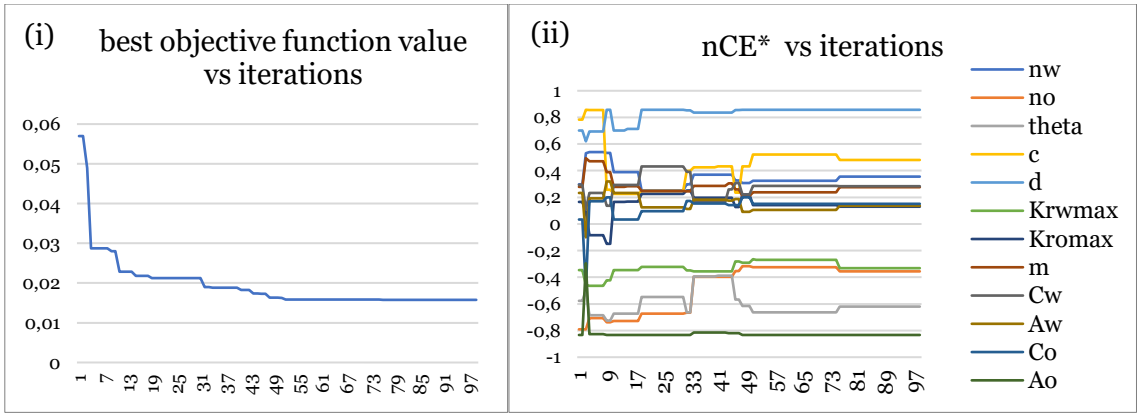

Figure 39: The graph (i) represents the best value obtained by evaluating the objective function during the iteration numbered on the horizontal axis. The graph (ii) represents the value of nCE for all the parameters of the simulation program that belong to the set of parameters that returned the best value of objective function shown in graph (i) for the same iterations.*

It has been possible to infer that the algorithm has reached a convergence since the value of the residuals remains constant for a large number of iterations. Despite the progress, the value has remained twice the minimum obtainable value and so the solution that has been identified is not the exact one. Observing the nCE*, it has been easy to understand that the identified parameters do not correspond to the correct solution. Additionally, the convergence of the algorithm has been confirmed noting that as the iterations increase the parameters chosen as solution do not change. These results should not be directly compared with the results previously shown because they represent two different conditions; in this case the algorithm has performed twice as many iterations.

5.3 FINAL VERSION OF THE WORKFLOW

Thanks to all the analyses described in the previous sections, a sufficient amount of information has been collected in order to refine the calibration process and to obtain reasonable results. Later on, the methodology has been tested under different conditions to evaluate its applicability. In the current chapter the calibrations for system with different wettability and for model with different degrees of refinement are described. In the end, the model is verified with a more altered dataset.

5.3.1 Best settings

The final idea has been to combine all the positive aspects seen from the previous analysis in order to create an effective and robust methodology. For this purpose, a grid coarser than the one available has been created. With this grid the methodology has been able to combine all the aspects previously seen returning the results in a reasonable time; i.e. the new grid would have been able to use a population of 100 individuals to carry out the calibration with a much lower time per iteration. In addition, the methodology would have exploited the positive aspects deriving from the calculation of the average between several cells in a similar way to the calibration carried out on the mono-dimensional model described in section 5.2.1.. Finally, the importance of the saturation component to the

entire objective function has been 10 times compared to the pressure drop component; this change has been made coherently with the observations reported in section 5.2.1.

The new grid had a refinement ratio respect to the coarse grid equal to the refinement ratio between the medium grid and the coarse grid (more details are available in chapter 3).

Coarsening information						
Grid name	**X**	**Y**	**z**	**cell tot**		**Rrefinement ratio**
Fine	42	42	178	313992	**F-C**	71,36181818
med	20,62236	20,62236	87,39951	37169,41	**F-M**	8,447592449
Coarse	10	10	44	4400	**M-C**	8,447592449
Very Coarse	5	5	21	525	**C-VC**	8,380952381

Table 10: Summary of all the information on the grids used. On the left side are reported the information about the refine ratios

The new grid had 525 cells and the proportions between the intervals of subdivision in the axes have been kept equal to the ones in the other grids. The very coarse grid has obtained a value of the saturation component of the objective function, calculated between the synthetic dataset and the saturation values obtained from the simulation conducted with the exact parameters using the new grid, lower than the one evaluated with the previous grid. This observation has been consistent with the observations already reported in section 5.2.1. for the averaging of the saturation values in the layers (mono-dimensional; result not reported).

The inversion procedure has received in input the same dataset seen in the section 5.1.3. and has applied all the setting of the methodology just explained. The results of the calibration process are shown below.

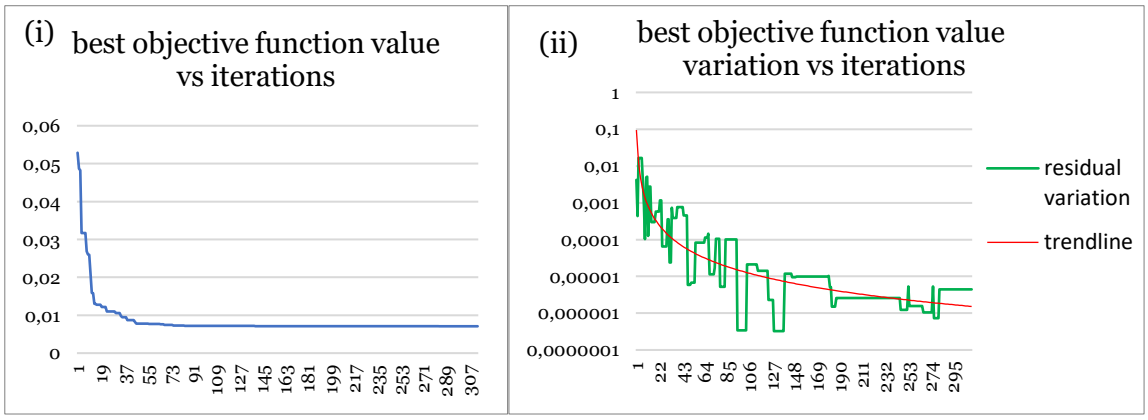

Figure 40: The graph (i) represents the best value obtained by evaluating the objective function during the iteration numbered on the horizontal axis. The graph (ii) represent the value of the last variation of best the objective function value reported in graph (i).

It can be seen from the figure 40 that despite all the upgrade in setting, the calculation of a large number of iterations has been necessary. The objective function best value and the objective function best value variation have been used as convergence criteria. From the

best objective function value graph, it has been noted that during the first 100 iterations the value drops abruptly, as expected, and quickly leads to a value very similar to the minimum obtainable. If only the observation of the residues had been used as a convergence criterion, the long plateau that is present between iteration 100 and iteration 250 would have induced to ending the calculation prematurely. Indeed, a second criterion has been added for the evaluation of the convergence. The variations of best objective function value have been used to add the necessary information. In order to have a usable graphic tool the new semi logarithmic graph has shown for each iteration the last reduction of the best objective function value. When these variations have become infrequent and small, the convergence could be inferred. The calculations have been stopped with confidence after 300 iterations, as it can be observed in the figure 40. Proceeding with the optimization after the plateau has been important to ensure that even the less significant parameters were calibrated.

The control over the values of the parameters obtained as a solution and the parameters with which the dataset has been generated confirmed the good quality of the solution.

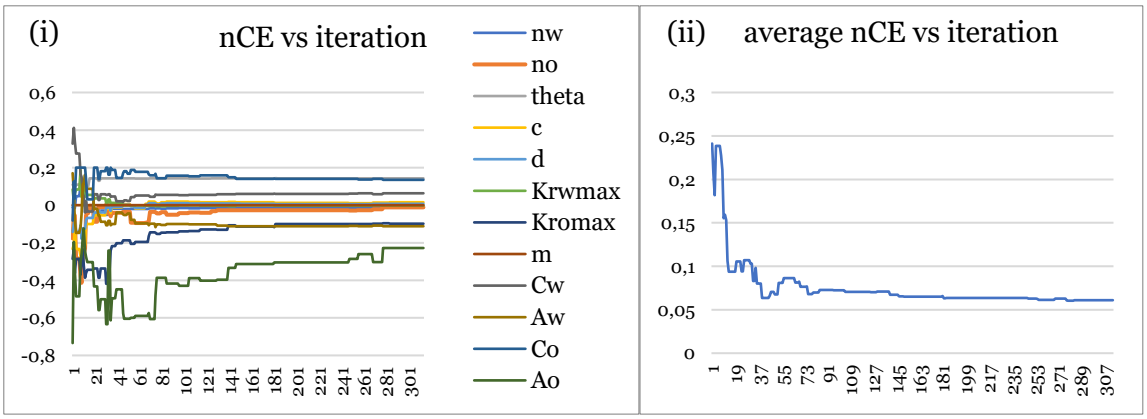

Figure 41:The graph (i) represents the value of nCE for all the parameters of the simulation program that belong to the set of parameters that returned the best value of objective function. The graph (ii) represent the average among all the parameters nCE represented in the graph (i).

From the graph representing the average normalised calibration error with respect to the exact solution values, it has been possible to notice that the error with which averagely the parameters have been calibrated is very low (less than 0.1). The normalised error for each individual parameter does not exceed 10%. The main criticality of this model is the very coarse grid. With a limited number of cells, the characteristics noted in the visual analysis of the real sample described in chapter 3 (diagonal layers) has not been captured. Moreover, the very coarse grid has deformed the cylindrical geometry; this phenomenon could lead to problems in the case of a sample with greater anisotropicity and inhomogeneity along the volume or with complex measurement errors. Therefore, the developed program has been verified only for systems that do not present the just described problems.

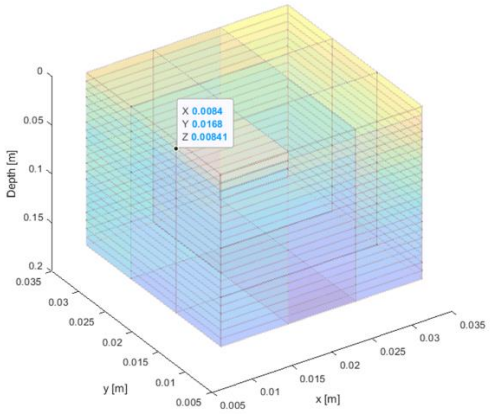

Figure 42:Very coarse grid

5.3.2 Workflow applicability

Once the workflow has been set up considering all the collected information, it has become necessary to check if the program is able to evaluate different datasets from the one seen above. For this purpose, synthetic datasets have been created to simulate different situations reflecting the possible real cases.

Before the methodology applicability tests, a new model update has been made available and a prior information has been measured from the research group that has implemented the model. Specifically, a correlation has been added which links the parameters of the Skjaeveland model. The correlation has identified the parameter C_o given the other parameters (A_o, A_w, C_w) and a new parameter n, which represents the saturation value for which the capillary pressure is equal to 0. The research group has also been able to experimentally evaluate the absolute permeability value (the parameter k). Using this parameter, the parameter m has been evaluated by inverting the Porosity-absolute permeability relationship (section 3.2.3.3).

$$m = \frac{(\log_{10} k - q)}{\phi} = 14.69 \qquad (5.15)$$

In this way the problems that could arise due to the plateau highlighted in the sensitivity analysis for parameter m have been solved.

Since the model has been modified, besides performing a process with a synthetic dataset generated in different condition, it has been verified if the code was still able to return results like those previously obtained in oil-wet conditions. The combinations of parameters have been chosen coherently with the wettability. It has also been verified if the relative permeability graphs obtained from the Corey model and if the graph obtainable with the Skjaeveland model possessed the appropriate characteristics. The analyses of the Corey graphs carried out in this regard are reported in the section 2.1.9 as an example of graphs with different wettability (figure 8).

Water-wet

	parameters	ub	lb
n_w	5,8	2	8
n_o	1,7	2	8
theta	62	40	150
c	0,3615	0,01	0,5
d	0,1316	0,01	0,5
K_{rwmax}	0,125	0	0,2
K_{romax}	0,74	0,5	1
m	14,69	-	-
C_w	0,34	0	0,5
A_w	0,569402	0,2	1,5
n	0,22	0,05	0,95
A_o	0,951299	0,9	1,5

Oil-wet

	parameters	ub	lb
n_w	3	2	8
n_o	7	2	8
theta	115	40	150
c	0,3615	0,01	0,5
d	0,1316	0,01	0,5
K_{rwmax}	0,7	0	0,2
K_{romax}	0,8	0,5	1
m	14,69	-	-
C_w	0,16	0	0,5
A_w	1,08	0,2	1,5
n	0,1	0,05	0,95
A_o	0,951299	0,9	1,5

Table 11: The table shows the values of the parameters used to generate the datasets in the two conditions (water wet and oil wet) and the domain for the parameters (upper and lower limit).

The objective function and the settings of the optimization algorithm have been kept the same as those seen in the previous subchapter (table 9)

The first application of the methodology has been done in water wet conditions. It must be noticed that the parameter theta has not been in the indeterminable condition (>120).

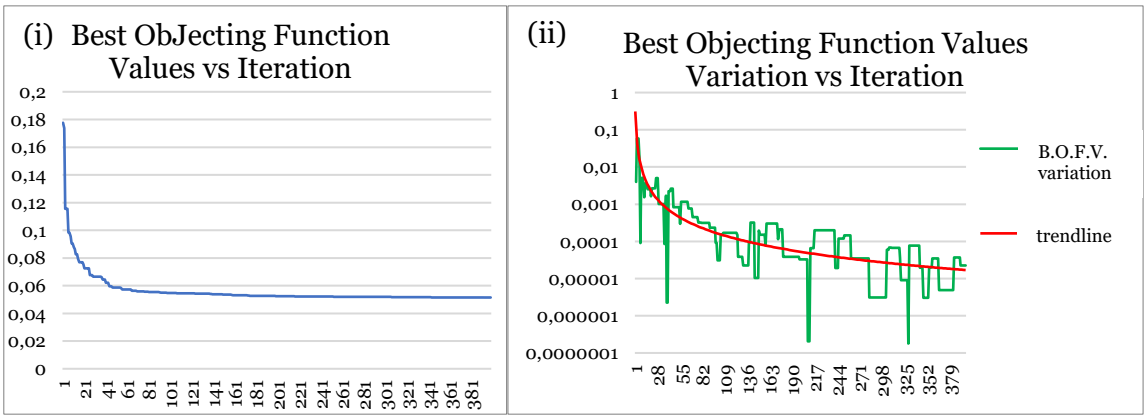

Figure 43: water-wet conditions. The graph (i) represents the best value obtained by evaluating the objective function during the iteration numbered on the horizontal axis. The graph (ii) represent the value of the last variation of best the objective function value reported in graph (i).

No automatic stopping criteria has been used as already done in the previous calibration; the result has been monitored manually. From the residue variation graph frequent variations have been noticed, it means that the solution is frequently updated to a better one. Hence, a large number of iterations have been performed in order to calibrate all the parameters. The algorithm has been stopped when the variations, even if frequent, were very small. 27 hours of calculation has been used from the algorithm to perform more than 350 iterations. From the graph of best objecting function values, it has been noticed that the algorithm quickly has led to a very low value and then it has slowed down the convergence.

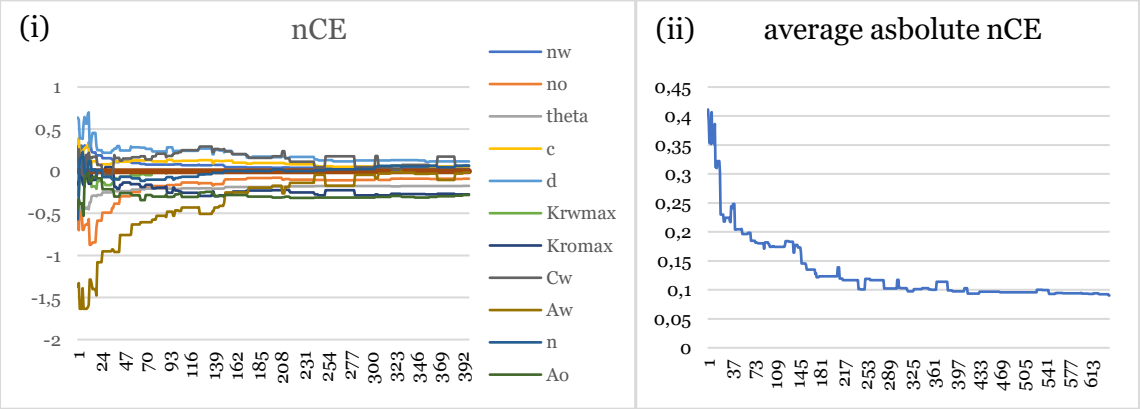

Figure 44:Water-wet conditions. The graph (ii) represents the value of nCE for all the parameters of the simulation program that belong to the set of parameters that returned the best value of objective function. The graph (ii) represent the average among all the parameters nCE represented in the graph (i)

The obtained solution has been good even using a water wet dataset. The obtained average normalized convergence error has been lower than 10%. The parameters that have been determined with a lower accuracy are A_o and K_{romax} consistently with the sensitivity analysis (section 5.1.4.).

The second analysis has been carried out on a synthetic dataset for a system tending towards oil-wet condition. The parameters are different from those successfully used in the previous section to verify not only the model updates but also the applicability to different wettability datasets.

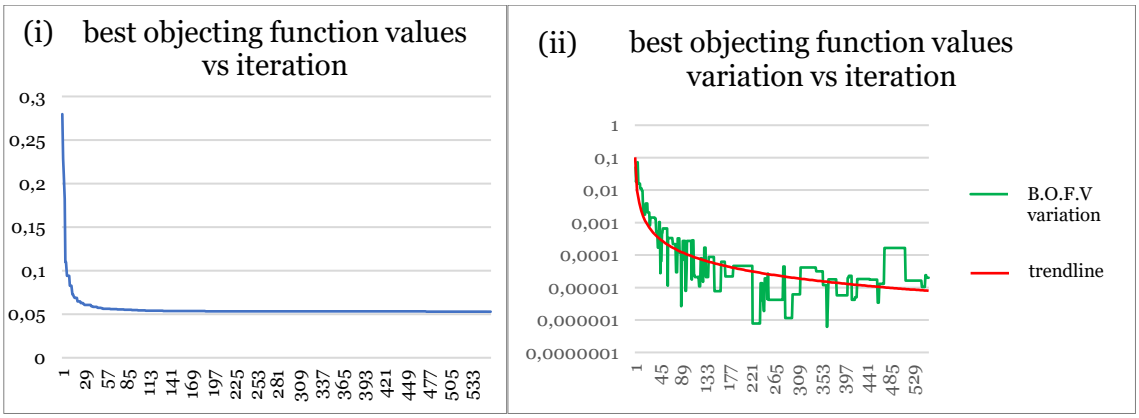

Figure 45:Oil-wet conditions. The graph (i) represents the best value obtained by evaluating the objective function during the iteration numbered on the horizontal axis. The graph (ii) represent the value of the last variation of best the objective function value reported in graph (i).

The stop criterion has been the same used for the water-wet dataset. Again, a rapid reduction in residues has been observed, and subsequently smaller variations led to infer the convergence of the optimization algorithm.

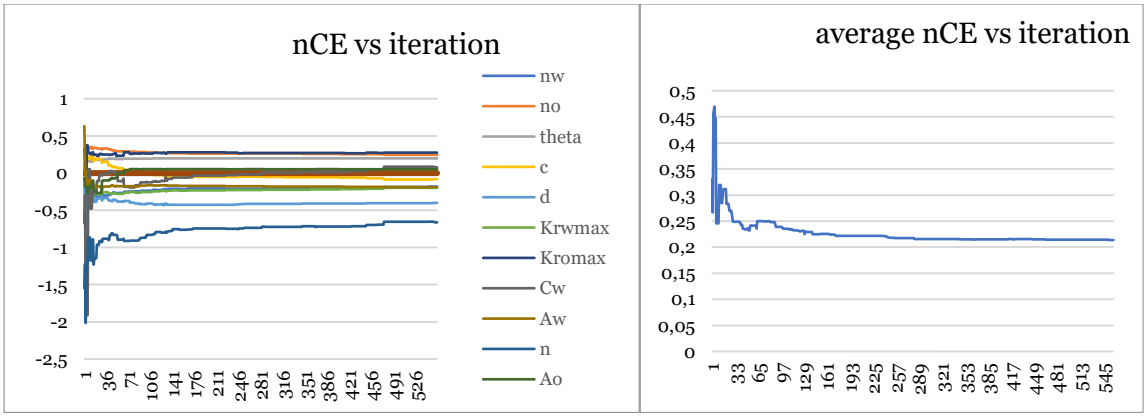

Figure 46:Oil wet condition. The graph (ii) represents the value of nCE for all the parameters of the simulation program that belong to the set of parameters that returned the best value of objective function. The graph (ii) represent the average among all the parameters nCE represented in the graph (i)

From all the graphs that show the calibration error, it has been possible to observe that in the first iterations the parameters have oscillated a lot, getting quite quickly close to the exact value, and then the calibration has proceeded slowly. The exceptions have been the parameters that, in the various sensitivity analysis, has shown to be less influential on the objective function value. The normalized calibration error of these parameters has reduced in the last iterations. A parameter that apparently has not been calibrated correctly is parameter n. In reality parameter n, besides having a low influence on the objective function value, has a very small value with respect to the range of values it can assume. Therefore, the normalisation with respect to the exact value makes the calibration error of this parameter seem very large with respect to what would be noted by normalising the same error on the range of values that it can assume.

Finally, the last analysis has been conducted on a dataset that simulates a larger measurement error. The calibration has been carried out to prove the applicability of the methodology in the case of experiments conducted with measuring instruments with worse characteristics. Since the real measurement instrument could not be analysed and therefore the error that it introduces in the making measure could not be determined, the worse measurement conditions have been simulated. The measurements have been carried out in the laboratory and in a controlled environment, so this worse measurement errors caused by the measuring instrument have been assumed well described by a Gaussian distribution with a variance equal to the 5% of the average value (saturation and pressure drop). Specifically, the function for data alteration has been used by setting the variance coefficient equal to 5% (see section 4.1.3.).

The parameters used to generate the dataset are the water wet parameters in the table 11.

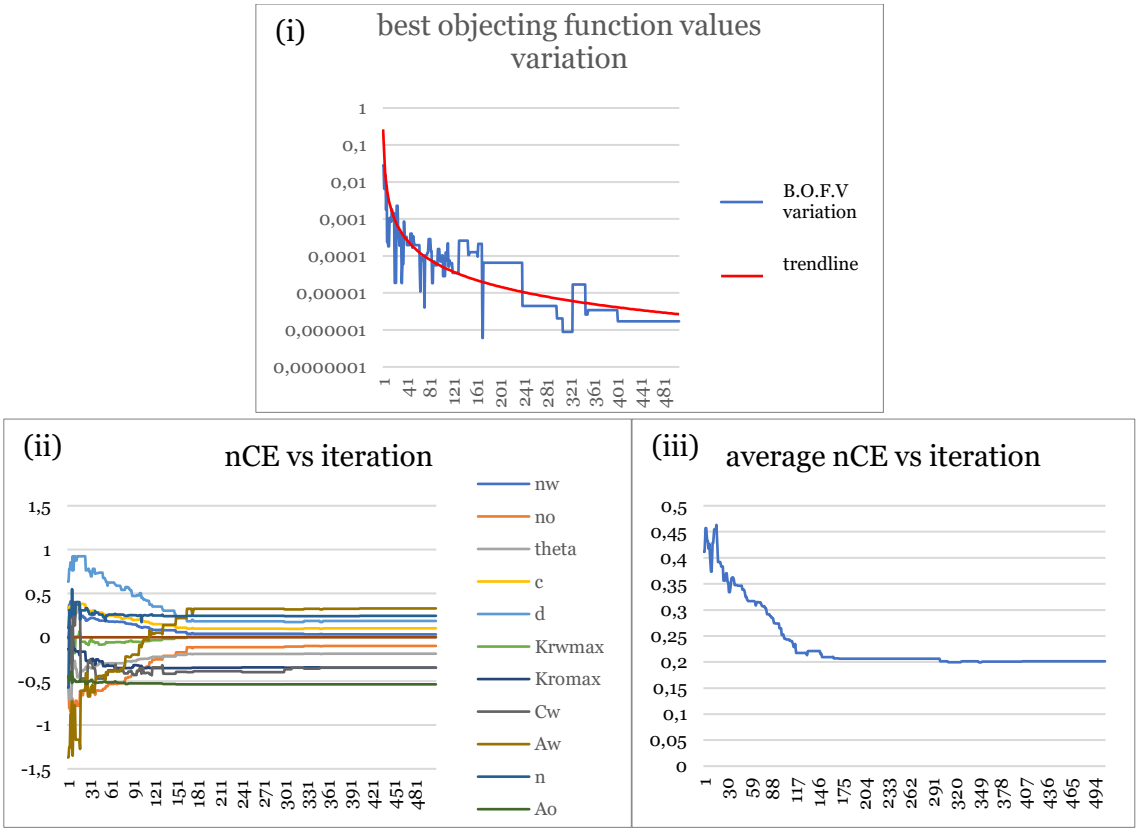

Figure 47: Increased measurement error. The graph (i) represent the value of the last variation of best the objective function value. The graph (ii) represents the value of nCE for all the parameters of the simulation program that belong to the set of parameters that returned the best value of objective function. The graph (iii) represent the average among all the parameters nCE represented in the graph (ii)

The stopping criterion has been the same used in all the previous analyses. The Entire optimization has taken more than 25 hours. Compared to the dataset generated in the same condition (water wet) with a more moderate alteration the results have shown a lower quality as expected. Another important aspect to be notice has been the normalised calibration error which has been reduced more slowly in the first iterations compared to conditions where the data set is less altered. This phenomenon indicated a more difficult search for the region where the exact solution has been located. The parameters that have been calibrated worse are those reported during the sensitivity analysis. Overall, the calculated solution is not too far from the exact solution.

6 CONCLUSION

The objective has been to create a multi-phase flow inversion methodology based on three-dimensional data at the laboratory scale. The creation of synthetic datasets that simulate data from a real test has been made possible thanks to the information available on the core sample experiment. In order to simulate the phenomena that characterise the flows of the experiments, a specific programme has been used; the latter has been specifically designed to study the experiment at the laboratory scale. The programme is able to simulate the two-phase flow inside a core sample; e.g. the one analysed in this study that characterises the injection of water inside a sample initially saturated with oil.

The use of synthetic data sets has made possible to introduce a series of advantages over the use of data from experiments; the main ones are: the possibility of knowing a priori the information (in the form of parameters that characterize the closure equation contained in the simulation program) that must be extrapolated from the data, the possibility of creating data that simulate experiments in different situations (different wettability) without having to conduct new experiments and the possibility of introducing a measurement error that simulates different qualities of the instrument.

The construction of the methodology has required a rich acquisition of information to allow the understanding of the phenomena that characterize the problem. The physics-based information has been integrated with the study of the inverse problem and of the optimization methods used within it. Thanks to an in-depth study of the simulation program and all the models contained within it, the limits within which each parameter can be identified have been defined and consequently the space in which the solution can be found have been determined. In order to guarantee a wide applicability of the methodology the use of a conservative approach has been fundamental; thanks to this approach, all the possible solutions have not been excluded by imposing too strict limits.

Starting from the theoretical knowledge acquired in the literature, a first attempt workflow for the solution of the inverse problem has been realized. Despite the improvements made to the simulation program, the methodology had some critical points in the first iterations of the optimization algorithm that did not allow to obtain a solution. In this regard, the choice of the appropriate optimisation algorithm has been a key aspect. Given the complexity of the simulation program, all the optimization algorithms that required the calculation of the derivative of the objective function have been discarded a priori. Therefore, the choice has been the population algorithms that thanks to their characteristics has proven to be adequate. Unfortunately, the first algorithm chosen, the particle swarm optimization, has led to problems in the evaluation of the objective function. Thanks to numerous analyses, the cause of the problem has been individuated as the evaluation of combinations of parameters which (often at the limits of space) did not reflect physically possible situations. These combinations of parameters have caused problems to the program for the calculation of the simulations. Therefore, the methodology has not been capable to obtain results to be evaluated within the objective function. The solution at this problem has been identified by analysing the phenomenon from which the particle swarm optimization has been inspired. Since the algorithm simulates the behaviour of a flock of birds that exchange information and explore the space to converge in a point of interest (the minimum of the objective function), the problem has occurred at the beginning of the optimization. In fact, during the first iterations, the swarm of particles has moved in a dispersive way leading to have many particles in areas of space where the combinations of parameters are critical for the program. Therefore, this

combination of parameters has caused problems to the simulations necessary for the evaluation of the objective function. The optimization algorithm has been replaced with the Differential Evolution, which if properly set, while maintaining the properties of the population algorithms, does not exhibit the same behaviour in the initial iterations.

Thanks to the differential evolution optimization algorithm the methodology has been able to obtain a result. The objective has therefore been changed becoming that of obtaining a set of parameters as similar as possible to that used for the generation of the synthetic data (the exact solution). The first improvement has been introduced in the objective function in which a component linked to the residues of the pressure drop at the ends of the sample has been added. The weight to be assigned to this component within the objective function has been selected thanks to a sensitivity analysis on the objective function. To the term linked to the saturation residue has been assigned a weight ten times greater than the one linked to the pressure drop term.

Another key point of the updates of the workflow has been the replacement of the grid used for the simulations required by the optimization algorithm. The first simulations have been performed with very fine grids that could take even minutes. These calculation times are not compatible with an optimisation algorithm that requires thousands of simulations. The solution identified has been the creation of a coarser grid that, in addition to greatly reducing the calculations, has shown to be effective in identifying parameters very similar to the exact solution. Furthermore, the reduction in calculation times has made it possible for the optimisation algorithm to use a larger population compatible with the need to determine 11 parameters. The main effect of the use of a larger population has been the ability to effectively explore the entire research domain by identifying the region where the exact solution is located. This effect has implied a determination of a solution composed of parameters very similar to those used to generate the synthetic dataset (the exact solution).

Finally, the project has included some tests to verify the applicability of the methodology in realistic cases. Specifically, the workflow has been demonstrated to be effective for systems with different wettability and to be able to determine the majority of the parameters under worse measurement error conditions.

The final version of the methodology has presented some difficulty in the determination of some of the parameters; specifically, Skjaeveland model parameters and the maximum relative permeability of the oil have presented the greater calibration error. Furthermore, it has been established that in the case in which the theta parameter is higher than 120, the parameter is not univocally identifiable ad so the S_{or} parameter is considered constant. One last criticality consists in the very coarse grid that does not allow to appreciate some characteristics of the sample (as the diagonal layer reported in chapter 3) and that could be important in cases of very inhomogeneous and anisotropic samples.

The greatest difficulties encountered during the development of the method have been: the blocking of the sample flow simulation model in the early stages of construction and the time required to test the various versions of the methodology, which have taken up to 30 hours each. Since the development of the workflow required several tests, the total computational cost has been very high.

Thanks to the work carried out, an effective methodology able to obtain important information from the core sample experiments has been developed. The main obtainable information are: the curves representing the trend of the relative permeability to the variation of the saturation of the phases themselves, the trend of the capillary pressure and other parameters that may be useful for the realization of models at the reserve scale. It is

envisaged that the methodology will be applied to real experiments. The workflow will return the results in a few hours if the calculation will be carried out in parallel processors.

APPENDIX A

Before the application within the workflow, a brief analysis has been made of the MATLAB functions that implement the two optimization algorithms used during the thesis work. The two functions are described in detail in the sections 5.1.2..

The two algorithms have been tested for functions that have plateau and local minima. The settings that have been imposed are the same used during the thesis analysis. A population of ten times the number of parameters has been used (equal to 100 for functions dependent on more than 10 parameters). The default weights have been left for the calculation of the velocity vector in the particle swarm optimization. The parameters used in the differential evolution algorithm were CR equal to 0.7 and F parameter equal to 0.3.

The first test has been made for Ackley's function, which has many local minima (figure 48).

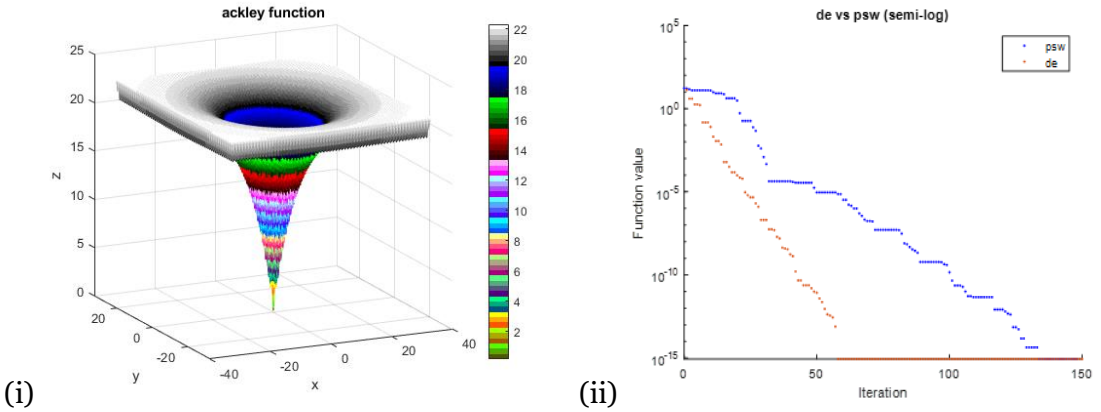

(i) (ii)

Figure 48: (i) 3D representation of the Ackley's function dependent on 2 variables (ii) value of the residue vs iteration, in orange the residues of differential evolution and in blue the residues of the particle swarm optimization.

The second test was made for Bale's function which has a plateau (figure 49).

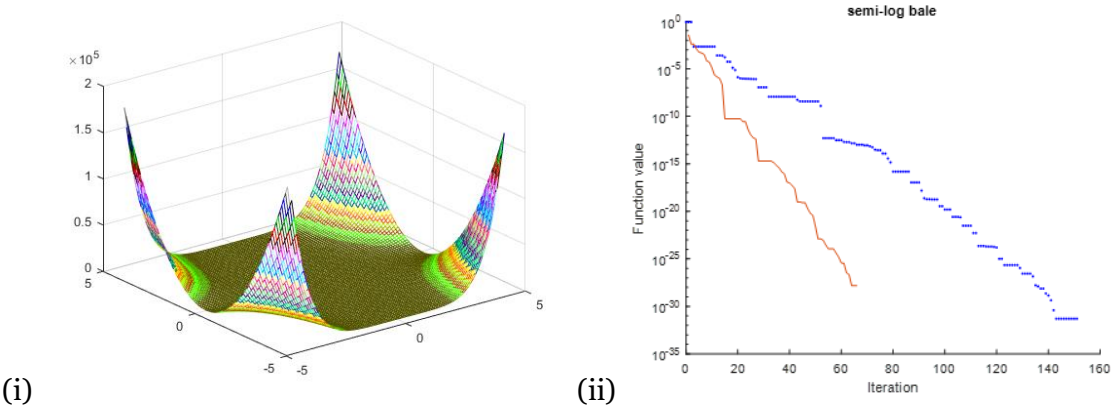

(i) (ii)

Figure 49: (i) 3D representation of the bale's function dependent on 2 variables (ii) value of the residue vs iteration, in orange the residues of differential evolution and in blue the residues of the particle swarm optimization,

The third test was conducted on the Bohachesky function (figure 50).

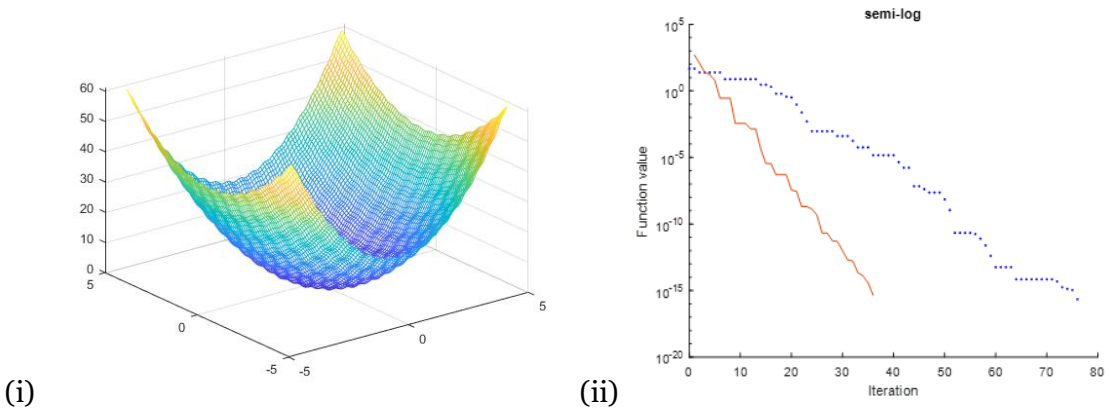

Figure 50: (i) 3D representation of the Bohachesky's function dependent on 2 variables (ii) value of the residue vs iteration, in orange the residues of differential evolution and in blue the residues of the particle swarm optimization

The above mentioned tests performed on two-dimensional functions with critical points (such as local minima and plateaus) showed that the functions have been able to quickly obtain the correct results. However, problems with few variables did not reflect the case studied in the thesis; therefore a 30-dimensional extension of the Ackley function has been also used. The function has many critical points such as the basic two-dimensional form. In this context the differential evolution has shown to be effective and correctly set. In particular it has been observed that with the parameter F=0.3 the function has been able to obtain the result avoiding a dispersive behaviour in space during the first iterations.

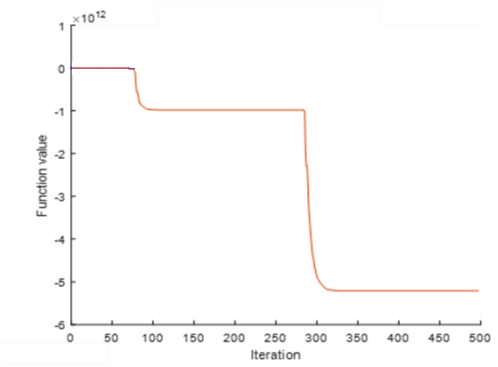

Figure 51:value of the residues with the differential evolution algorithm

APPENDIX B

This appendix reports the results of the sensitivity analysis described in section 5.1.4.. During the local sensitivity analysis all the parameters (except the one analysed that varies) are fixed to the values in green reported in table 8. For each parameter are reported in order: the component of the objective function related to saturation residues (eq 5.12), the component of the objective function related to the pressure drop residues (eq 5.13) and the objective function defined as the combination of two just mentioned components.

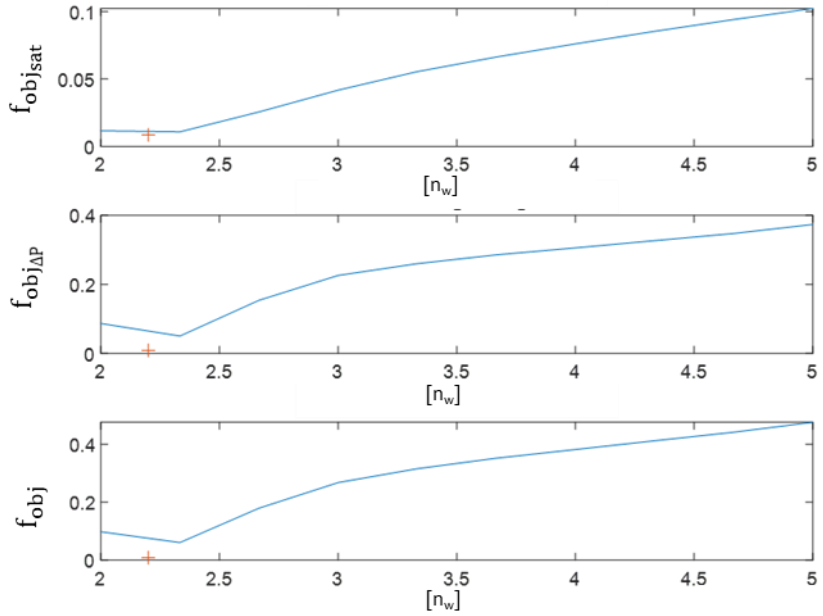

Figure 52: The graphs show result of the sensitivity analysis. On the horizontal axes are reported the values assumed by the parameter n_w while on the vertical axis are reported in order from top to bottom: the value of the component linked to the saturation residues of the objective function, the value of the component linked to the pressure drop residues of the objective function and the value assumed by the objective function. in red is reported the minimum value obtainable by the objective function in the exact value of the parameter under analysis (in all graphs).

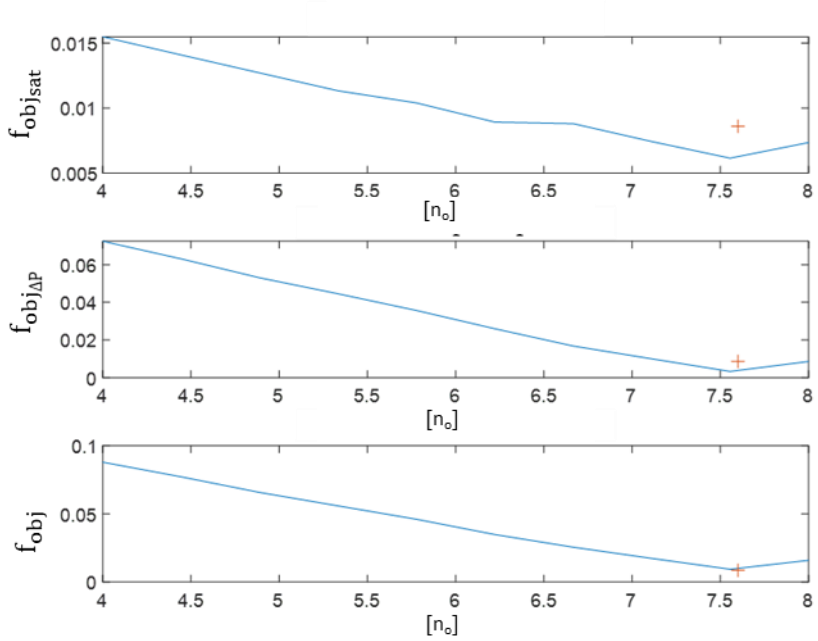

Figure 53: The graphs show result of the sensitivity analysis. On the horizontal axes are reported the values assumed by the parameter n_o while on the vertical axis are reported in order from top to bottom: the value of the component linked to the saturation residues of the objective function, the value of the component linked to the pressure drop residues of the objective function and the value assumed by the objective function. in red is reported the minimum value obtainable by the objective function in the exact value of the parameter under analysis (in all graphs).

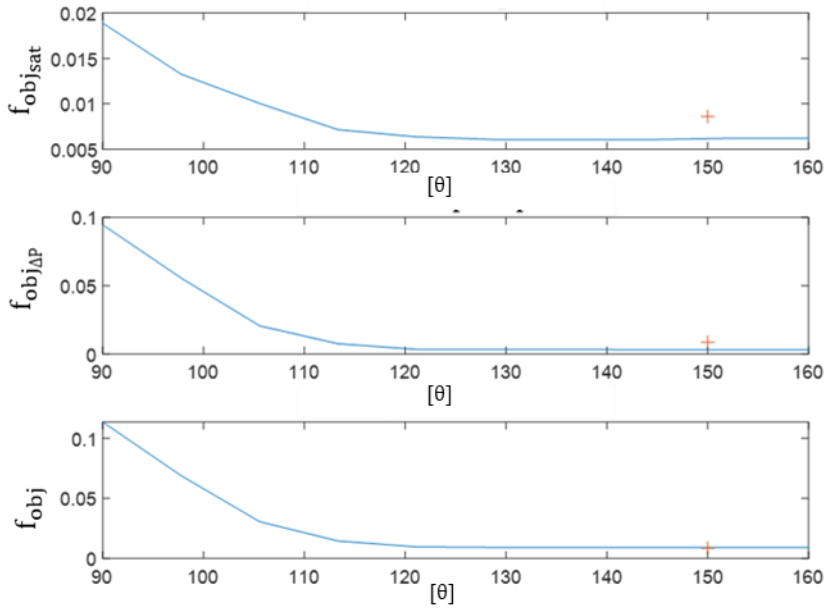

Figure 54: The graphs show result of the sensitivity analysis. On the horizontal axes are reported the values assumed by the parameter theta while on the vertical axis are reported in order from top to bottom: the value of the component linked to the saturation residues of the objective function, the value of the component linked to the pressure drop residues of the objective function and the value assumed by the objective function. in red is reported the minimum value obtainable by the objective function in the exact value of the parameter under analysis (in all graphs).

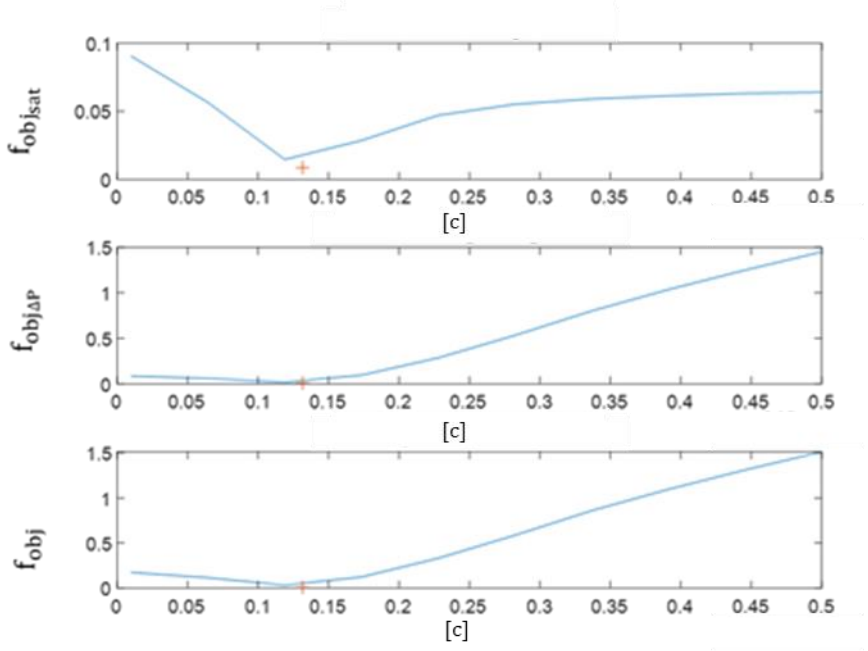

Figure 55: The graphs show result of the sensitivity analysis. On the horizontal axes are reported the values assumed by the parameter c while on the vertical axis are reported in order from top to bottom: the value of the component linked to the saturation residues of the objective function, the value of the component linked to the pressure drop residues of the objective function and the value assumed by the objective function. in red is reported the minimum value obtainable by the objective function in the exact value of the parameter under analysis (in all graphs).

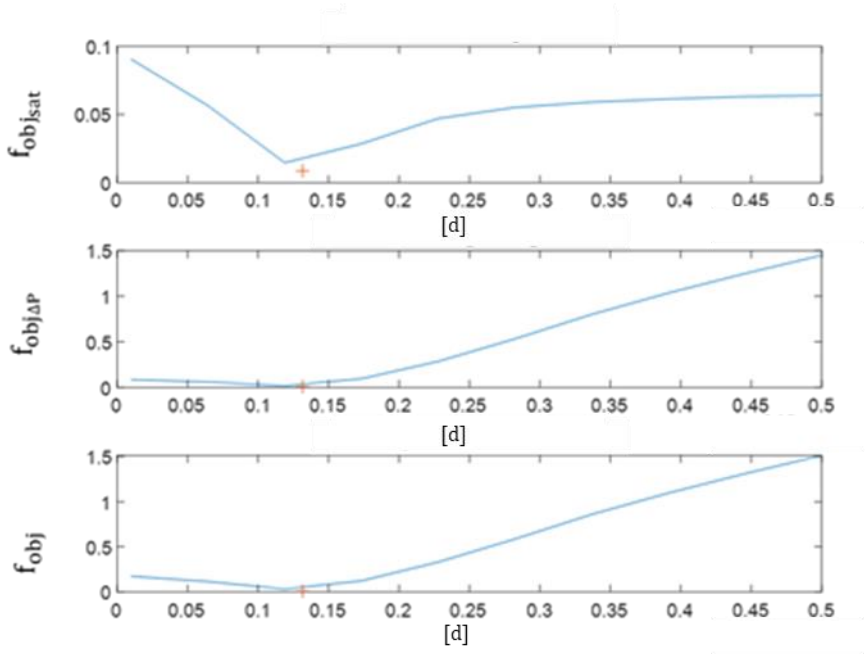

Figure 56: The graphs show result of the sensitivity analysis. On the horizontal axes are reported the values assumed by the parameter d while on the vertical axis are reported in order from top to bottom: the value of the component linked to the saturation residues of the objective function, the value of the component linked to the pressure drop residues of the objective function and the value assumed by the objective function. in red is reported the minimum value obtainable by the objective function in the exact value of the parameter under analysis (in all graphs).

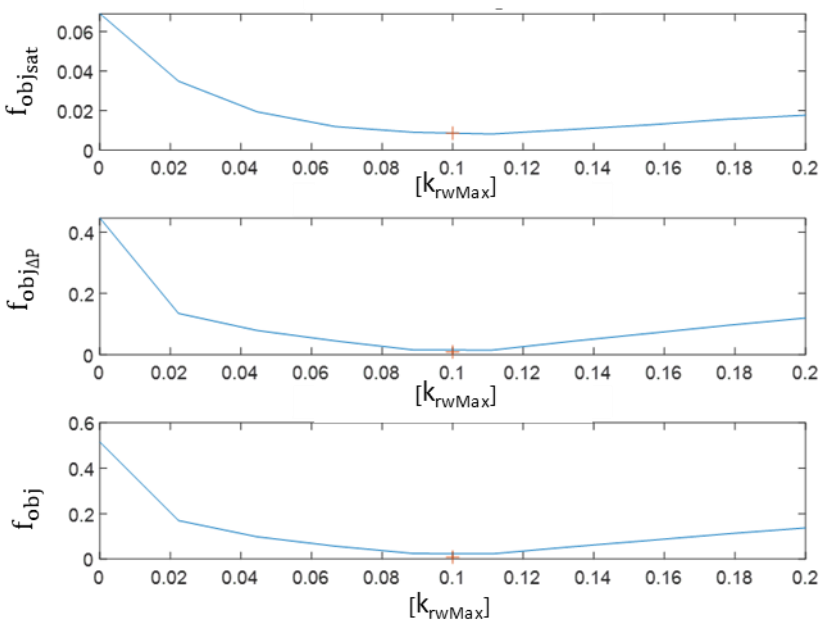

Figure 57: The graphs show result of the sensitivity analysis. On the horizontal axes are reported the values assumed by the parameter k_{rwMax} while on the vertical axis are reported in order from top to bottom: the value of the component linked to the saturation residues of the objective function, the value of the component linked to the pressure drop residues of the objective function and the value assumed by the objective function. in red is reported the minimum value obtainable by the objective function in the exact value of the parameter under analysis (in all graphs).

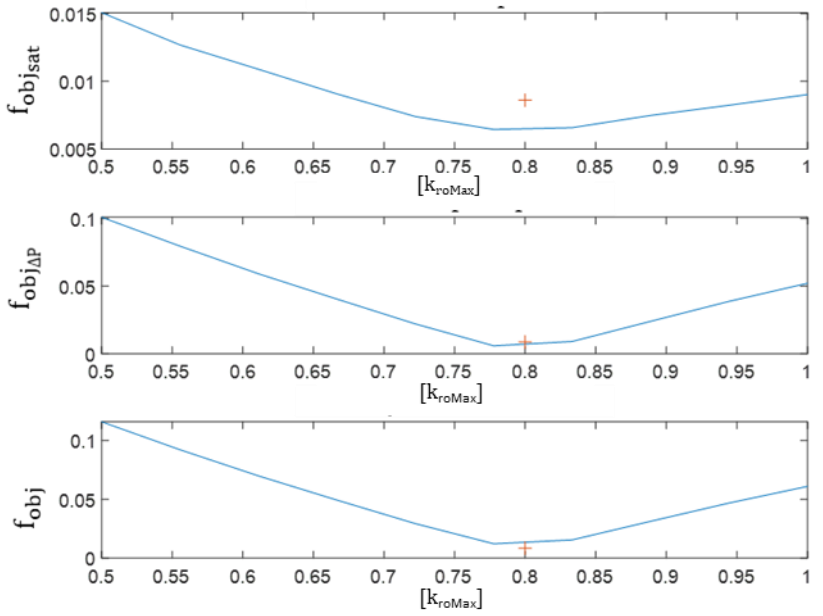

Figure 58: The graphs show result of the sensitivity analysis. On the horizontal axes are reported the values assumed by the parameter k_{roMax} while on the vertical axis are reported in order from top to bottom: the value of the component linked to the saturation residues of the objective function, the value of the component linked to the pressure drop residues of the objective function and the value assumed by the objective function. in red is reported the minimum value obtainable by the objective function in the exact value of the parameter under analysis (in all graphs).

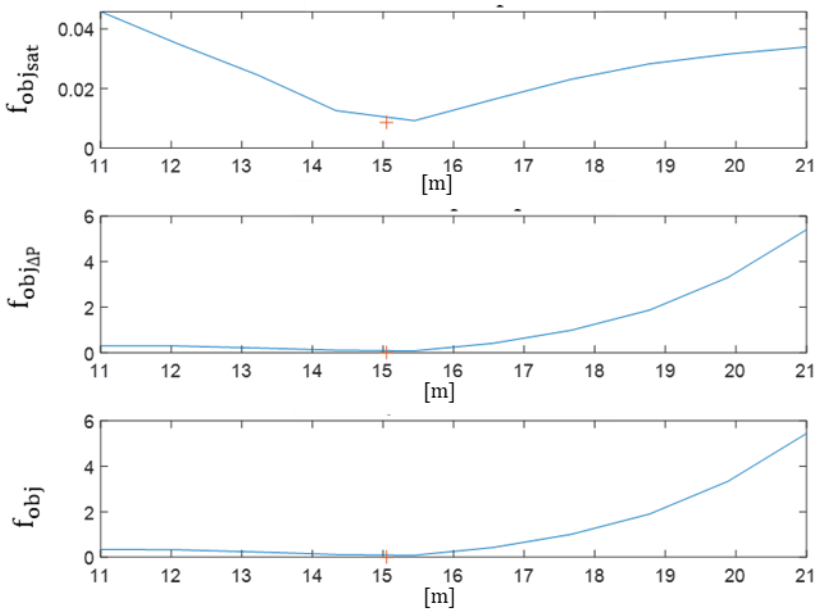

Figure 59: The graphs show result of the sensitivity analysis. On the horizontal axes are reported the values assumed by the parameter m while on the vertical axis are reported in order from top to bottom: the value of the component linked to the saturation residues of the objective function, the value of the component linked to the pressure drop residues of the objective function and the value assumed by the objective function. in red is reported the minimum value obtainable by the objective function in the exact value of the parameter under analysis (in all graphs).

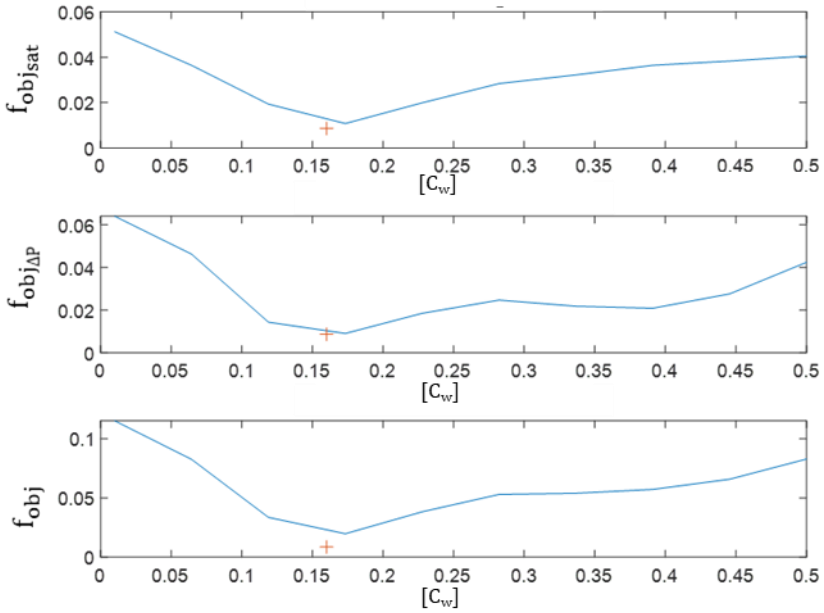

Figure 60: The graphs show result of the sensitivity analysis. On the horizontal axes are reported the values assumed by the parameter C_w while on the vertical axis are reported in order from top to bottom: the value of the component linked to the saturation residues of the objective function, the value of the component linked to the pressure drop residues of the objective function and the value assumed by the objective function. in red is reported the minimum value obtainable by the objective function in the exact value of the parameter under analysis (in all graphs).

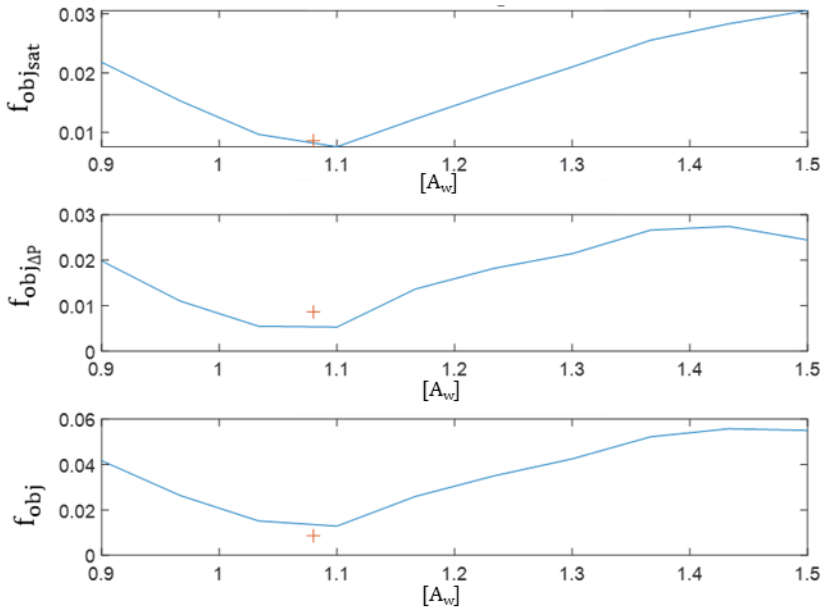

Figure 61: The graphs show result of the sensitivity analysis. On the horizontal axes are reported the values assumed by the parameter A_w while on the vertical axis are reported in order from top to bottom: the value of the component linked to the saturation residues of the objective function, the value of the component linked to the pressure drop residues of the objective function and the value assumed by the objective function. in red is reported the minimum value obtainable by the objective function in the exact value of the parameter under analysis (in all graphs).

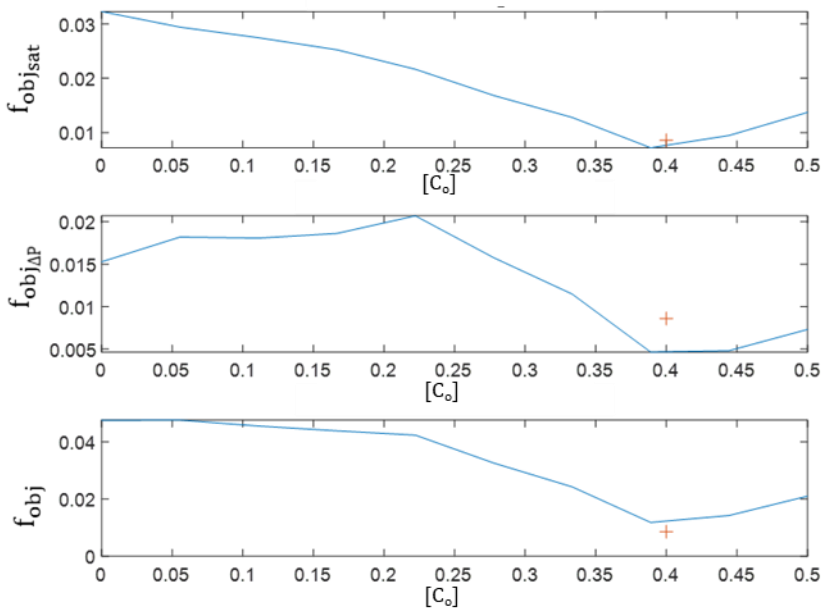

Figure 62: The graphs show result of the sensitivity analysis. On the horizontal axes are reported the values assumed by the parameter C_o while on the vertical axis are reported in order from top to bottom: the value of the component linked to the saturation residues of the objective function, the value of the component linked to the pressure drop residues of the objective function and the value assumed by the objective function. in red is reported the minimum value obtainable by the objective function in the exact value of the parameter under analysis (in all graphs).

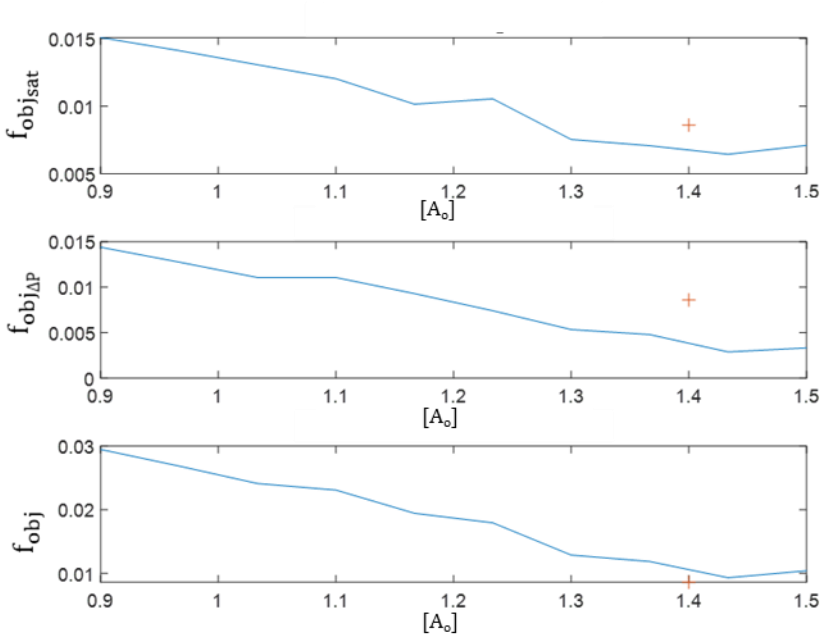

Figure 63: The graphs show result of the sensitivity analysis. On the horizontal axes are reported the values assumed by the parameter A_o while on the vertical axis are reported in order from top to bottom: the value of the component linked to the saturation residues of the objective function, the value of the component linked to the pressure drop residues of the objective function and the value assumed by the objective function. in red is reported the minimum value obtainable by the objective function in the exact value of the parameter under analysis (in all graphs).

APPENDIX C

In this appendix are reported the results of the sensitivity analysis of the program for the simulation of multiphase flows in the final version. The sensitivity analysis was carried out in the same way to that described in section 5.1.4.. During the local sensitivity analysis all the parameters (except the one analysed that varies) are fixed at the values in green reported in table 8. The figures below show for each parameter the graphs, from top to bottom: the component of the objective function linked to the saturation residues (eq. 12), the component of the objective function linked to the pressure drop residues (eq. 13) and the objective function defined as the sum of the two just mentioned components.

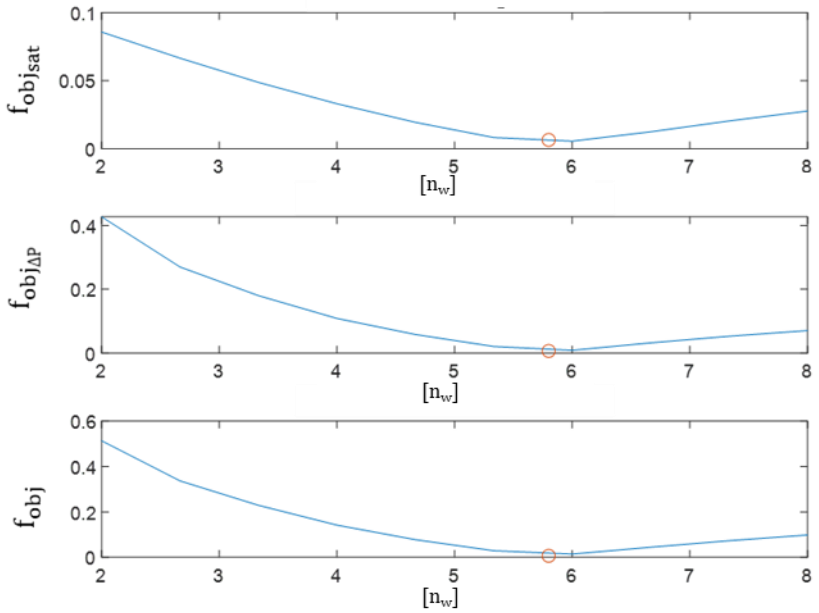

Figure 64: The graphs show result of the sensitivity analysis. On the horizontal axes are reported the values assumed by the parameter n_w while on the vertical axis are reported in order from top to bottom: the value of the component linked to the saturation residues of the objective function, the value of the component linked to the pressure drop residues of the objective function and the value assumed by the objective function. in red is reported the minimum value obtainable by the objective function in the exact value of the parameter under analysis (in all graphs).

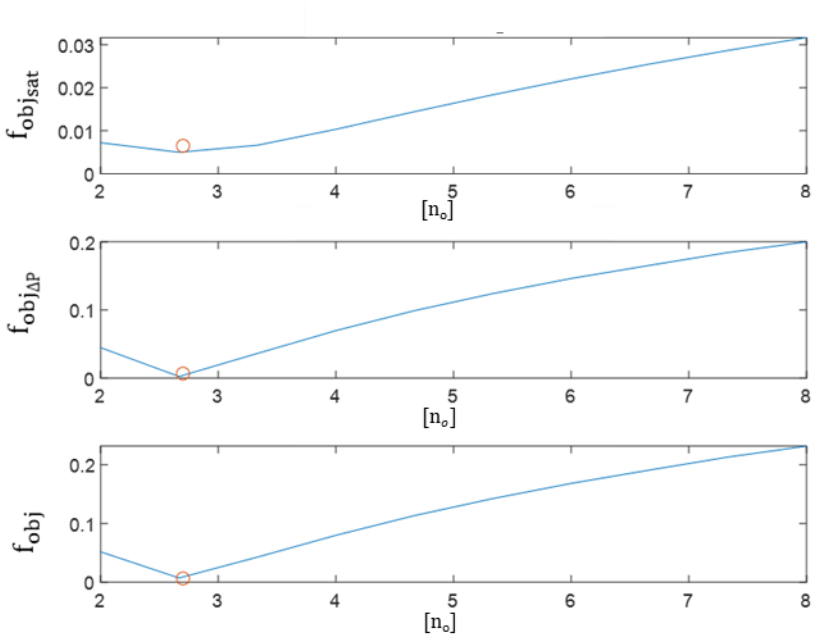

Figure 65: The graphs show result of the sensitivity analysis. On the horizontal axes are reported the values assumed by the parameter n_o while on the vertical axis are reported in order from top to bottom: the value of the component linked to the saturation residues of the objective function, the value of the component linked to the pressure drop residues of the objective function and the value assumed by the objective function. in red is reported the minimum value obtainable by the objective function in the exact value of the parameter under analysis (in all graphs).

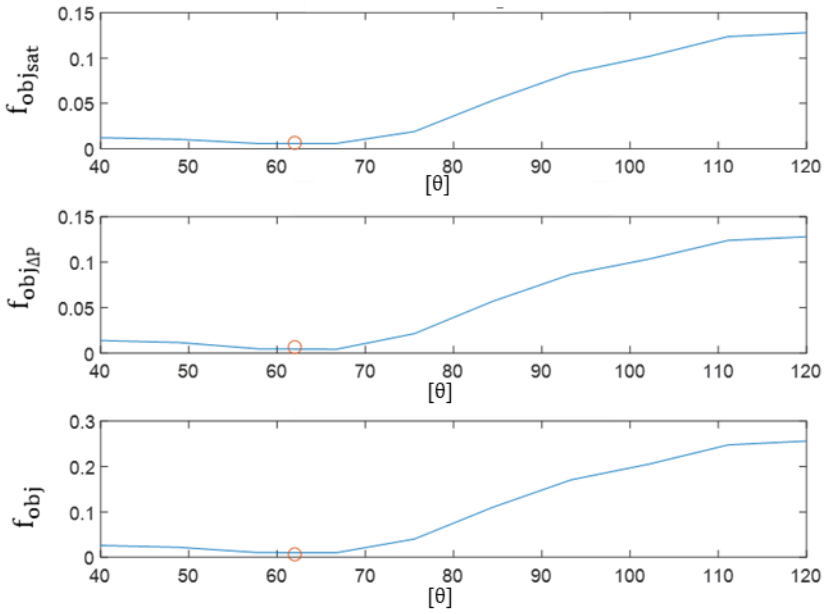

Figure 66: The graphs show result of the sensitivity analysis. On the horizontal axes are reported the values assumed by the parameter theta while on the vertical axis are reported in order from top to bottom: the value of the component linked to the saturation residues of the objective function, the value of the component linked to the pressure drop residues of the objective function and the value assumed by the objective function. in red is reported the minimum value obtainable by the objective function in the exact value of the parameter under analysis (in all graphs).

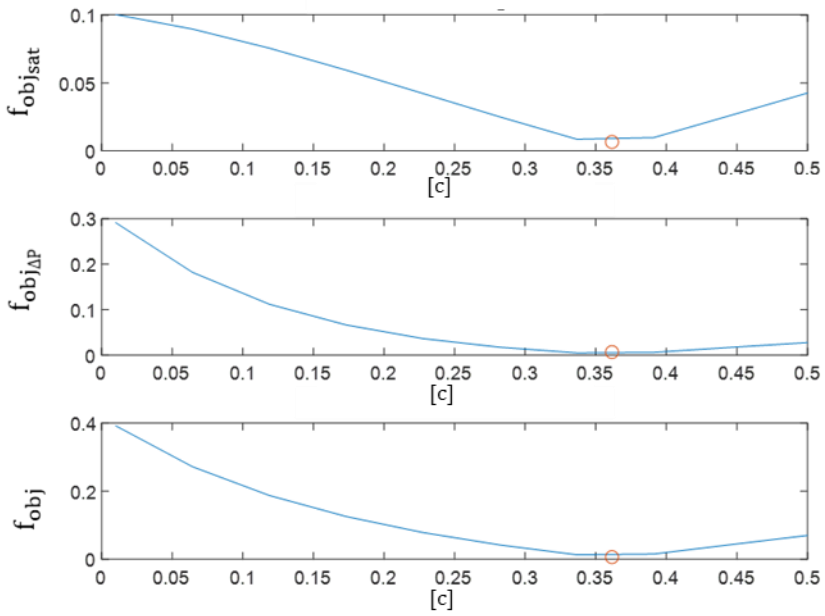

Figure 67: The graphs show result of the sensitivity analysis. On the horizontal axes are reported the values assumed by the parameter c while on the vertical axis are reported in order from top to bottom: the value of the component linked to the saturation residues of the objective function, the value of the component linked to the pressure drop residues of the objective function and the value assumed by the objective function. in red is reported the minimum value obtainable by the objective function in the exact value of the parameter under analysis (in all graphs).

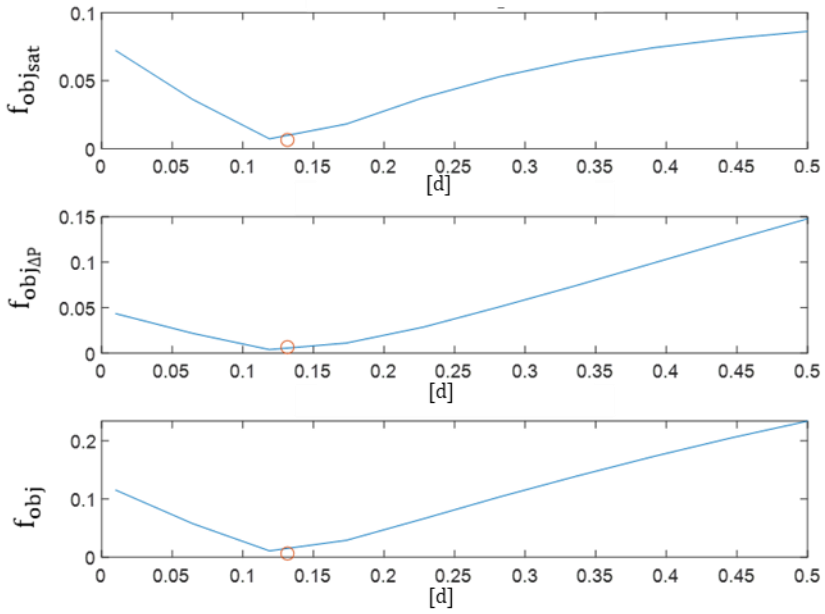

Figure 68: The graphs show result of the sensitivity analysis. On the horizontal axes are reported the values assumed by the parameter d while on the vertical axis are reported in order from top to bottom: the value of the component linked to the saturation residues of the objective function, the value of the component linked to the pressure drop residues of the objective function and the value assumed by the objective function. in red is reported the minimum value obtainable by the objective function in the exact value of the parameter under analysis (in all graphs).

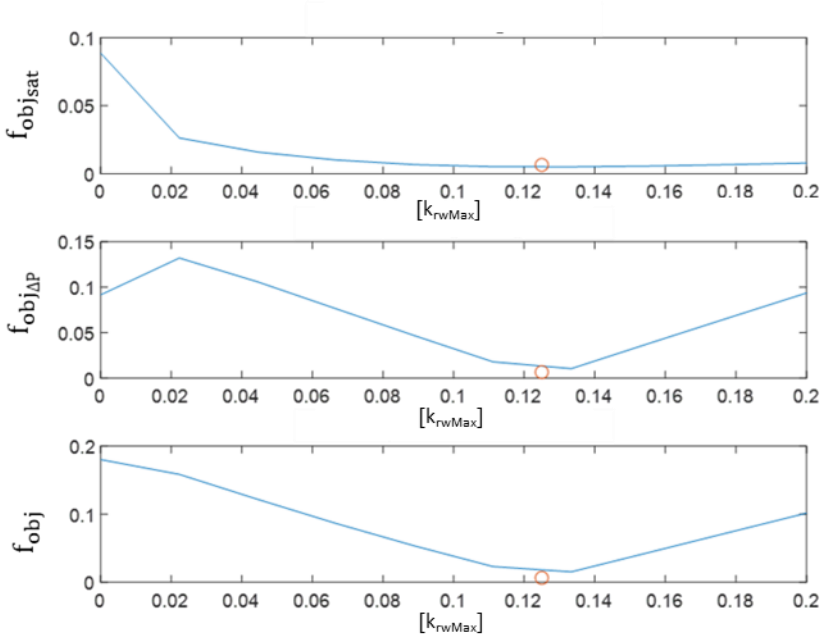

Figure 69: The graphs show result of the sensitivity analysis. On the horizontal axes are reported the values assumed by the parameter k_{rwMax} while on the vertical axis are reported in order from top to bottom: the value of the component linked to the saturation residues of the objective function, the value of the component linked to the pressure drop residues of the objective function and the value assumed by the objective function. in red is reported the minimum value obtainable by the objective function in the exact value of the parameter under analysis (in all graphs).

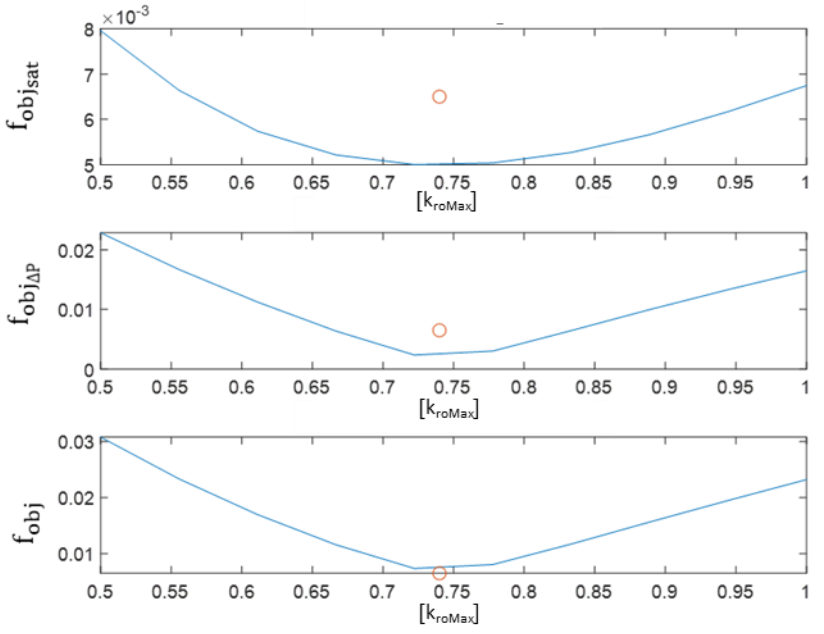

Figure 70: The graphs show result of the sensitivity analysis. On the horizontal axes are reported the values assumed by the parameter k_{roMax} while on the vertical axis are reported in order from top to bottom: the value of the component linked to the saturation residues of the objective function, the value of the component linked to the pressure drop residues of the objective function and the value assumed by the objective function. in red is reported the minimum value obtainable by the objective function in the exact value of the parameter under analysis (in all graphs).

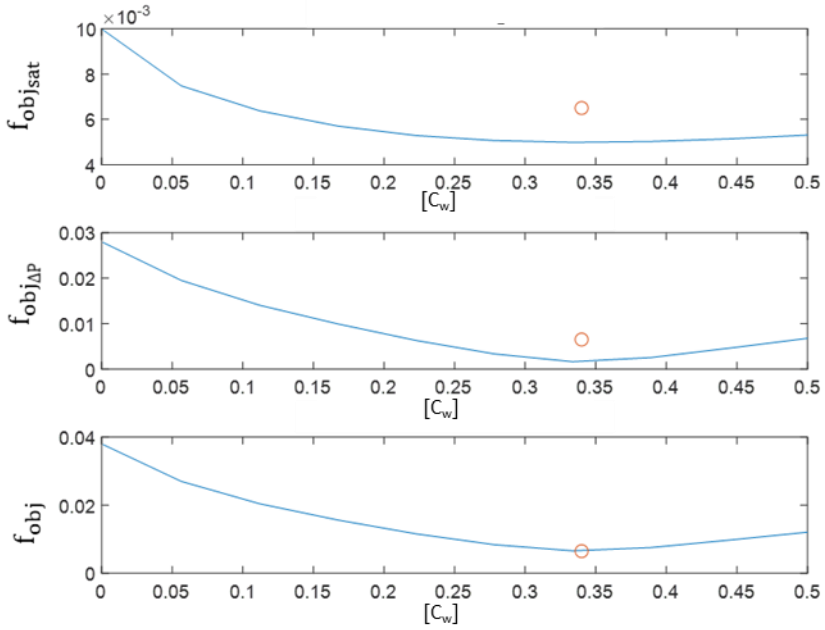

Figure 71: The graphs show result of the sensitivity analysis. On the horizontal axes are reported the values assumed by the parameter C_w while on the vertical axis are reported in order from top to bottom: the value of the component linked to the saturation residues of the objective function, the value of the component linked to the pressure drop residues of the objective function and the value assumed by the objective function. in red is reported the minimum value obtainable by the objective function in the exact value of the parameter under analysis (in all graphs).

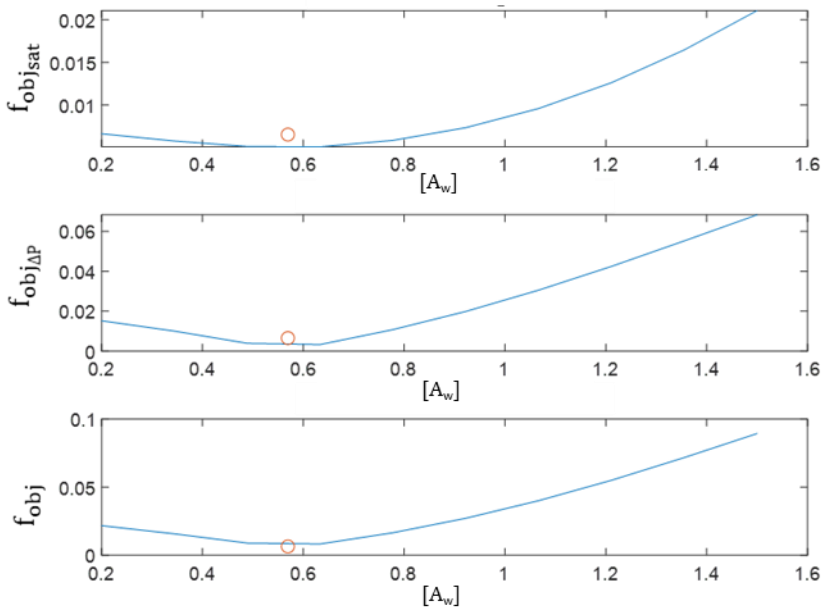

Figure 72: The graphs show result of the sensitivity analysis. On the horizontal axes are reported the values assumed by the parameter A_w while on the vertical axis are reported in order from top to bottom: the value of the component linked to the saturation residues of the objective function, the value of the component linked to the pressure drop residues of the objective function and the value assumed by the objective function. in red is reported the minimum value obtainable by the objective function in the exact value of the parameter under analysis (in all graphs).

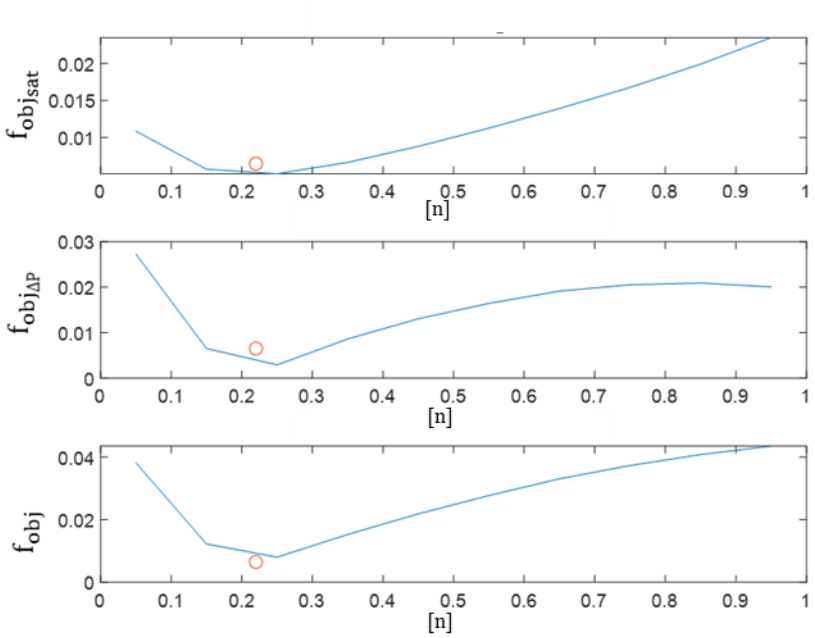

Figure 73: The graphs show result of the sensitivity analysis. On the horizontal axes are reported the values assumed by the parameter n while on the vertical axis are reported in order from top to bottom: the value of the component linked to the saturation residues of the objective function, the value of the component linked to the pressure drop residues of the objective function and the value assumed by the objective function. in red is reported the minimum value obtainable by the objective function in the exact value of the parameter under analysis (in all graphs).

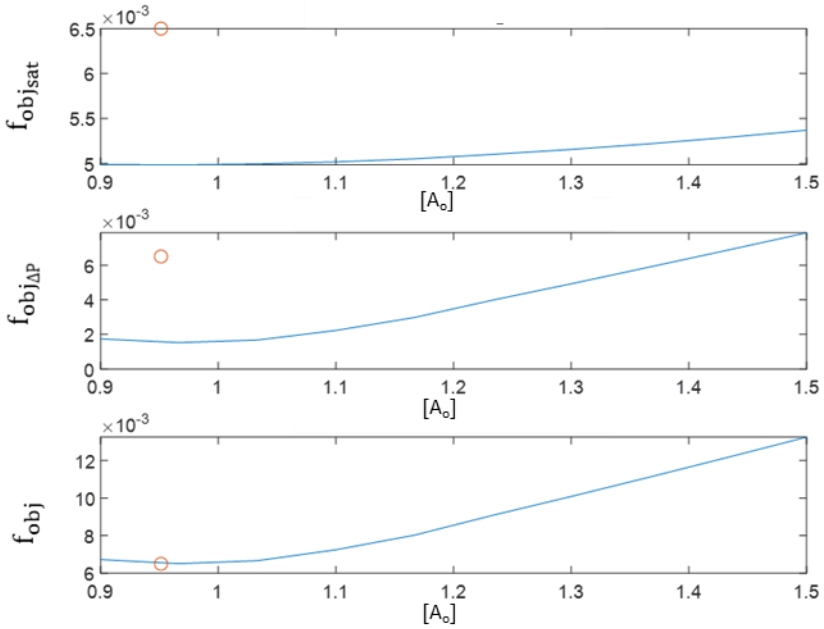

Figure 74: The graphs show result of the sensitivity analysis. On the horizontal axes are reported the values assumed by the parameter A_o while on the vertical axis are reported in order from top to bottom: the value of the component linked to the saturation residues of the objective function, the value of the component linked to the pressure drop residues of the objective function and the value assumed by the objective function. in red is reported the minimum value obtainable by the objective function in the exact value of the parameter under analysis (in all graphs).

The figures below show for each parameter the graphs, from top to bottom: the component of the objective function linked to the saturation residues, the component of the objective function linked to the pressure drop residues and the objective function defined as the weighted sum of the two just mentioned components with a weight 10 times greater for the component linked to the saturation.

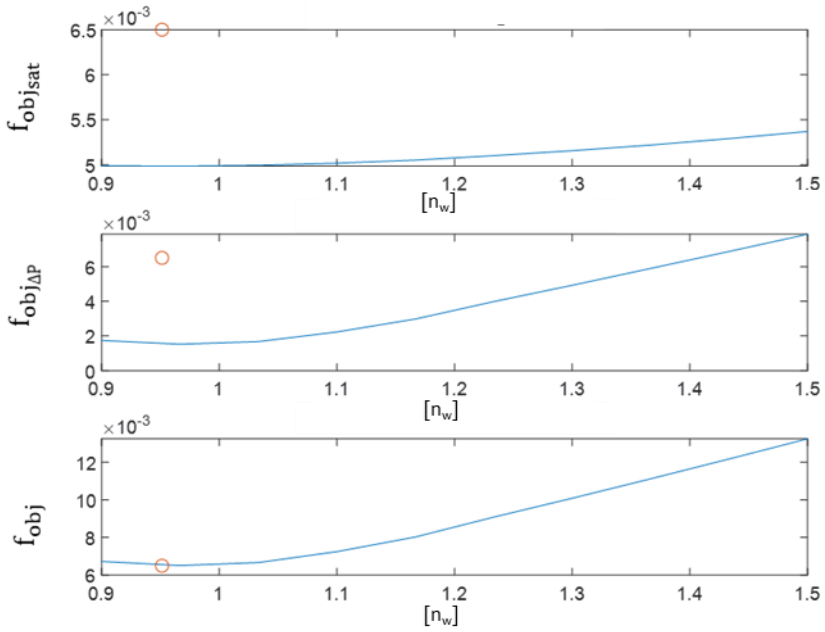

Figure 75: The graphs show result of the sensitivity analysis. On the horizontal axes are reported the values assumed by the parameter n_w while on the vertical axis are reported in order from top to bottom: the value of the component linked to the saturation residues of the objective function, the value of the component linked to the pressure drop residues of the objective function and the value assumed by the objective function. in red is reported the minimum value obtainable by the objective function in the exact value of the parameter under analysis (in all graphs).

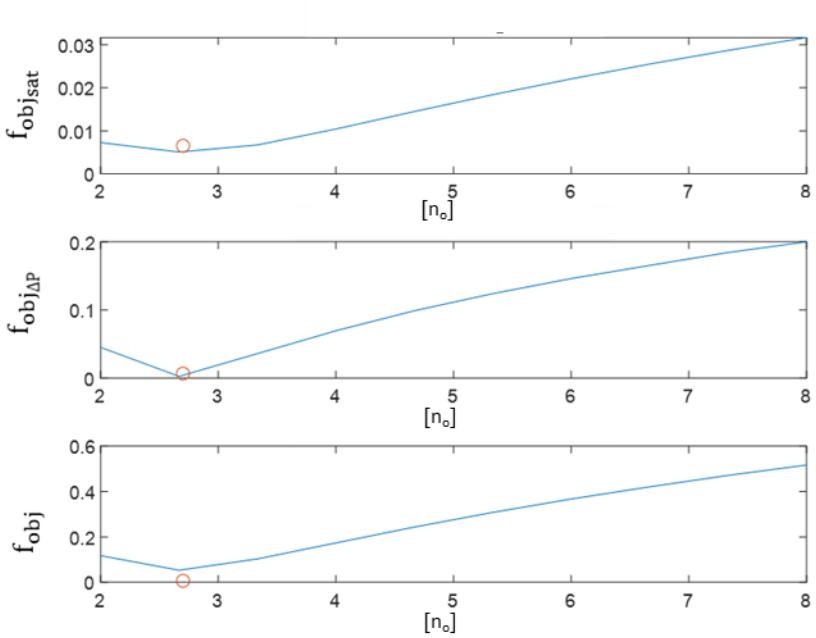

Figure 76: The graphs show result of the sensitivity analysis. On the horizontal axes are reported the values assumed by the parameter n_o while on the vertical axis are reported in order from top to bottom: the value of the component linked to the saturation residues of the objective function, the value of the component linked to the pressure drop residues of the objective function and the value assumed by the objective function. in red is reported the minimum value obtainable by the objective function in the exact value of the parameter under analysis (in all graphs).

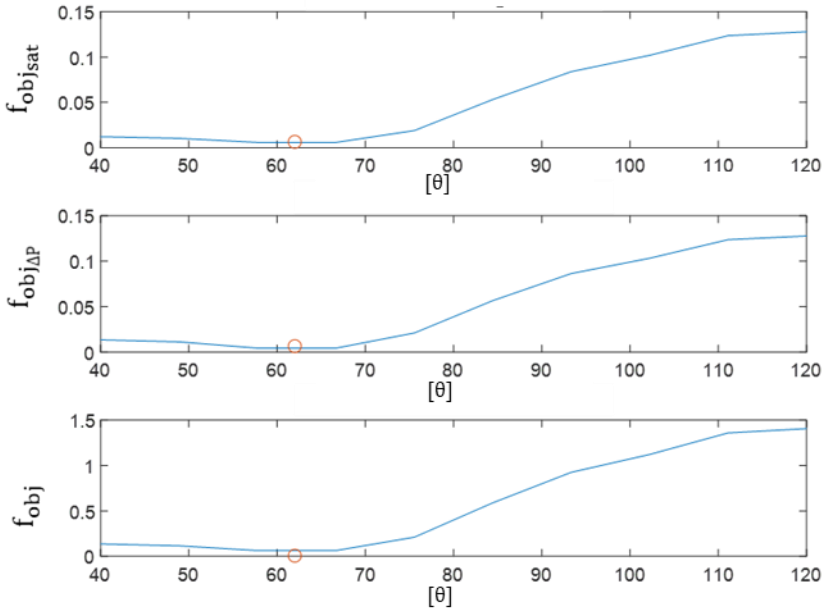

Figure 77: The graphs show result of the sensitivity analysis. On the horizontal axes are reported the values assumed by the parameter theta while on the vertical axis are reported in order from top to bottom: the value of the component linked to the saturation residues of the objective function, the value of the component linked to the pressure drop residues of the objective function and the value assumed by the objective function. in red is reported the minimum value obtainable by the objective function in the exact value of the parameter under analysis (in all graphs).

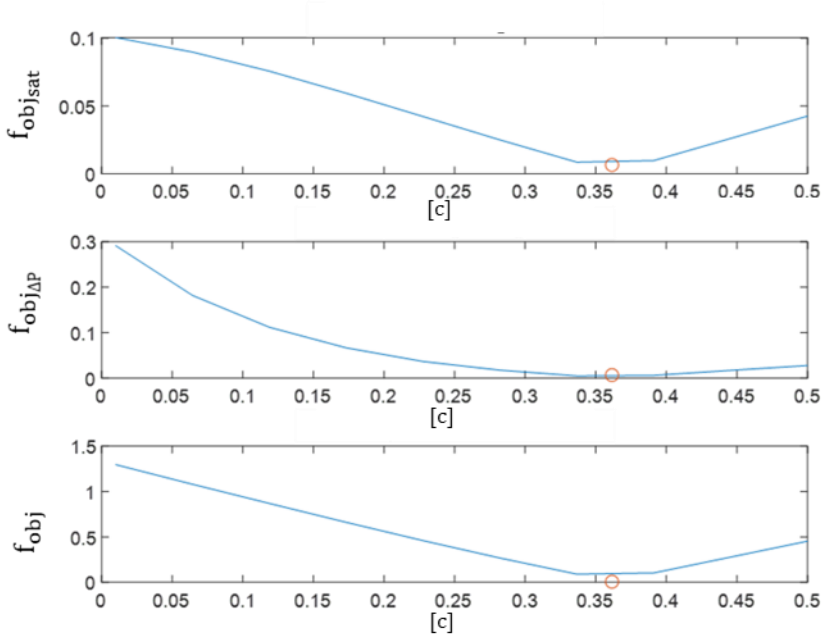

Figure 78: The graphs show result of the sensitivity analysis. On the horizontal axes are reported the values assumed by the parameter c while on the vertical axis are reported in order from top to bottom: the value of the component linked to the saturation residues of the objective function, the value of the component linked to the pressure drop residues of the objective function and the value assumed by the objective function. in red is reported the minimum value obtainable by the objective function in the exact value of the parameter under analysis (in all graphs).

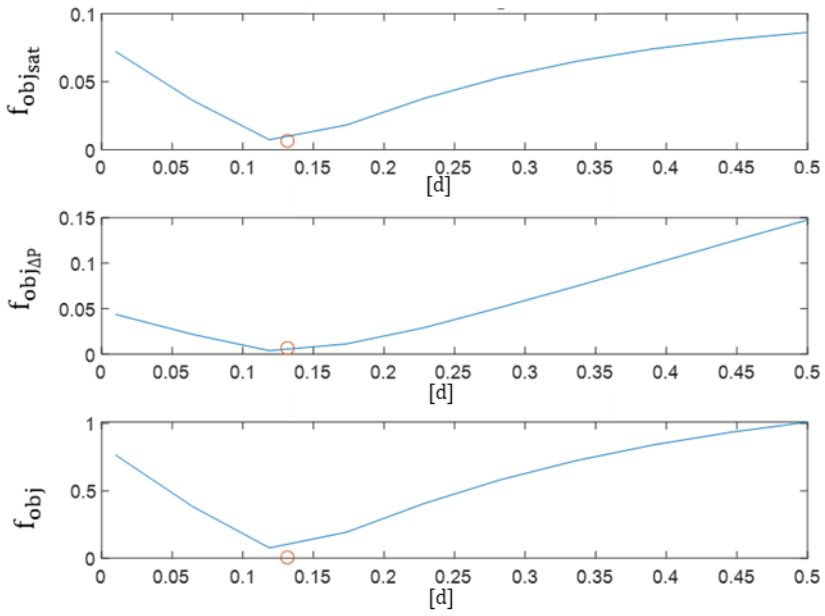

Figure 79: The graphs show result of the sensitivity analysis. On the horizontal axes are reported the values assumed by the parameter d while on the vertical axis are reported in order from top to bottom: the value of the component linked to the saturation residues of the objective function, the value of the component linked to the pressure drop residues of the objective function and the value assumed by the objective function. in red is reported the minimum value obtainable by the objective function in the exact value of the parameter under analysis (in all graphs).

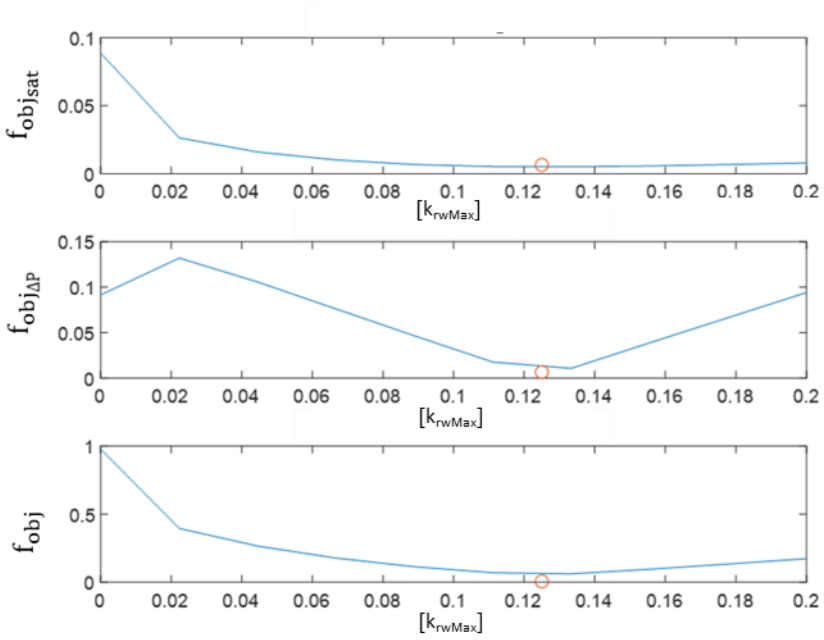

Figure 80; The graphs show result of the sensitivity analysis. On the horizontal axes are reported the values assumed by the parameter k_{rwMax} while on the vertical axis are reported in order from top to bottom: the value of the component linked to the saturation residues of the objective function, the value of the component linked to the pressure drop residues of the objective function and the value assumed by the objective function. in red is reported the minimum value obtainable by the objective function in the exact value of the parameter under analysis (in all graphs).

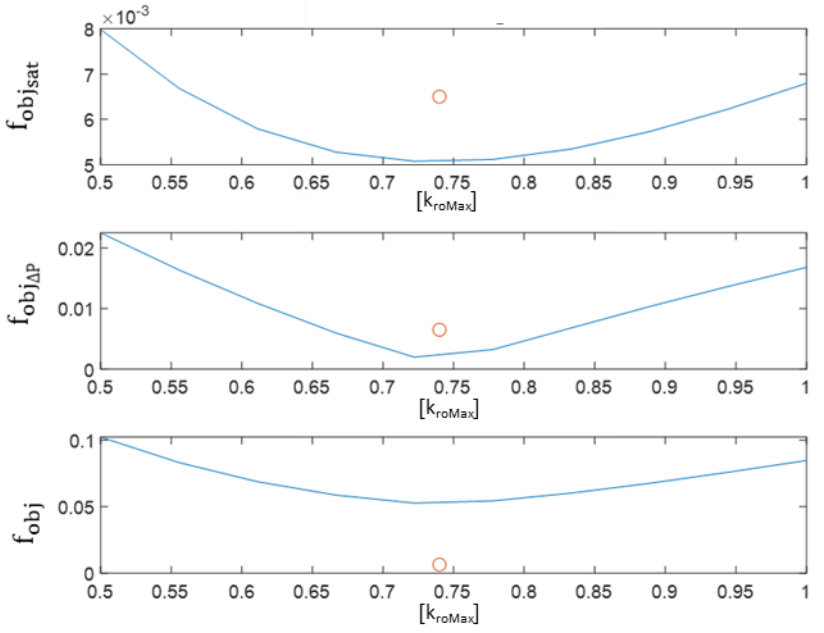

Figure 81: The graphs show result of the sensitivity analysis. On the horizontal axes are reported the values assumed by the parameter k_{roMax} while on the vertical axis are reported in order from top to bottom: the value of the component linked to the saturation residues of the objective function, the value of the component linked to the pressure drop residues of the objective function and the value assumed by the objective function. in red is reported the minimum value obtainable by the objective function in the exact value of the parameter under analysis (in all graphs).

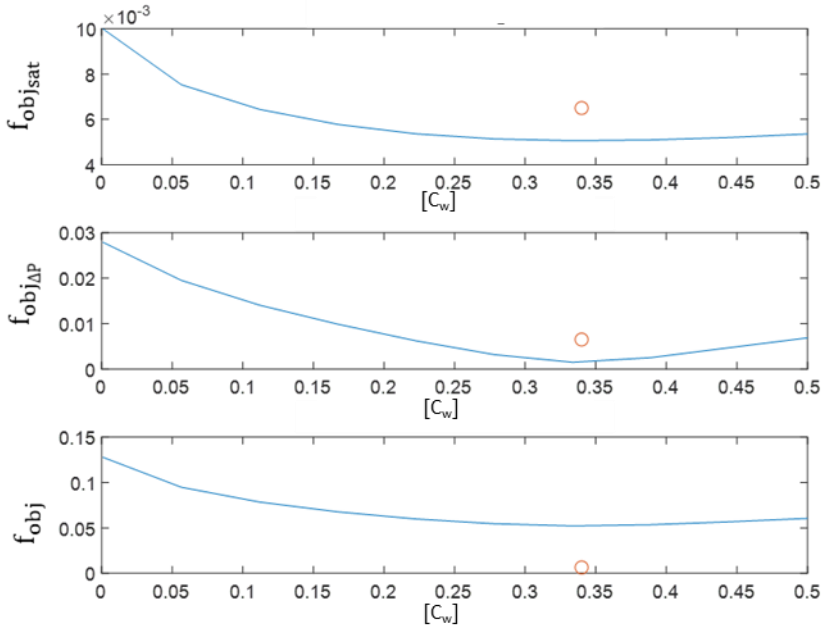

Figure 82: The graphs show result of the sensitivity analysis. On the horizontal axes are reported the values assumed by the parameter C_w while on the vertical axis are reported in order from top to bottom: the value of the component linked to the saturation residues of the objective function, the value of the component linked to the pressure drop residues of the objective function and the value assumed by the objective function. in red is reported the minimum value obtainable by the objective function in the exact value of the parameter under analysis (in all graphs).

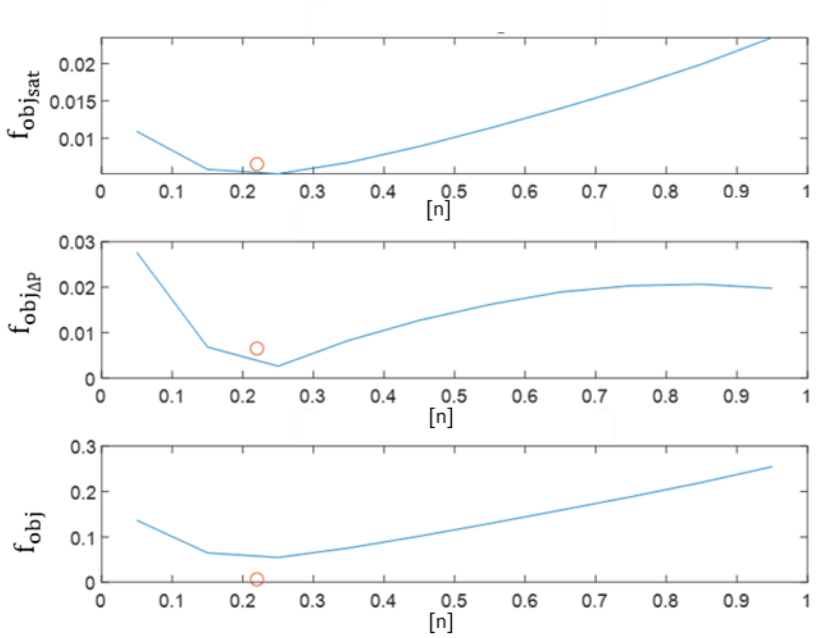

Figure 83: The graphs show result of the sensitivity analysis. On the horizontal axes are reported the values assumed by the parameter n while on the vertical axis are reported in order from top to bottom: the value of the component linked to the saturation residues of the objective function, the value of the component linked to the pressure drop residues of the objective function and the value assumed by the objective function. in red is reported the minimum value obtainable by the objective function in the exact value of the parameter under analysis (in all graphs).

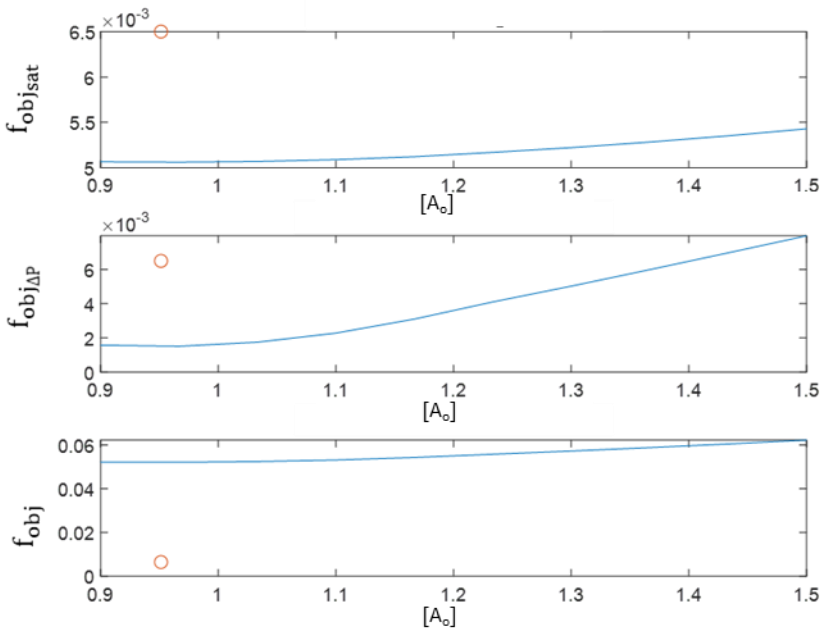

Figure 84: The graphs show result of the sensitivity analysis. On the horizontal axes are reported the values assumed by the parameter A_o while on the vertical axis are reported in order from top to bottom: the value of the component linked to the saturation residues of the objective function, the value of the component linked to the pressure drop residues of the objective function and the value assumed by the objective function. in red is reported the minimum value obtainable by the objective function in the exact value of the parameter under analysis (in all graphs).

APPENDIX D

Since one of the critical issues that has been identified in the latest version of the workflow consists in the deformation of the geometry caused by the grid created to reduce the calculation time of the optimization algorithm, a new grid able to better interpolate a cylindrical geometry (characteristic of core samples) has been proposed.

An octagonal grid has been chosen because it is able to better interpolate data from the dataset.

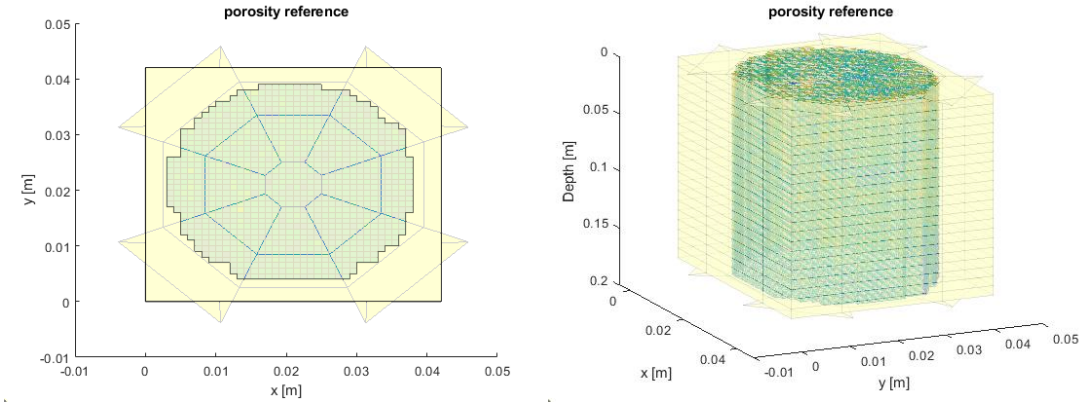

Figure 85: octagonal grid superimposed on the cells where a measurement is present

The interpolation of parameters has been certainly one of the critical points of the grid development. There has not been a specific function in the MRST toolbox to interpolate data for this kind of unstructured geometry. For this purpose, an algorithm has been written to identify the closest vertices to each cell centre, and therefore to find the vertices of the volume of each cell. Using the assigned vertices, all the measurements present inside the volume has been identified and interpolated obtaining the average value of porosity and initial saturation for each volume of the octagonal grid.

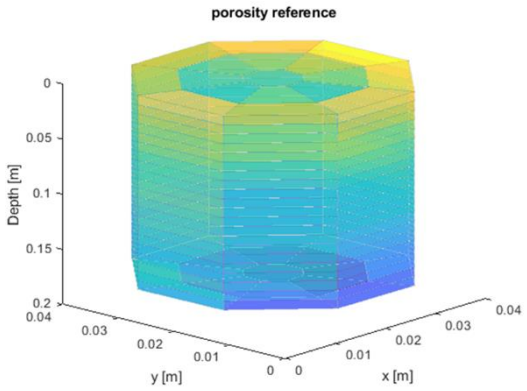

Figure 86: upscaled value on the octagonal grid

No useful simulations have been carried out with this type of grid. The unstructured grid of this type would require a suitable flow model.

The realization of a model for the simulation of multi-phase flows would have required: the use of new codes able to treat the errors introduced with an unstructured grid, a

validation process and the specific expedients that have been left for a future project (for the development of a new specific methodology).

REFERENCES

[1] J. Bear, Dynamics of fluids in porous media, New York NY: Dover, 1972.

[2] G. Mavko, J. Dvorkin and T. Mukerji, The Rock Physics Handbook, Cambridge University Press, 2003.

[3] M. J. Blunt, The Imperial College Lectures in Petroleum Engineering 2, Reservoir Engineering-World Scientific, 2017.

[4] J. Bear and A. Cheng, Modeling Groundwater Flow and Contaminant Transport, Springer, 2010.

[5] H. Versteeg and W. Malalasekra, An Introduction to Computational Fluid Dynamics The Finite Volume Method (2nd Edition), Prentice Hall, 2007.

[6] J. Carrera, "State of the art of the inverse problem applied to the flow and solute transport equations," in *Ground Water Flow and Quality Modelling*, D. Reidel Publishing Company, 1988, pp. 549-583.

[7] M. Riva and A. Guadagnini, *Inverse Problem in Reservoir Engineering (Politecnico di Milano Lectures in Transport Phenomena In Petroleum Reservoir),* 2017.

[8] J. Wilson and m. Dettinger, "Steady state vs. transient parameter estimation," in *ASCE conference on "Verification of Mahematical and Physical models in Hydraulic Engieneering*", University of Meriland, 1978.

[9] A. Akaike, "A new look at statistical model identification," *IEEE Transactions on Automatic Control,* Vols. AC-19, pp. 716-722, 1974.

[10] A. Akaike, "On entropy maximization principle," in *Applications of statistics*, 1977, pp. 27-41.

[11] R. Kashyap, "Optimal choice of AR and MA parts in autoregressive moving average models," in *Transactions on Pattern Analysis and Machine Intelligence*, 1982, pp. 99-104.

[12] J. Carrera and S. P. Neuman, "Esitmation of aquifer parameters under transient and steady-state condition, 3. application on synthetic and field data," *Water Resour. Res,* vol. 2, no. 22, pp. 228-242, 1986.

[13] K. E. Parsopoulos and M. N. Vrahatis, Particle Swarm Optimization and Intelligence: Advances and Applications, New York: Hershey, 2010.

[14] H. B. Curry, "The Method of Steepest Descent for Non-linear Minimization Problems," *Quart. Appl. Math.,* vol. 3, no. 2, p. 258–261, 1944.

[15] C. Lemarechal, “Cauchy and the Gradient Method,” *Documenta Mathematica,* vol. Extra, p. 251–254, 2012.

[16] y. J. Kochenderfer and T. A. Wheeler, Algorithms for Optimization, The MIT Press, 2019.

[17] X. Yang, “A Brief History of Optimization,” in *Engineering Optimization*, Wiley, 2010, p. 1–13.

[18] Powell, “An Efficient Method for Finding the Minimum of a Function of Several Variables Without Calculating Derivatives,” *Computer Journal,* vol. 7, no. 2, pp. 155-162, 1964.

[19] R. Hooke and T. A. Jeeves, “Direct Search Solution of Numerical and Statistical Problems,” *Journal of the ACM (JACM),* vol. 8, no. 2, pp. 212-229, 1961.

[20] R. G. Regis, “On the Properties of Positive Spanning Sets and Positive Bases,” *Optimization and Engineering,* vol. 17, no. 1, pp. 229-262, 2016.

[21] G. Hinton and S. Roweis, “Stochastic Neighbor Embedding,” *Advances in Neural Information Processing Systems,* 2003.

[22] D. E. Goldberg, “Genetic Algorithms,” in *Search, Optimization, and Machine*, Addison-Wesley, 1989.

[23] R. Fletcher, “On the Barzilai–Borwein Method,” in *Optimization and Control with Applications. Applied Optimization*, Boston, Springer, 2005.

[24] R. Storn and K. Price, “Differential Evolution – A Simple and Efficient Heuristic for Global Optimization over Continuous Spaces,” *Journal of Global Optimization ,* vol. 11, p. 341–359, 1997.

[25] J. Kennedy and R. Eberhart, “Particle swarm optimization,” in *International Conference on Neural Networks*, Perth, WA, Australia, 1995.

[26] J. Sheldon, C. Harris and D. Bavly, “ A method for general reservoir behavior simulation on digital computers,” in *Fall Meeting of the Society of Petroleum Engineers of AIME*, Denver, Colorado, 1960.

[27] P. Jacquard, “Permeability distribution from field pressure data,” *SPE journal,* vol. 5, p. 281–294, 1965.

[28] K. Thomas and L. Hellums, “A nonlinear automatic history matching technique for reservoir simulation models,” *SPE journal,* vol. 12, no. 6, 1972.

[29] R. Kulkarni, A. Watson, J. Nordtvedt, A. Brancolini and O. Johnsen, “Estimation of multiphase flow functions from dynamic displacement data: applications of NMR imaging,” in *SPE European Petroleum Conference*, Milan, Italy, 1996.

[30] R. Liu, H. Liu, X. Li, J. Wang and C. Pang, “Calculation of oil and water relative permeability for extra low,” in *CPS/SPE International Oil and Gas*, Beijing, China, 2010.

[31] M. Honarpour and S. Mahmood, “Relative-permeability measurements: an overview,” *J. Petroleum Technol,* vol. 40, pp. 963-966, 1988.

[32] S. Ucan, F. Civan and R. Evans, “Uniqueness and simultaneous predictability of relative permeability and,” *J. Can. Petroleum Technol.,* vol. 4, no. 36, pp. 52-61, 1997.

[33] A. Watson, R. Kulkarni, J. Nordtvedt, A. Sylte and H. Urkedal, “ Estimation of porous media flow functions,” *Meas. Sci. Technol.,* vol. 6, no. 9, pp. 898-905, 1998.

[34] C. Chardaire-Riviere, G. Chavent, J. Jaffre, J. Liu and B. Bourbiaux, “Simultaneous estimation of relative permeability and capillary pressure,” *SPE Form. Eval.,* vol. 2, no. 7, pp. 283-289, 1992.

[35] X. Sun and K. Mohanty, “Estimation of flow functions during drainage using genetic algorithm,” *SPE j.,* vol. 4, no. 10, pp. 449-457, 2005.

[36] L. Mohamed, M. Christie and V. Demyanov, “Comparison of stochastic sampling algorithms for uncertainty quantification,” in *Proceedings of the SPE Reservoir Simulation Symposium*, Woodlands, Texas, 2009.

[37] Y. Hajizadeh, A. Michael and V. Demyanov, “Ant colony optimization for history matching and uncertainty quantification of reservoir models,” *J. Pet. Sci. Eng.,* no. 77, pp. 78-92, 2011.

[38] Y. Hajizadeh, A. Michael and V. Demyanov, “Comparative study of novel population-based optimization algorithms for history matching and uncertaintyquantification quantification,” in *Abu Dhabi International Petroleum Exhibition and Conference*, Abu Dhabi, 2010.

[39] Y. Zhang, H. Li and D. Yang, “Simultaneous Estimation of Relative Permeability and Capillary Pressure Using Ensemble-Based History Matching Techniques,” *Transp Porous Med ,* no. 94, pp. 259-276, 2012.

[40] E. C. Santhosh and J. S. Sangwai, “A hybrid differential evolution algorithm approach towards assisted history matching and uncertainty quantification for reservoir models,” *Journal of Petroleum Science and Engineering,* no. 142, pp. 21-35, 2016.

[41] M. Mahdaviara, N. A. Menad, M. Ghazanfari and A. Hemmati-Sarapardeh, “Modeling relative permeability of gas condensate reservoirs: Advanced computational frameworks,” *Journal of Petroleum Science and Engineering,* no. 189, 2020.

[42] J. Tian, C. Qi, Y. Sun, Z. M. Yaseen and B. T. Pham, “Permeability prediction of porous media using a combination of computational fuid dynamics and hybrid machine learning methods,” *Engineering with Computers .*

[43] F. Di Maio, *Artificial intelligence and advanced simulation for the safety, reliability and maintenance of energy systems (Politecnico di Milano Lectures in Energy Engineering),* 2019.

[44] Sintef, “MRST - MATLAB Reservoir Simulation Toolbox,” [Online]. Available: https://www.sintef.no/projectweb/mrst/. [Accessed 10 8 2020].

[45] J. E. Castillo, “Mathematical aspects of numerical grid generation-Society for Industrial and Applied Mathematics,” *Frontiers in applied mathematics,* no. 8, 1987.

[46] K. A. Lie, An Introduction To Reservoir Simulation Using Matlab/Gnu Octave, Cambridge University Press, 2019.

[47] SPE, “Petro wiki: Relative permeability models,” 2016 1 19. [Online]. Available: https://petrowiki.org/Relative_permeability_models#cite_note-r1-1. [Accessed 12 8 2020].

[48] A. T. Corey, “The Interrelation Between Gas and Oil Relative Permeabilities,” *Preoducer Montly,* pp. 38-41, 1954.

[49] R. Brooks and A. Corey, “Hydraulic Properties of Porous Media,” *Hydrology Papers,* no. 3, 1964.

[50] S. Skjaeveland, L. Siqveland, A. Kjosavik, W. Hammervold Thomas and V. G. A., “Capillary Pressure Correlation for Mixed-Wet Reservoirs,” *SPE Reservoir Eval. & Eng.,* vol. 3, pp. 60-67, 200.

[51] SPE, “PetroWiki: Permeability determination,” 24 6 2015. [Online]. Available: https://petrowiki.org/Permeability_determination#cite_ref-r3_3-0. [Accessed 10 5 2020].

[52] A. Li, W. Ding, J. He, P. Dai, S. Yin and F. Xie, “Investigation of pore structure and fractal characteristics of organic-rich shale reservoirs: A case study of Lower Cambrian Qiongzhusi formation in Malong block of eastern Yunnan Province, South China.,” *Marine and Petroleum Geology,* vol. 70, 2015.

[53] McGraw-Hill Dictionary of Scientific and Technical Terms, *Synthetic data,* 2009.

[54] E. Barse, H. Kvarnström and E. Jonsson, “Synthesizing test data for fraud detection systems,” in *19th Annual Computer Security Applications Conference*, 2003.

[55] Rubin, “Statistical Analysis of Masked Data,” *Journal of Official Statistics,* vol. 9, p. 407–426, 1993.

[56] Ente Nazionale Italiano di Unificazione (UNI), “Guida all'espressione dell'incertezza di misura, Milano, 2000.

[57] MATLAB, “MATLAB: help centre, filmissing,” [Online]. Available: https://it.mathworks.com/help/matlab/ref/fillmissing.html.

[58] MATLAB, “MATLAB: Help Centre, Particle Swarm Optimizarion,” [Online]. Available: https://it.mathworks.com/help/gads/particle-swarm-optimization-algorithm.html.

[59] Buehren and Markus, “MATLAB Central File Exchange, Differential Evolution,” 2020. [Online]. Available: https://www.mathworks.com/matlabcentral/fileexchange/18593-differential-evolution.

[60] Tarek and H. A., “Fundamentals of Rock Properties,” in *Reservoir Engineering Handbook*, 2018, pp. 167-281.

[61] R. L. Morris and W. P. Biggs, “Using Log-Derived Values Of Water Saturation And Porosity,” *Society of Petrophysicists and Well-Log Analysts,* 1967.

[62] E. Spiteri, R. Juanes, M. Blunt and F. & Orr, “ A New Model of Trapping and Relative Permeability Hysteresis for All Wettability Characteristics,” *Spe Journal,* vol. 13, pp. 277-288, 2008.

[63] A. i, M. Ratto, T. Andres, F. Campolongo, J. Cariboni, D. Gatelli, M. Saisana and S. Tarantola, Global Sensitivity Analysis, The Primer. John Wiley & Sons., 2008.

[64] MATLAB, “MATLAB: Help Centre, What is Sensitivity Analysis?,” [Online]. Available: https://it.mathworks.com/help/sldo/ug/what-is-sensitivity-analysis.html.

[65] J. Arabas, Z. Michalewicz and J. Mulawka, “GAVaPS-a genetic algorithm with varying population size,” in *First IEEE Conference on Evolutionary Computation*, Orlando, FL, 1994.